Copy

[redacted]

NASA TM X-840

NASA TM X-840

[redacted]

X 63 15024

(NASA-TM-X-840) LONGITUDINAL AERODYNAMIC CHARACTERISTICS AT MACH NUMBERS FROM 0.28 TO 2.50 OF A MULTIPURPOSE TACTICAL AIRPLANE CONFIGURATION HAVING — W.P. Phillips, et al (NASA) Jul. 1963 109 p

N72-73183

Unclas

00/99 31923

TECHNICAL MEMORANDUM

X-840

LONGITUDINAL AERODYNAMIC CHARACTERISTICS AT MACH NUMBERS FROM 0.28 TO 2.50 OF A MULTIPURPOSE TACTICAL AIRPLANE CONFIGURATION HAVING VARIABLE-SWEEP WINGS AND EXTERNALLY MOUNTED ENGINES

By W. Pelham Phillips and Robert T. Taylor

Langley Research Center
Langley Station, Hampton, Va.

CLASSIFICATION CHANGED
UNCLASSIFIED
TO
By Authority of
Date

Details of illustrations in this document may be better studied on microfiche

[redacted]

NATIONAL AERONAUTICS AND SPACE ADMINISTRATION

WASHINGTON July 1963

[redacted]

[redacted]

NATIONAL AERONAUTICS AND SPACE ADMINISTRATION

TECHNICAL MEMORANDUM X-840

LONGITUDINAL AERODYNAMIC CHARACTERISTICS AT MACH NUMBERS FROM 0.28 TO 2.50 OF A MULTIPURPOSE TACTICAL AIRPLANE CONFIGURATION HAVING VARIABLE-SWEEP WINGS AND EXTERNALLY MOUNTED ENGINES*

By W. Pelham Phillips and Robert T. Taylor

SUMMARY

An investigation was conducted in the Langley 7- by 10-foot high-speed tunnel and in the Langley Unitary Plan wind tunnel at Mach numbers from 0.28 to 2.50 to determine the subsonic, transonic, and supersonic longitudinal aerodynamic characteristics of a variable-sweep airplane configuration having externally mounted engines. The configuration was investigated at wing-sweep angles of 25°, 35°, 45°, 55°, 75°, and 90°.

The highest value of trimmed maximum lift-drag ratio (at model Reynolds number) at subsonic speeds was found to be 14.3 for the wing in the 25° sweep position. At supersonic speeds the higher values of maximum lift-drag ratio were found for the configuration having the wings swept back 75°. Only a slight reduction in zero lift drag was obtained by increasing the wing sweep from 75° to 90°; however, a marked reduction in wave drag at a Mach number of 1.2 was noted as a result of improvements in the area distribution (as compared with a preliminary configuration), and a reduction in the maximum cross-sectional area.

With regard to the longitudinal stability characteristics, the aerodynamic-center location was approximately the same for the configurations having the wing swept 25° and 75° at a Mach number of 0.60. However, a rearward aerodynamic-center movement of 22.5 percent $\bar{c}$ accompanies an increase in Mach number from 0.85 to 2.50 with the wing in the 75° sweep position. The variation of pitching moment with lift at high lift coefficients was made more linear by notching the outboard wing panels.

INTRODUCTION

In anticipation of future requirements for multipurpose land and carrier-based attack aircraft, the National Aeronautics and Space Administration has

[redacted]

undertaken the aerodynamic investigation of a lightweight configuration which would exceed the versatility levels of contemporary aircraft. This configuration would combine carrier and short field utility with acceptable high or extremely low altitude supersonic strike capability and would exhibit good performance characteristics in either subsonic cruise or loiter missions. Previous wind-tunnel studies for a larger configuration (60,000-pound class) with internal engines have indicated that these demands may be met while maintaining acceptable longitudinal stability levels with the incorporation of outboard pivoted variable-sweep wings. (See ref. 1.) A limited amount of research has been conducted on the lighter weight configuration having a high-fineness-ratio fuselage and externally mounted engines. References 2 and 3 summarize the low subsonic to transonic and supersonic speed performance and longitudinal stability characteristics for one such configuration having both weight and size restraints. This configuration incorporated the aforementioned type of variable-wing geometry, twin externally mounted engines, and an internal weapons bay. Larger weapon loads were possible with external storing.

Although references 2 and 3 have shown the feasibility of a lightweight configuration with externally mounted engines, it was felt that a better proportioned configuration embodying refined transonic design could be developed which would achieve higher levels of performance throughout the proposed flight envelope. Therefore, a model was designed and constructed which satisfied identical size limitations as that of references 2 and 3. The design and construction phases incorporated component and overall proportioning so that the equivalent body for the airplane configuration, in the 90° sweep condition, conformed to a minimum drag body. A scaled model was then tested in the Langley 7- by 10-foot high-speed tunnel and in the Langley Unitary Plan wind tunnel at Mach numbers from 0.28 to 2.5.

The purpose of this paper is to present the aerodynamic performance and longitudinal stability characteristics resulting from these wind-tunnel studies. Also presented are the effects of several external store configurations and horizontal-tail location and size. The effect of a leading-edge modification in the form of notches on the outboard wing panels is also included.

In order to expedite publication, only a minimum of analysis is included herein.

COEFFICIENTS AND SYMBOLS

The results are referred to the stability axis system with all coefficients being nondimensionalized with respect to the wing geometric characteristics in the 75° leading-edge-sweep condition. The moment reference point is located at 50.9 percent of the model length and at the intersection of the model reference plane and the plane of symmetry.

C_L lift coefficient, $\frac{\text{Lift}}{qS}$

C_{L_α} lift-curve slope, $\frac{dC_L}{d\alpha}$, per degree

C_D drag coefficient, $\frac{\text{Drag}}{qS}$

C_{D_i} internal drag coefficient of engine nacelles

$C_{D,0}$ zero-lift drag coefficient

C_m pitching-moment coefficient, $\frac{\text{Pitching moment}}{qS\bar{c}}$

$(L/D)_{max}$ maximum lift-drag ratio

$C_{m_{C_L}}$ pitching-moment-curve slope, $\frac{dC_m}{dC_L}$

b wing span (75° sweep condition), 1.557 ft

$\bar{c}$ mean aerodynamic chord (75° sweep condition), 0.863 ft

i incidence angle, deg (positive when trailing edge is down)

$p_{t,\infty}$ free-stream stagnation pressure, lb/sq ft

M free-stream Mach number

q free-stream dynamic pressure, $\frac{1}{2}\rho V^2$, lb/sq ft

R Reynolds number per foot

S reference area (75° sweep condition), 1.2097 sq ft

V free-stream velocity, ft/sec

α angle of attack, deg

Λ_{LE} leading-edge sweep angle, deg

ρ air density, slugs/cu ft

Subscripts:

t horizontal tail

w wing

Components of model:

B	body (including canopy)
H	horizontal tail (subscript 1 indicates original tails; subscript 2, the 1.6 inch shorter span tails)
N	engine nacelles
V	vertical tail
W	wing (subscripts 1 and 2 indicate unnotched and notched wing, respectively)

AIRPLANE CONFIGURATION

The airplane configuration was area contoured in the 90° sweep condition, for a Mach number of unity, to provide conformity between its normal area distribution (with a $M = 1.2$, at sea level, engine inlet stream tube removed), and that of a Sears-Haack body having restrictions in length and volume. The configuration had a high wing combined with a low horizontal tail and external engine nacelles. Each inboard wing panel was fixed at a leading-edge sweep angle of 60° and contained an outboard-panel pivot axis at 48.2 percent of the wing semispan $\left(\Lambda_{LE} = 75^{\circ}\right)$ and 49.2 percent of the body length. The leading-edge sweep of the outboard wing panels varied from 25° to 90°. The maximum cross-sectional area of the configuration was 21 square feet and the total wetted area was 1,608 square feet for $\Lambda_{LE} = 90^{\circ}$.

WIND-TUNNEL MODEL

The wind-tunnel model used in the investigation was scaled to 6.31 percent of the full-size configuration, a small part of the aft portion of the fuselage being removed to allow for the model support sting.

Sketches of the model are shown in figure 1. In an attempt to obtain the most accurate representation of the flow condition at the aft end of the model, a narrow rectangular support sting was used and the scaled fuselage lines were maintained back to the points at which the fuselage surface actually intersected the sting cavity. The cross-sectional-area diagram of the model is compared with that of a Sears-Haack body of revolution of figure 2. These area distributions are identical up to fuselage station 38 where fuselage surface intersection with the sting cavity first occurs.

Airfoil sections of the outboard wing panels were 7.5-percent-thick modified NACA 2408 (streamwise in the $\Lambda_{LE} = 25^{\circ}$ condition) (see table I), while the streamwise inboard panel sections varied from a NACA 65A005.2 airfoil section

$(i_w = -1.207)$ at the root chord to the 7.5-percent $(i_w = 0^\circ)$ outboard panel sections. The empennage components had NACA 65A004 airfoil sections. The outboard wing panels could be set at sweep angles of 25°, 35°, 45°, 55°, 65°, 75°, and 90°.

Engine nacelles for the model had a constant internal diameter while the exteriors were scaled from the airplane configuration. The straight-through interiors were used to expedite data-reduction processes while simulating nacelle-fuselage interference effects.

Photographs of the sting-mounted model are shown in figure 3 with $\Lambda_{LE} = 75^\circ$.

The external stores are shown in figure 4. The GAR-8 (Sidewinder) stores were mounted in pairs beneath the inboard wing panel so that the wing-pivot axes lay in a plane perpendicular to both store axes of symmetry and passed through the store centers of gravity. The ASM-N-7B (Bullpup-B) stores were positioned in a similar manner with only one store beneath each wing pivot.

TEST APPARATUS AND MEASUREMENTS

Tunnels

The tests were made in the Langley 7- by 10-foot high-speed wind tunnel at Mach numbers from 0.28 to 1.15 and in the Langley Unitary Plan wind tunnel low Mach number test section at Mach numbers of 1.65, 2.00, and 2.50.

The Langley 7- by 10-foot high-speed tunnel is of the atmospheric continuous-flow type having a rectangular test section equipped with longitudinal rows of perforations along the upper and lower walls to permit continuous operation from low subsonic speeds to $M = 1.15$ with negligible choking or blockage effects. No data were taken at Mach numbers from 1.03 to 1.15 to avoid impingement on the model of boundary-reflected disturbances.

The low Mach number test circuit of the Unitary Plan wind tunnel is of the variable-pressure, continuous-flow type and is equipped with an asymmetric sliding block at the test-section throat to allow continuous variation in test-section Mach number from about 1.47 to 2.9. Control of pressure, temperature, and humidity in the test medium is provided and schlieren detection is used to avoid data acquisition at Mach numbers where boundary-reflected waves impinged on the model.

Reynolds number as a function of Mach number is shown in figure 5 for both the 7- by 10-foot high-speed wind tunnel and the Unitary Plan wind tunnel through the speed range of the investigation.

Measurements

A sting-mounted six-component strain-gage balance was utilized throughout the investigation to provide force and moment measurements. In most of the tests run

in the Langley 7- by 10-foot high-speed wind tunnel, measurements were made between angle-of-attack limits of -6° and 12° through a Mach number range inclusive of 0.6 and 1.15. However, both angle of attack and Mach number were restricted by balance load limits and model wing deflections at low sweep angles. The remainder of the low-speed tests were conducted at about $M = 0.28$ through an angle-of-attack range extending from -1° to 24°.

The supersonic wind-tunnel tests were likewise restricted in angle of attack in the lower sweep conditions, the maximum α range extending from -5° to 22°.

All tests were for transition fixed by utilization of No. 180 grain size (0.0035-inch nominal diameter) carborundum particles along the 5-percent chord lines of the wing $\left(\Lambda_{LE} = 75^{\circ}\right)$ and empennage components and circumferentially at the 10-percent station of the fuselage and engine nacelles.

Corrections

No corrections are required for the effects of blockage on the free-stream dynamic pressures and Mach numbers for tests run in the transonic throat of the Langley 7- by 10-foot high-speed tunnel or the low Mach number test section of the Langley Unitary Plan wind tunnel. Also, no data are presented from either test series in a speed range where boundary-reflected disturbances impinged on the model.

The angle of attack has been corrected for flow angularity (where necessary) and for deflections in the balance and sting-support system under aerodynamic load.

The drag data were adjusted to correspond to the condition of free-stream static pressure in the balance cavity. Nacelle drag due to internal flow was calculated, turbulent skin friction on the nacelle interiors being assumed, and subtracted from the drag measurements. These internal drag coefficients (based on the wing reference area) are shown as a function of Mach number in figure 6.

No corrections for sting-support interference effects on the force and moment data have been applied, except the correction inherent in the chamber pressure adjustment to the drag.

DISCUSSION

The basic data are presented as curves of C_m, C_D, and α as a function of C_L. The subsonic to transonic data are given in figures 7 to 16, and the supersonic data are given in figures 17 to 21. All supersonic data are for the configuration having the outboard wing panels notched (W_2). Summary curves of $(L/D)_{max}$ and $C_{D,0}$ for the various sweep angles are shown in figure 22 as functions of the Mach number. These curves were prepared for the condition of zero horizontal-tail incidence.

The data indicate that the model had an untrimmed $(L/D)_{max}$ of about 14.5 at a Mach number of about 0.60 with the wing leading edge swept 25°. A trimmed $(L/D)_{max}$ value of 14.3 is indicated in figure 8 for the previously mentioned conditions. The value of $M(L/D)_{max}$ for the model is approximately 10.6 and occurs at a Mach number of about $M = 0.85$ and a leading-edge sweep of 45°.

At supersonic speeds the model had higher values of $(L/D)_{max}$ with the wing leading edge swept 75° than with any other sweep angle of the investigation. At a Mach number of 2.0 the untrimmed $(L/D)_{max}$ is about 4.5.

For flights at low altitudes and high speed, the value of zero lift drag is important to range because the aircraft is forced to fly at very low lift coefficients $\left(C_L \approx 0\right)$. Figure 22(b) is a plot of $C_{D,0}$ against Mach number for several wing leading-edge sweeps. The sweep angle having the lowest drag at transonic speeds is seen to be 90°; however, this increase in sweep affords only a very slight reduction in the transonic zero lift-drag values for the wing swept to 75°. Also plotted is a curve of $C_{D,0}$ against Mach number for the configuration of reference 2 at $\Lambda_{LE} = 75°$. Comparison shows a significant reduction in wave drag at $M = 1.2$ due to the smaller maximum cross section and improved area distribution of the present configuration. Further comparison shows an increase in the drag-rise Mach number from about $M = 0.80$ to about $M = 0.90$ for the configuration of the present paper.

The lift-curve slope C_{L_α} assumes a great deal of importance in low-altitude high-speed missions, in that it affects the "ride" or gust-response characteristics of an aircraft. Although the acceptable gust-response characteristics on such a mission have yet to be quantitatively defined, reductions in C_{L_α} will, of course, provide lower gust response. Figure 23 shows the variation of C_{L_α} with Mach number for several wing sweeps. At a Mach number of $M = 0.80$, a reduction in C_{L_α} from 0.081 to 0.048 occurs because of sweeping of the wing from 25° to 75°. Increasing the sweep angle to 90° further reduced C_{L_α} to a value of 0.034.

Figures 15, 16, and 21 show the effect of the addition of 4 GAR-8 (Sidewinder) and 2 ASM-N-7B (Bullpup-B) stores on the longitudinal aerodynamic characteristics. The incremental drag at zero lift, which represents the major effect of store addition, is presented in figure 24 as a function of Mach number. Figures 15 and 16 indicate a nonlinearity in pitching-moment characteristics as well as a general reduction in stability due to the addition of the ASM-N-7B stores.

The variation of static margin with sweep angle for the cases of horizontal tail on and tail off is shown in figure 25 for a Mach number of 0.60. As has been pointed out in reference 1 the aerodynamic-center progression with sweep for an outboard-pivot location tends to move rearward to some intermediate sweep angle and then gradually moves forward at higher sweep angles. A comparison of the longitudinal stability levels at sweep angles of 25° and 75° (horizontal tail on)

for both the present configuration and that of reference 2 indicates a reduction in aft movement of the aerodynamic center with increasing sweep of about 15 percent $\bar{c}$. (See fig. 25.) The effect of Mach number on the aerodynamic-center position is shown in figure 26 for several wing sweeps. The effect of increasing Mach number is to move the aerodynamic center aft. For a sweep angle of 75°, the aerodynamic center moves 22.5 percent $\bar{c}$ when the Mach number is increased from 0.85 to 2.50.

Variation of pitching-moment coefficient with lift coefficient at a Mach number of $M = 0.28$ is shown in figure 27 for the complete configuration $\left(BW_1VH_1N\right.$ and $\left.BW_2VH_1N\right)$. Nonlinear variation of pitching-moment coefficient with lift coefficient occurs above a C_L of about 0.6. Notching the outboard wing panels as shown in figure 1(d) appears to extend the linear portion of the curve to higher lift coefficients, in the low-sweep range, and thereby provides better trim characteristics at the low speeds and high lifts desirable for short-field take-off and landing.

Changes in the original horizontal-tail planform and location were investigated and the results are shown in figure 14. Over the range of variables investigated the original tail position and planform show more linear pitching-moment-coefficient variations at low lift coefficient throughout the sweep range investigated.

CONCLUDING REMARKS

Subsonic and supersonic wind-tunnel tests which were conducted on a model of a lightweight, multipurpose airplane configuration having variable-sweep wings and externally mounted engines indicated a trimmed maximum lift-drag ratio (at model Reynolds numbers) of 14.3 at a Mach number of 0.60 with a wing sweep of 25°. At supersonic speeds the highest values of maximum lift-drag ratio were found for the configuration having the wings swept back 75°. The lowest values of zero lift drag (for increased range at low altitudes and high speeds) occur with the wing swept back 90°. However, reducing the sweep angle to 75° results in only a very slight increase in zero-lift drag coefficient at transonic speeds. The wave drag at a Mach number of 1.2 was considerably less for the present configuration than for that of NASA TM X-734 as a result of the improvement in the area distribution and reduction of maximum cross section.

With regard to the longitudinal stability characteristics at a Mach number of 0.60, increasing the wing sweep from 25° to 75° results in only a slight difference in the aerodynamic-center location; however, a rearward aerodynamic-center movement of 22.5 percent mean aerodynamic chord accompanies an increase in Mach number from 0.85 to 2.50 for the 75° sweep position.

Notching the outboard wing panels provided more linear pitching-moment variation with lift at high lift coefficients for sweep angles up to 45° at a Mach number of 0.28.

Langley Research Center,
National Aeronautics and Space Administration,
Langley Station, Hampton, Va., May 8, 1963.

REFERENCES

1. Spencer, Bernard, Jr.: Stability and Control Characteristics at Low Subsonic Speeds of an Airplane Configuration Having Two Types of Variable-Sweep Wings. NASA TM X-303, 1960.

2. Taylor, Robert T., Alford, William J., Jr., and Phillips, W. Pelham: Preliminary Investigation of Subsonic and Transonic Longitudinal Aerodynamic Characteristics of a Variable-Sweep Airplane Configuration Having Externally Mounted Engines. NASA TM X-734, 1962.

3. Foster, Gerald V., and Spearman, M. Leroy: Aerodynamic Characteristics at a Mach Number of 2.01 of a Variable-Sweep Airplane Configuration With Body-Mounted Podded Engines and Having an Equivalent-Body Fineness Ratio of 9.8. NASA TM X-687, 1962.

TABLE I.- AIRFOIL COORDINATES FOR OUTBOARD-WING PANELS

[Streamwise in $\Lambda_{LE} = 25^{\circ}$ position]

Ordinate, percent chord	Upper surface, percent chord	Lower surface, percent chord
0	0	0
1.128	1.380	-1.045
2.337	1.977	-1.420
4.794	2.829	-1.750
7.273	3.471	-1.800
9.768	3.987	-1.767
14.778	4.776	-1.673
19.809	5.320	-1.580
24.852	5.677	-1.485
29.900	5.875	-1.391
40.000	5.869	-1.202
50.039	5.473	-1.019
60.068	4.820	-.830
70.081	3.942	-.642
80.078	2.858	-.455
90.054	1.575	-.268
95.033	.855	-.177
100.000	.084	-.084
L.E. radius: 0.70 percent chord		

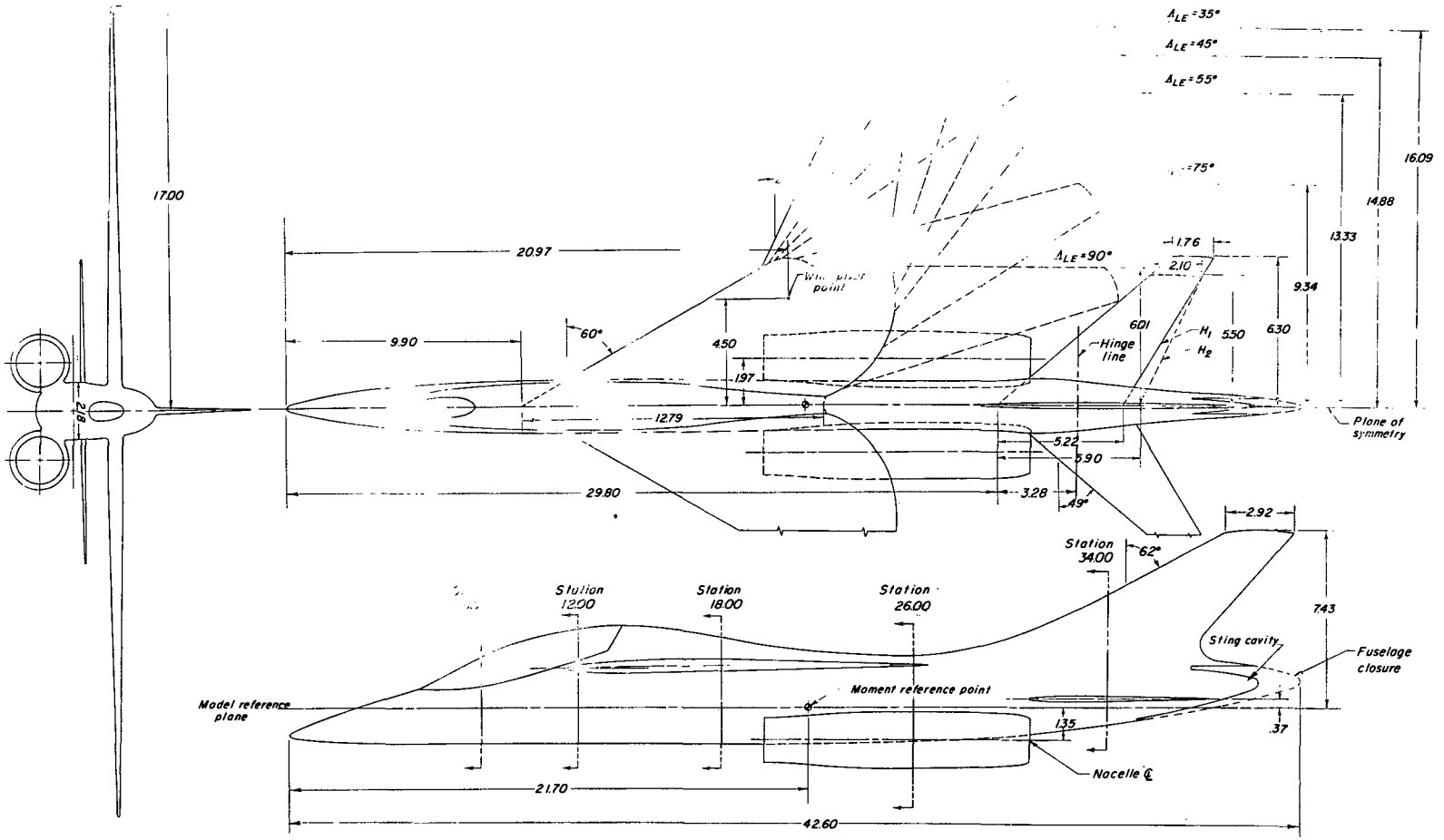

(a) Three-view drawing.

Figure 1.- Details of the configuration model. All linear dimensions are in inches.

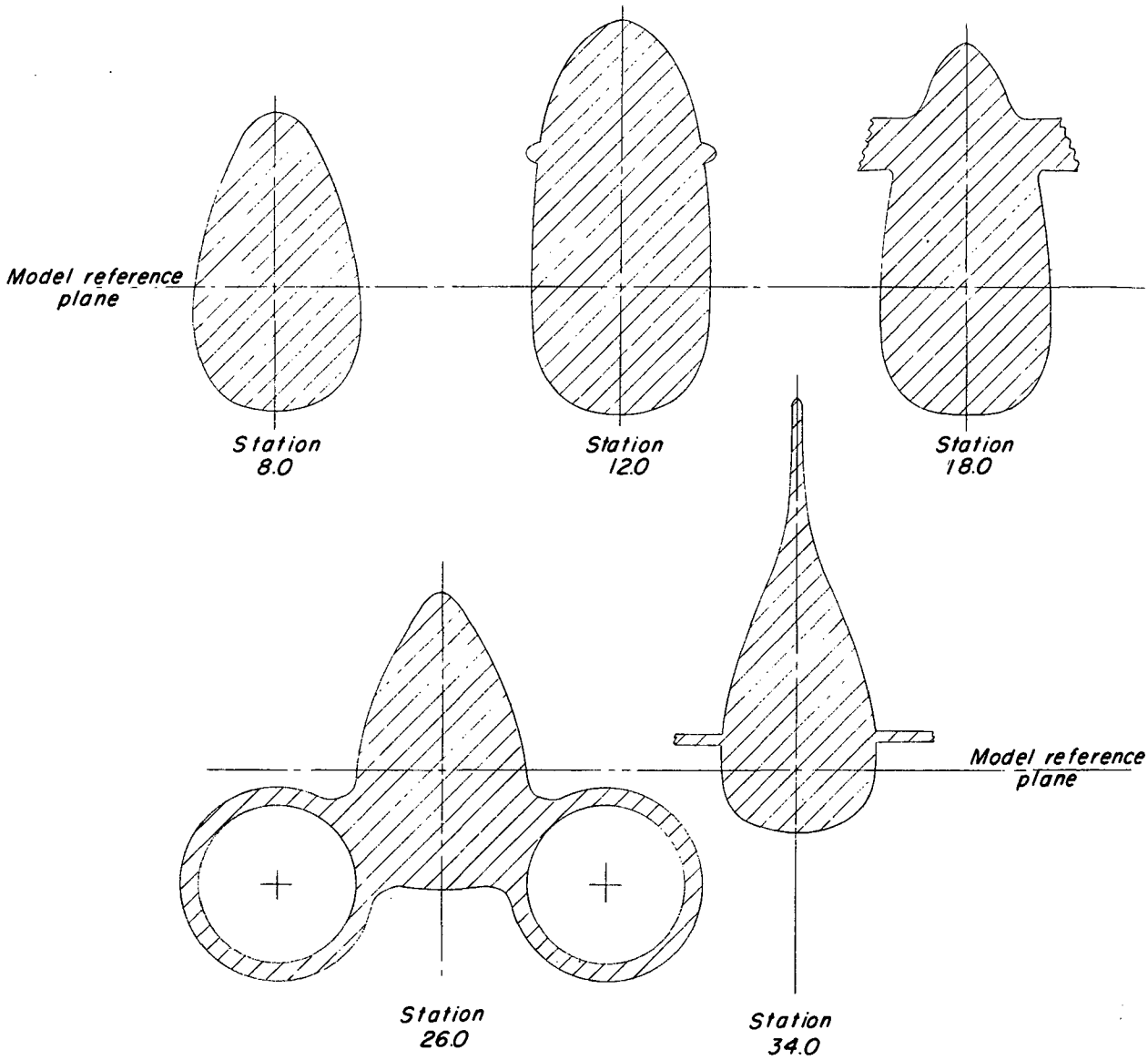

(b) Fuselage cross sections at stations specified in inches from the nose.

Figure 1.- Continued.

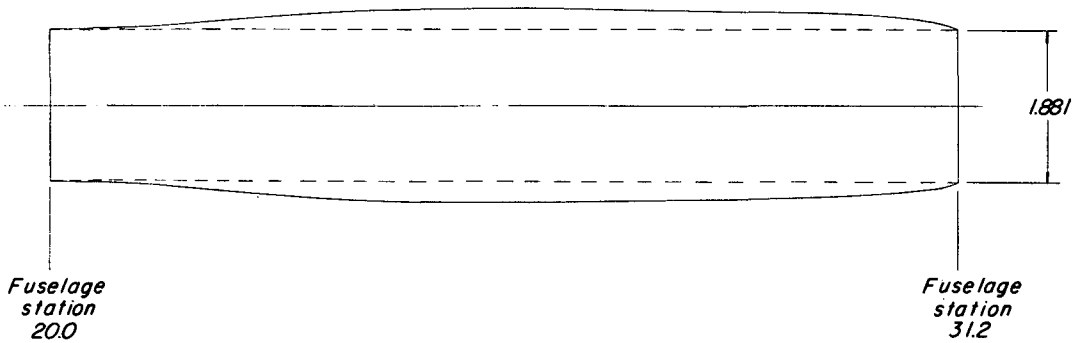

Nacelle coordinates	
Fuselage station, in.	Outside diam. in.
20.0	1.881
21.0	1.915
22.0	2.077
23.0	2.226
24.0	2.334
25.0	2.362
26.0	2.362
27.0	2.351
28.0	2.323
29.0	2.285
30.0	2.214
31.0	2.044
31.2	1.881
Inside diameter=1.881 in.	

(c) Engine nacelles.

Figure 1.- Continued.

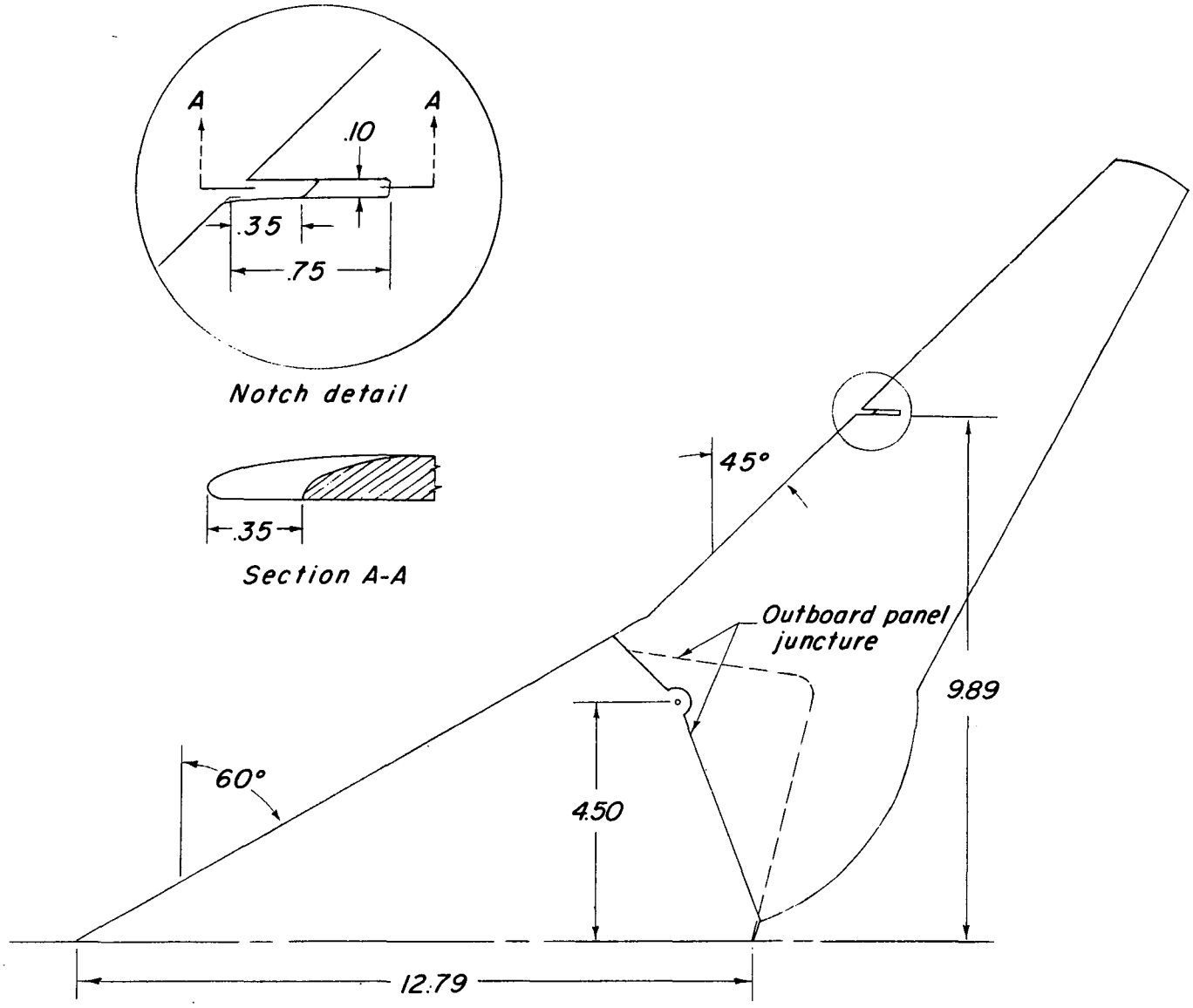

(d) Wing panel characteristics.

Figure 1.- Concluded.

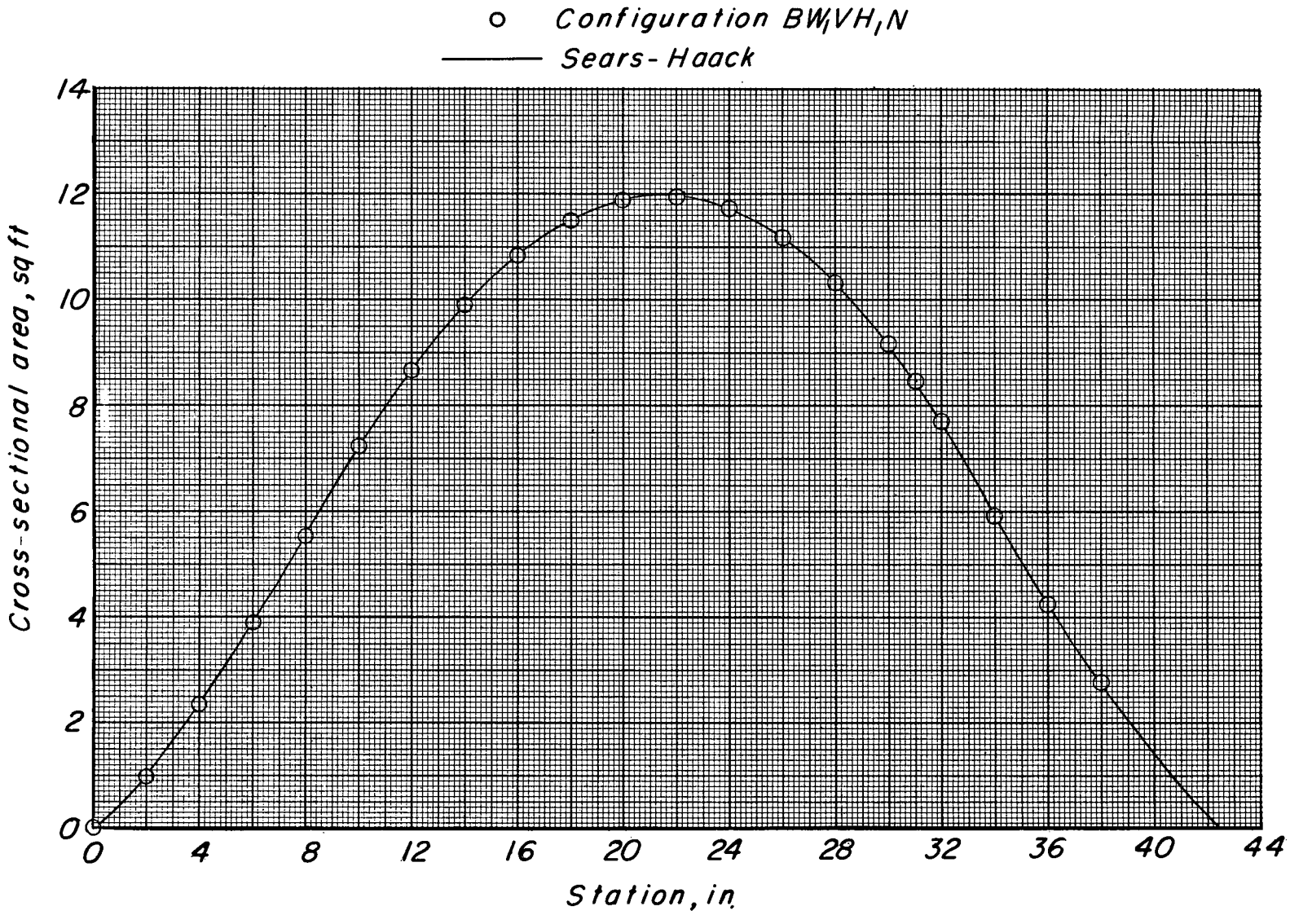

Figure 2.- Cross-sectional-area diagram of configuration $BWVH_1N$ with $\Lambda_{LE} = 90^{\circ}$ (excluding duct area) and a Sears-Haack body.

CONFIDENTIAL

Reproduced from best available copy.

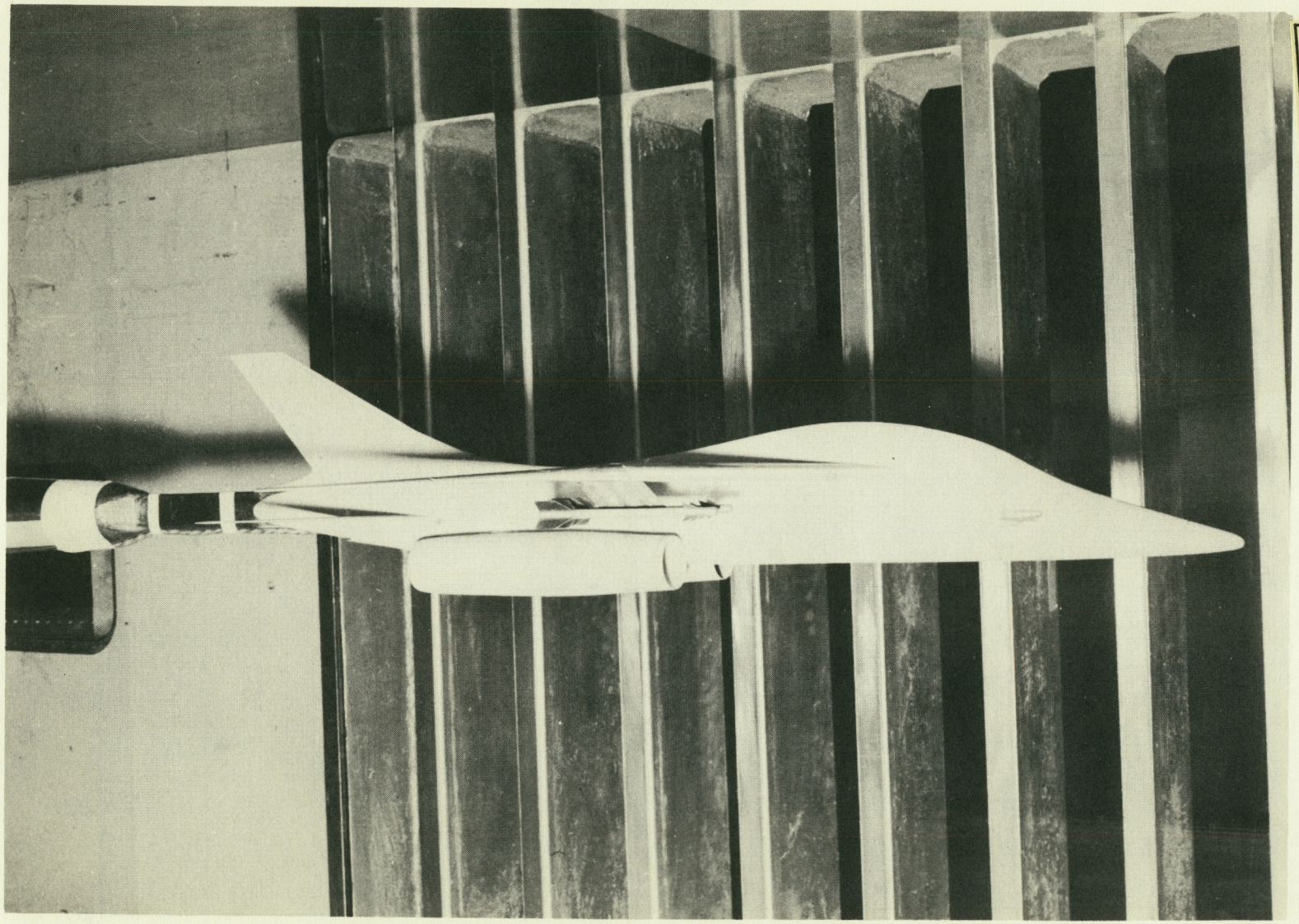

(a) Side view. L-62-1199

Figure 3.- Photographs of configuration BW_1VH_1N having two GAR-8 stores mounted at each wing-pivot point $\left(\Lambda_{LE} = 75^{\circ}\right)$.

CONFIDENTIAL

Reproduced from best available copy.

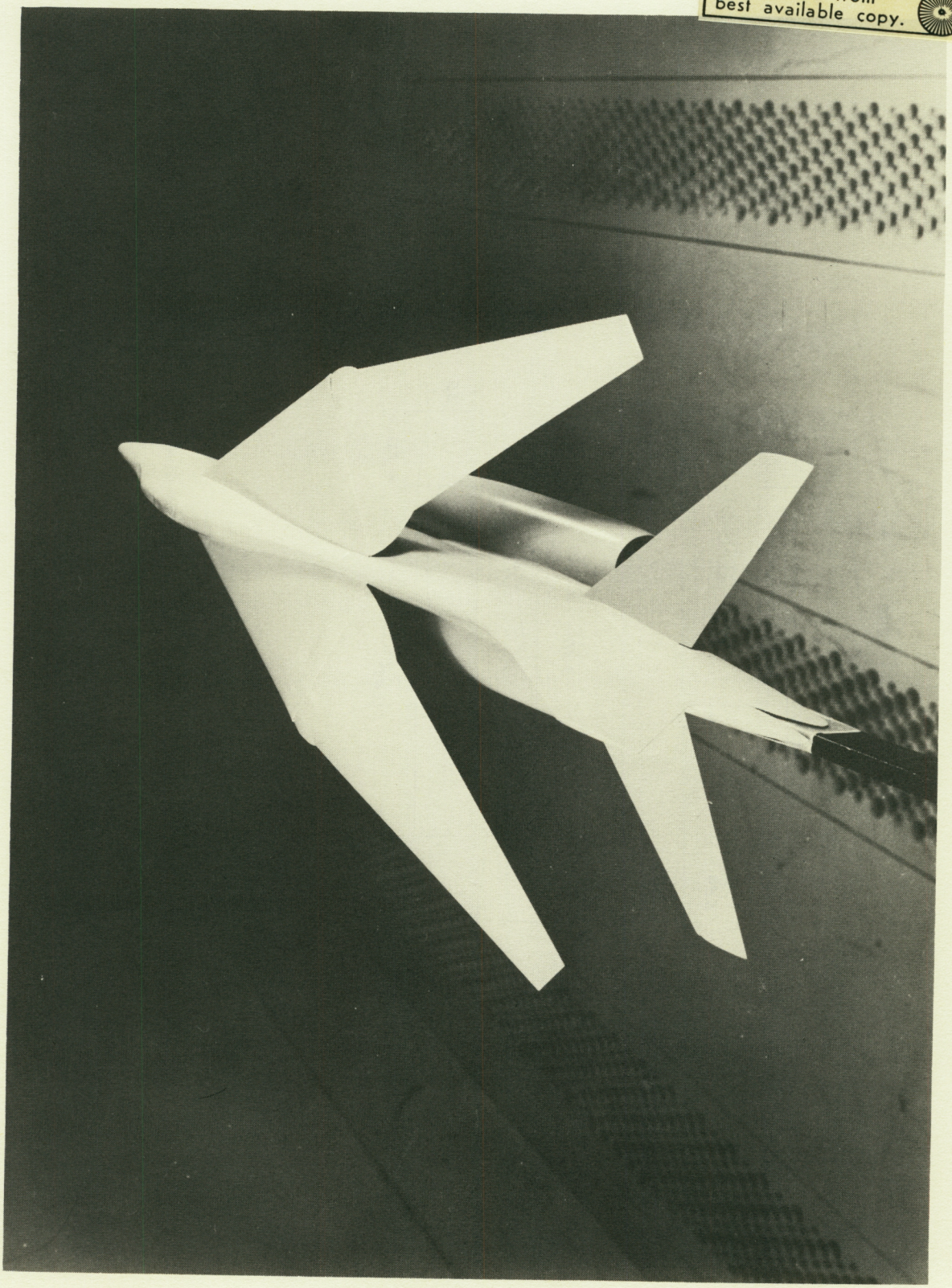

L-61-7588

(b) Three-quarter rear view.

Figure 3.- Concluded.

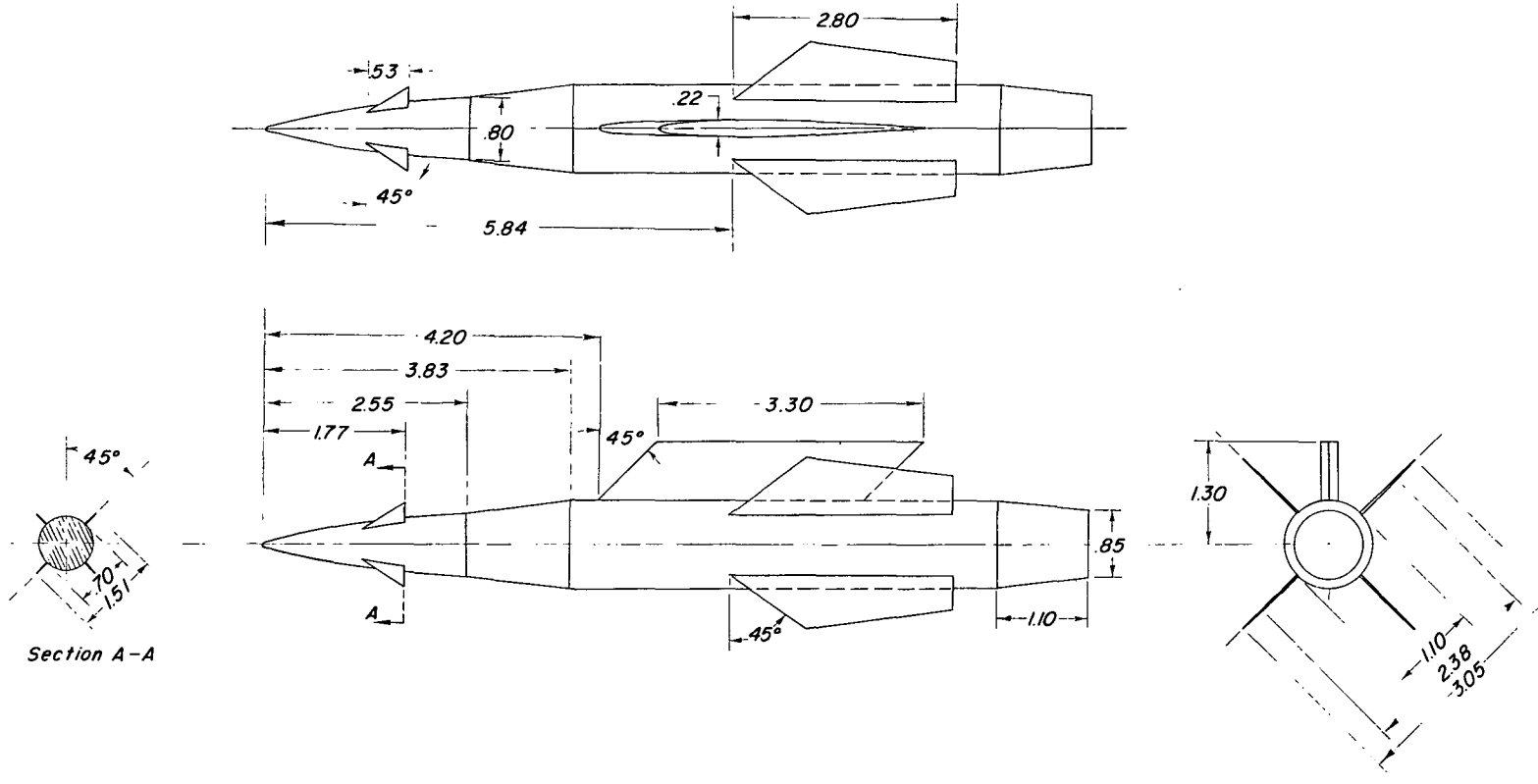

(a) ASM-N-7B (Bullpup B) stores.

Figure 4.- Three-view drawings of external stores. All linear dimenions are in inches.

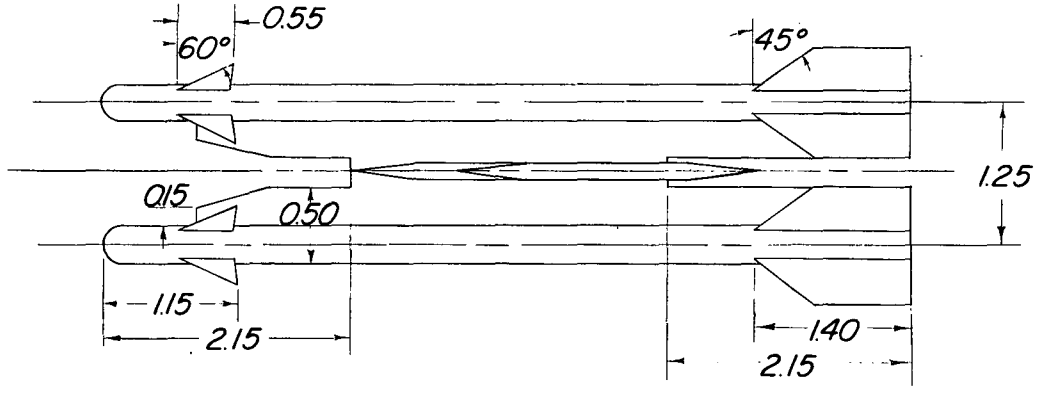

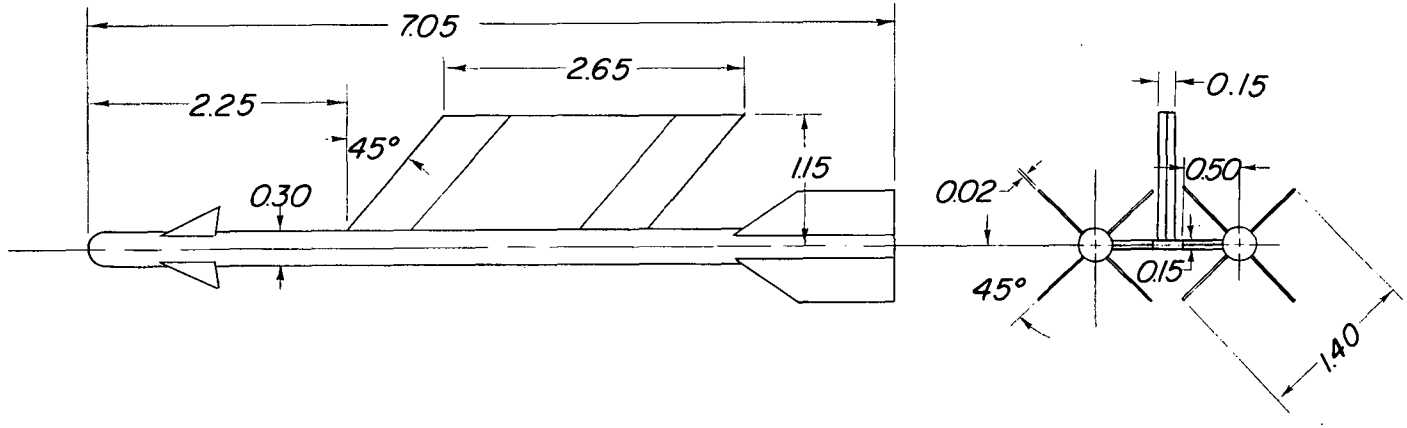

(b) GAR-8 (Sidewinder) stores.

Figure 4.- Concluded.

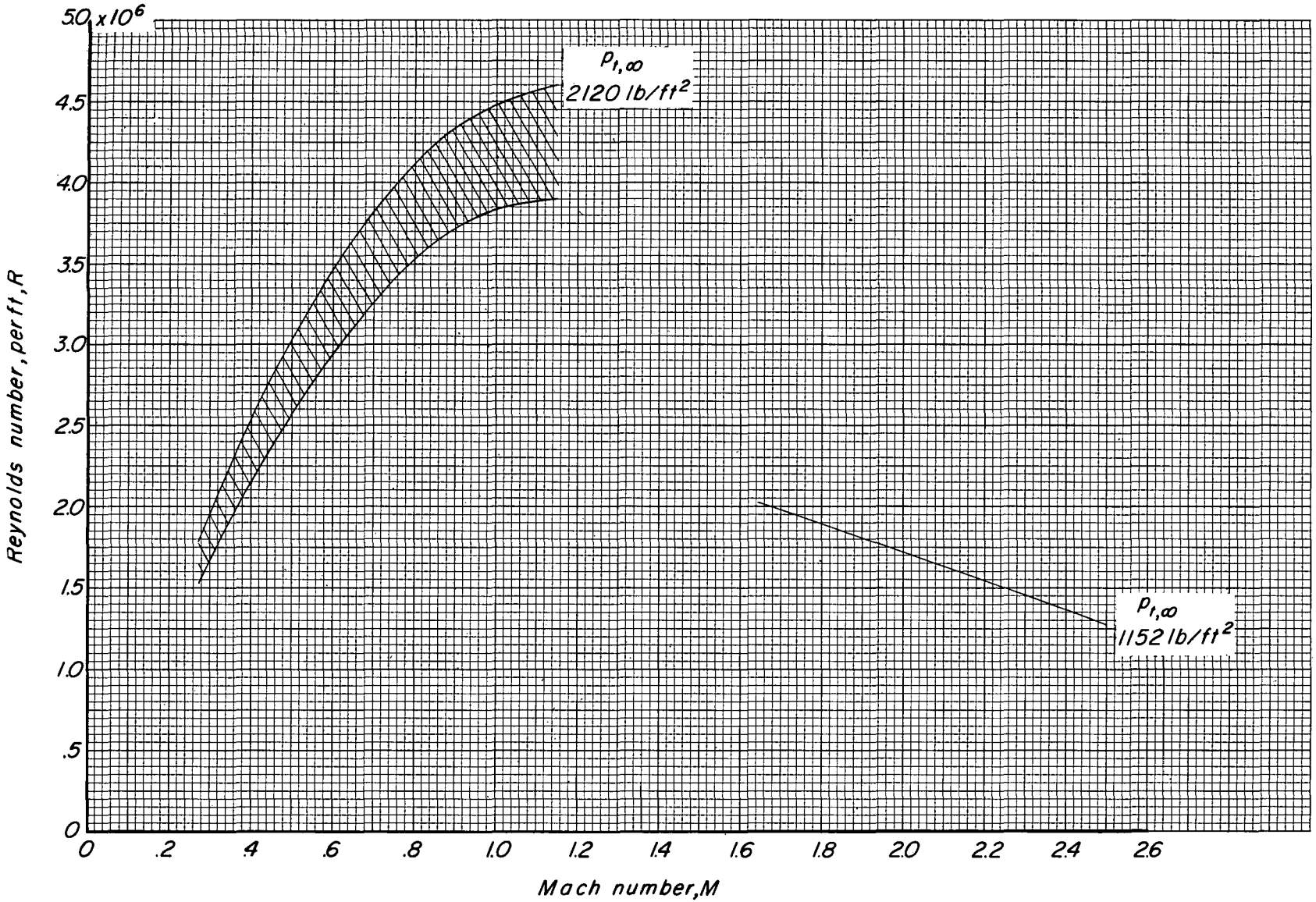

Figure 5.- Reynolds number (based on a reference length of 1 foot) variation with Mach number.

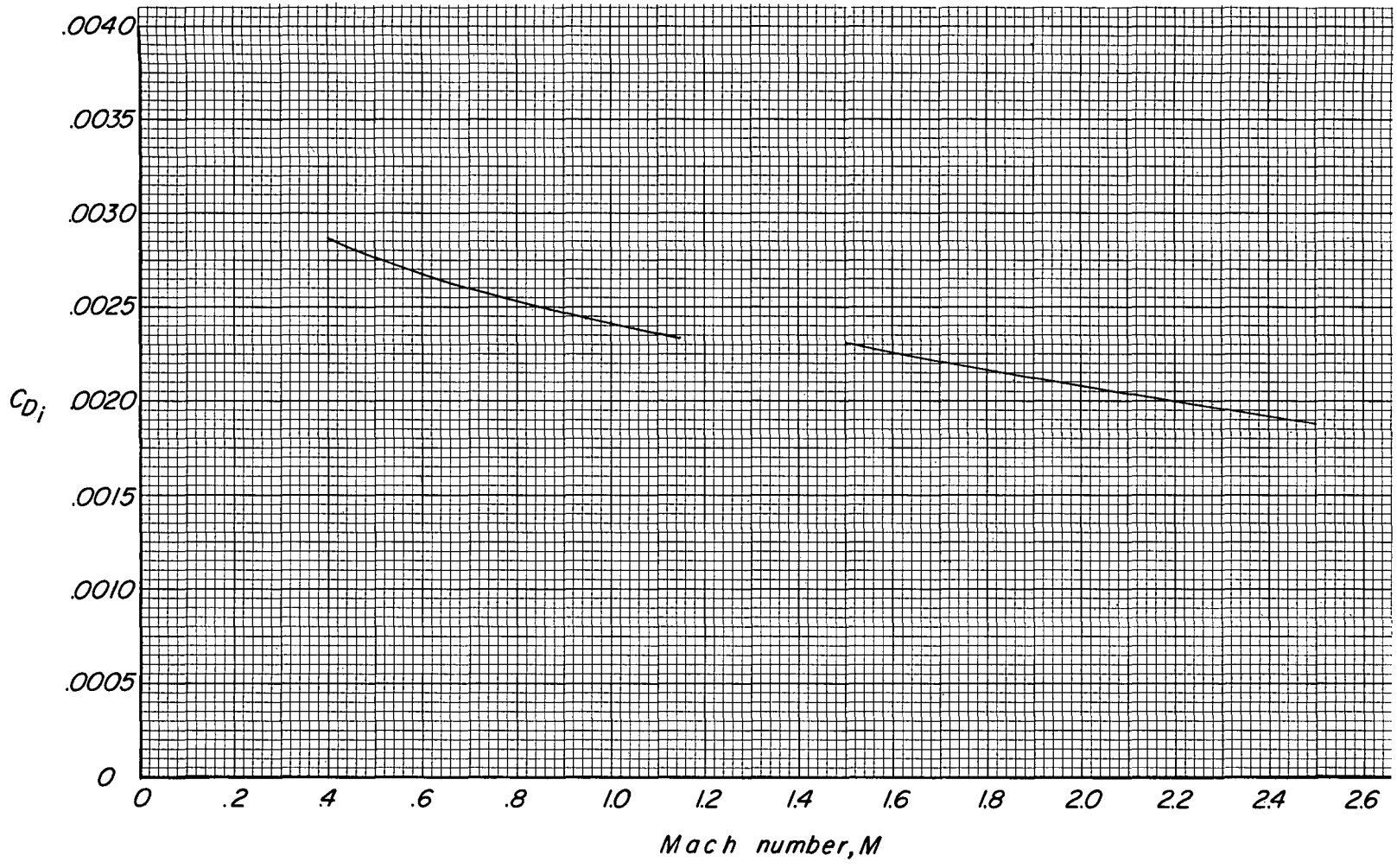

Figure 6.- Computed values for internal drag coefficient of nacelles as a function of Mach number.

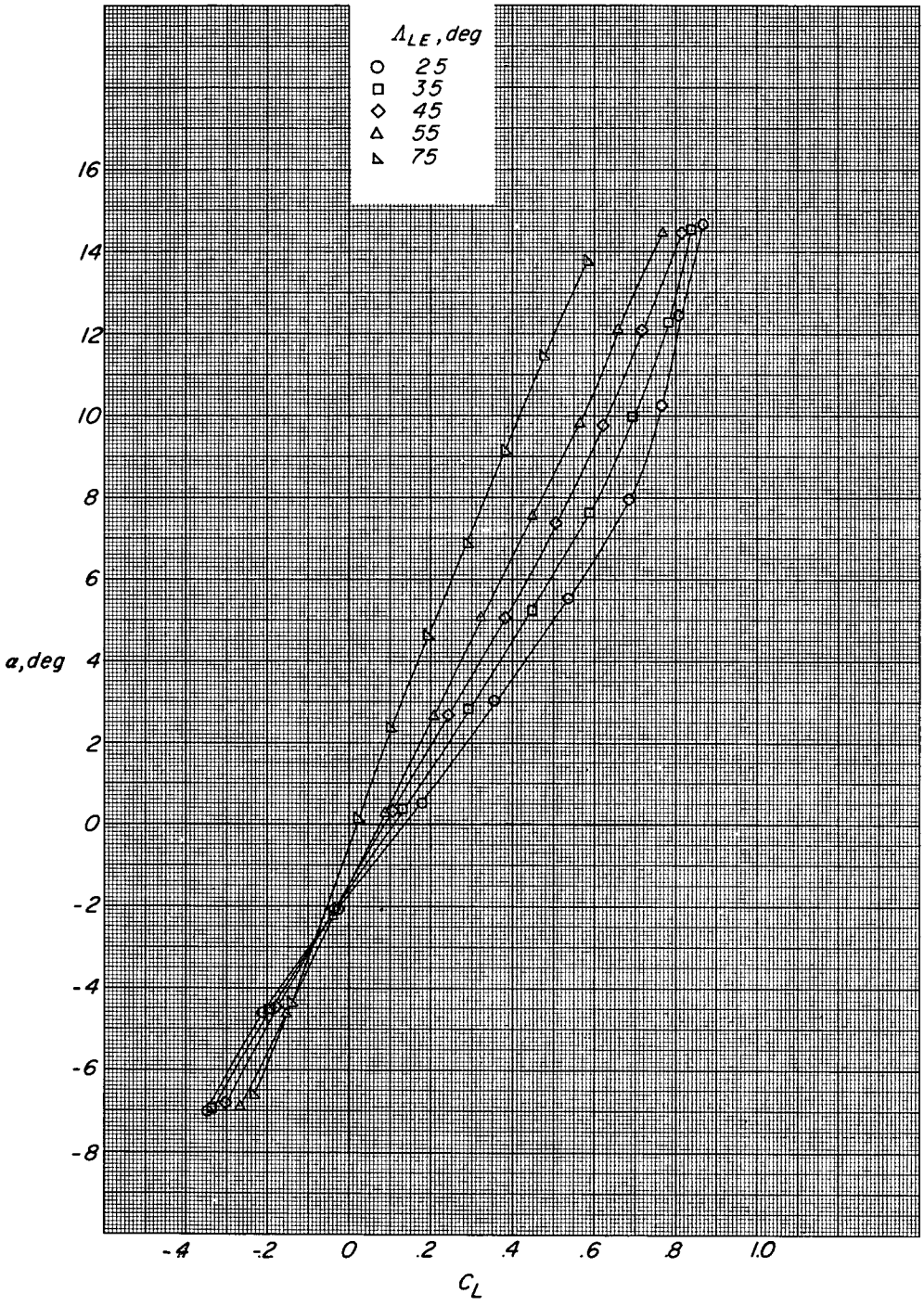

(a) Angle of attack.

Figure 7.- The effect of wing sweep on the aerodynamic characteristics for configuration BW_1VN at M = 0.6.

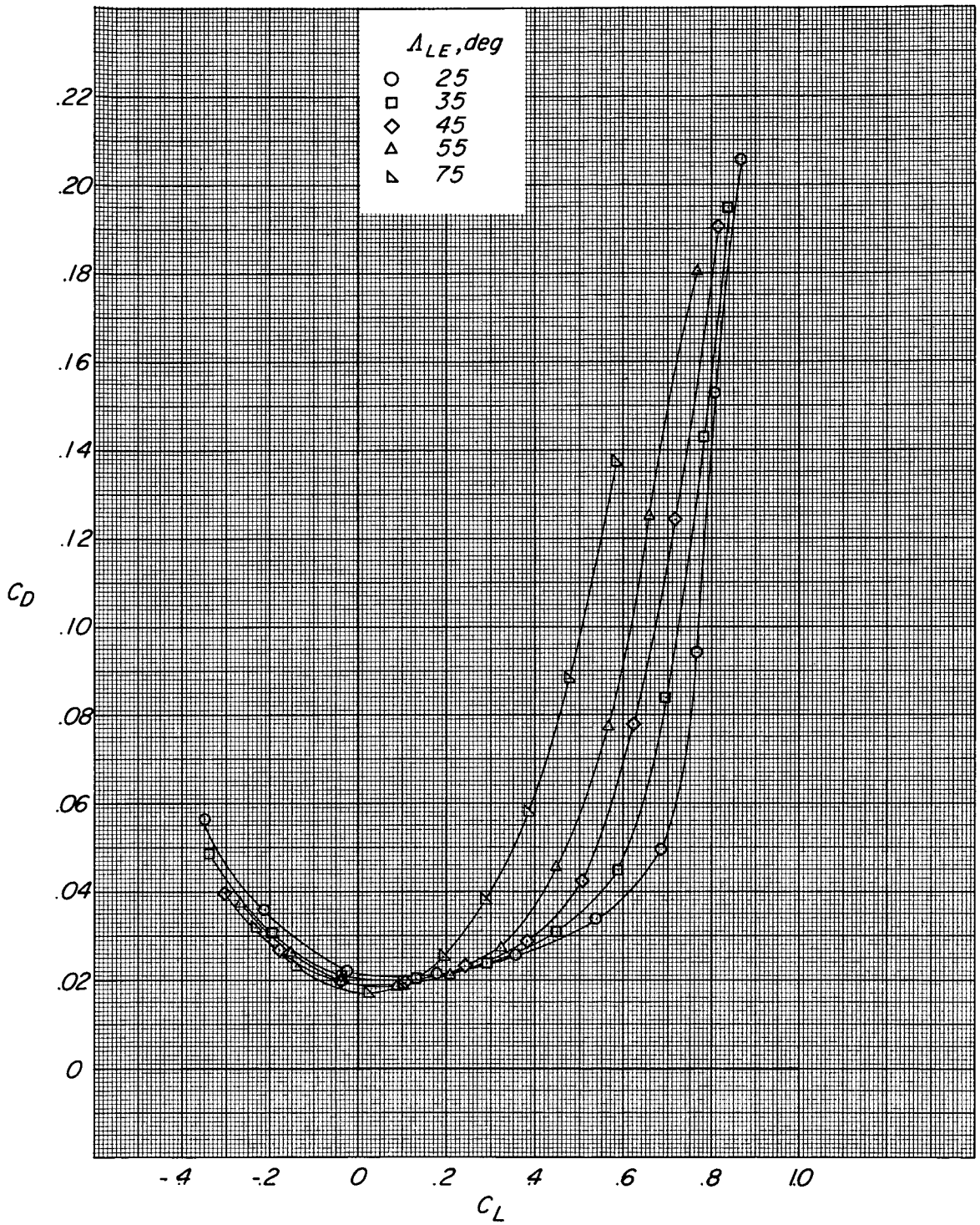

(b) Drag coefficient.

Figure 7.- Continued.

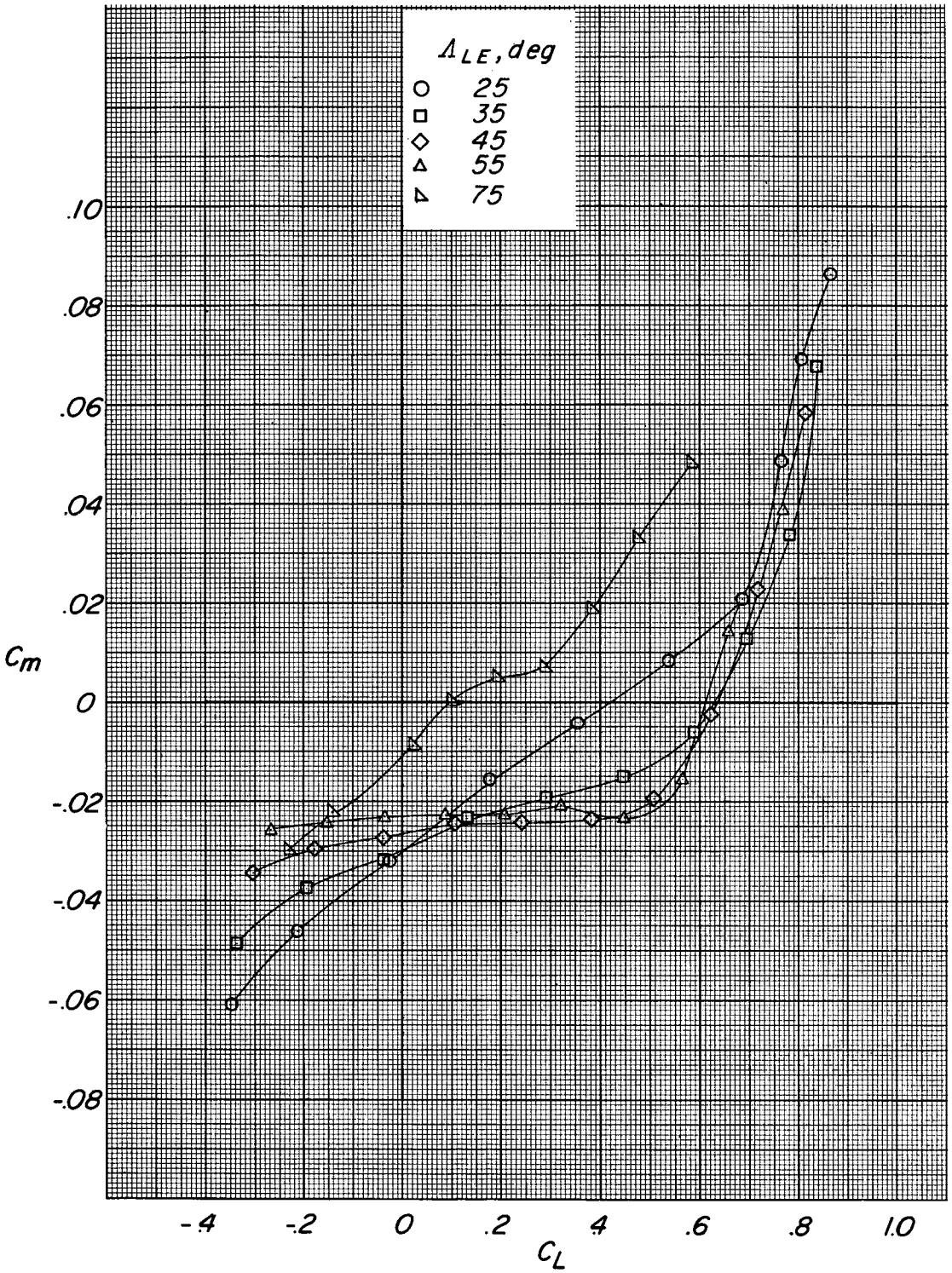

(c) Pitching-moment coefficient.

Figure 7.- Concluded.

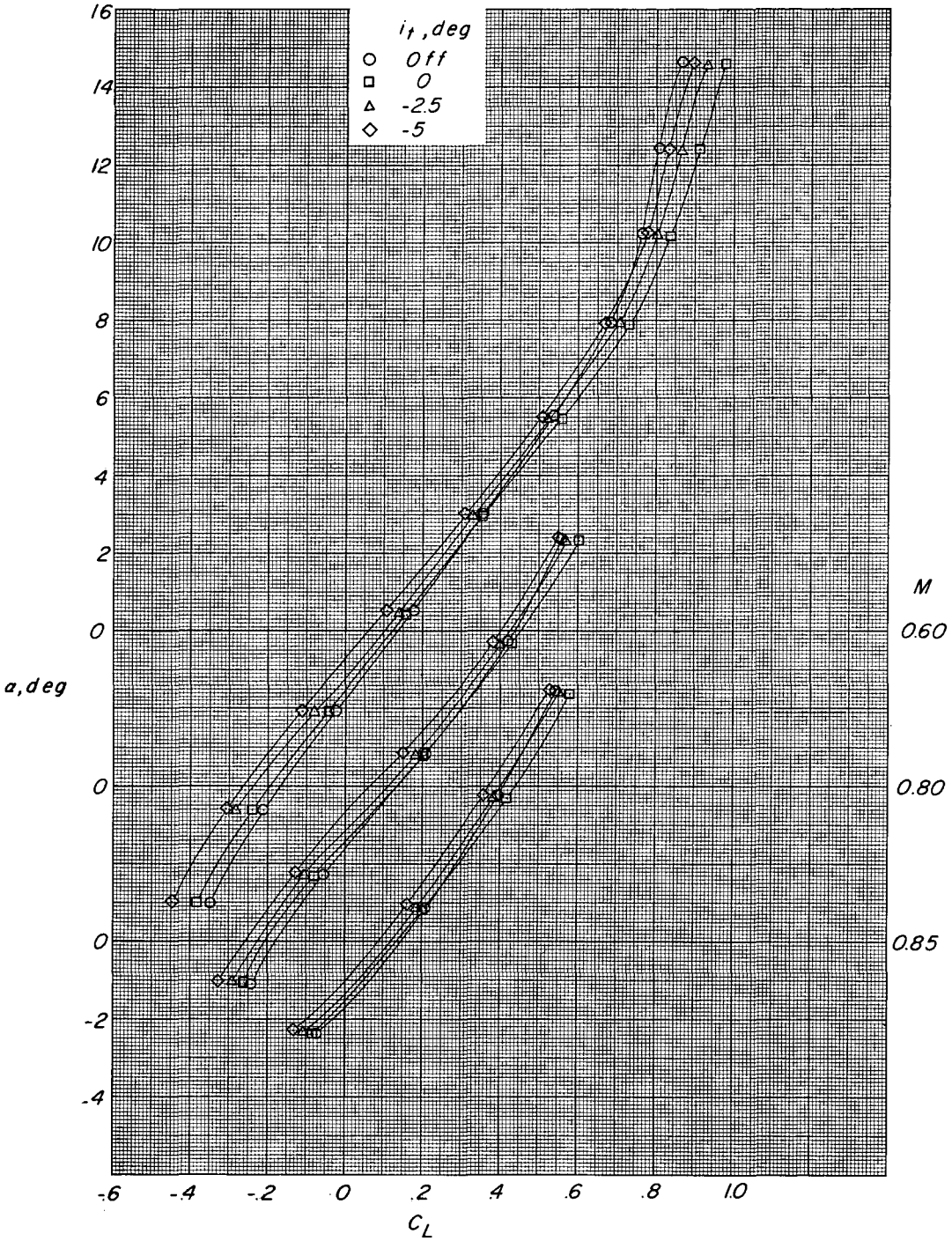

(a) Angle of attack.

Figure 8.- Aerodynamic characteristics for configuration BW_1VH_1N at $\Lambda_{LE} = 25^{\circ}$.

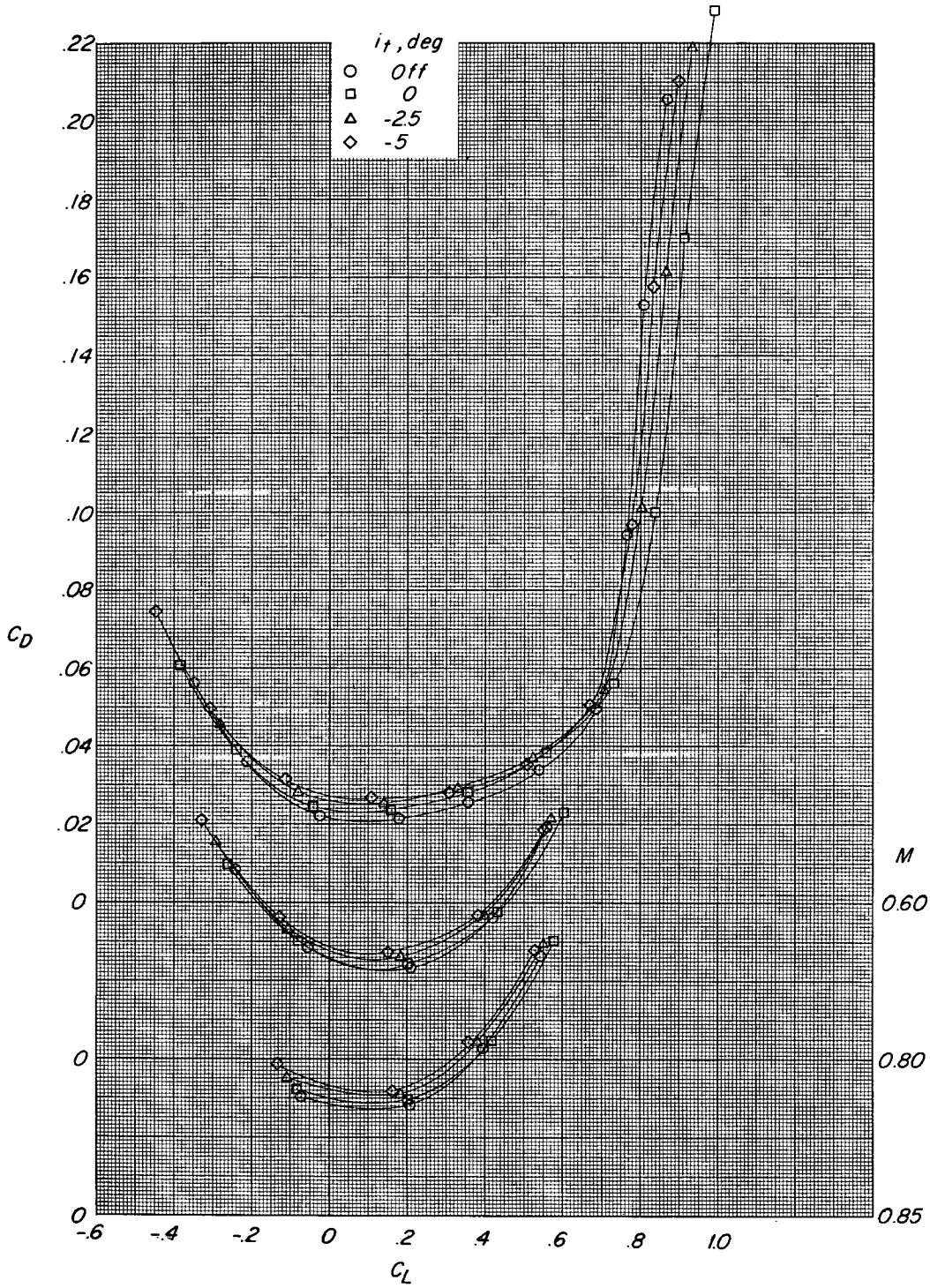

(b) Drag coefficient.

Figure 8.- Continued.

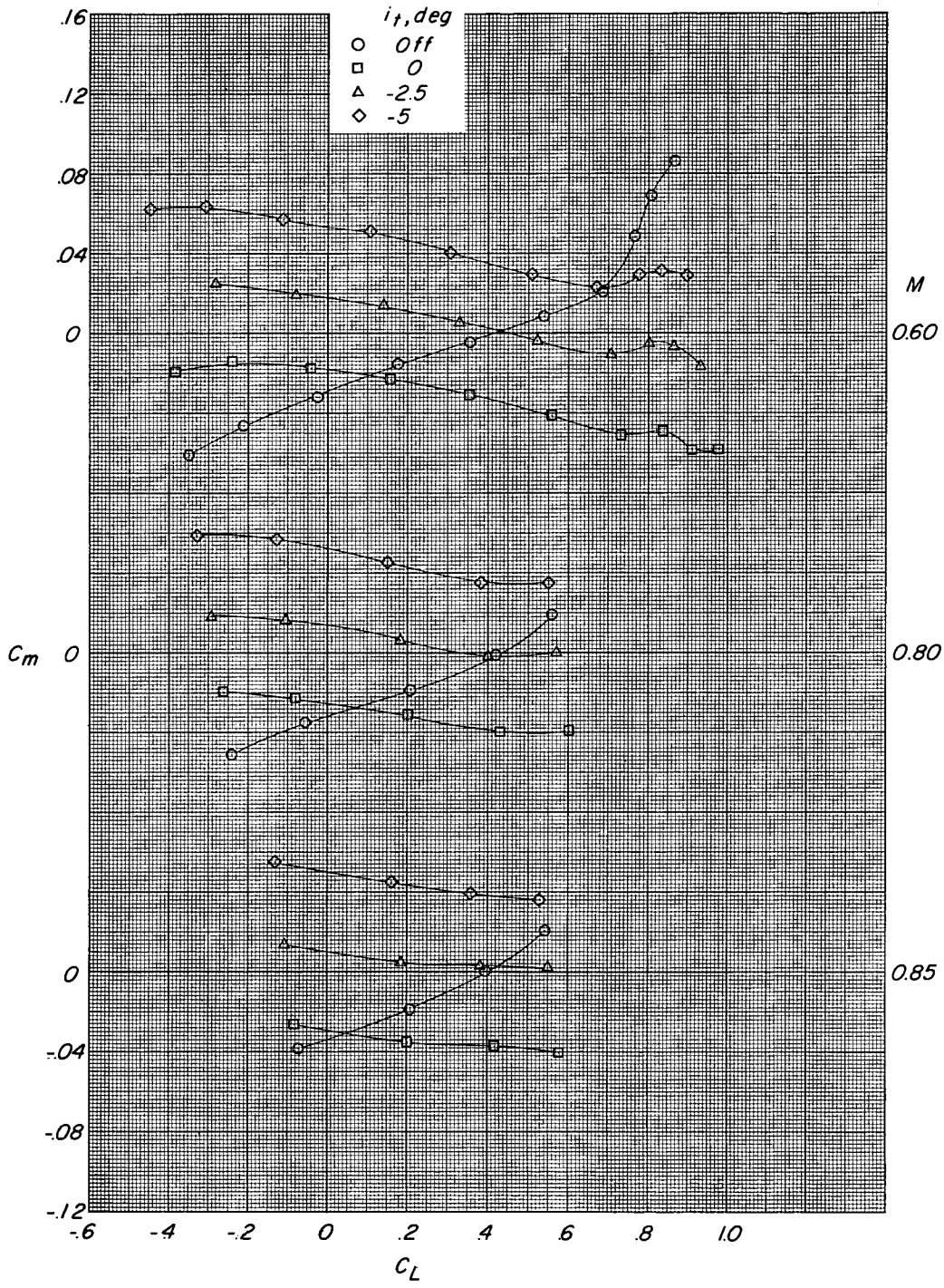

(c) Pitching-moment coefficient.

Figure 8.- Concluded.

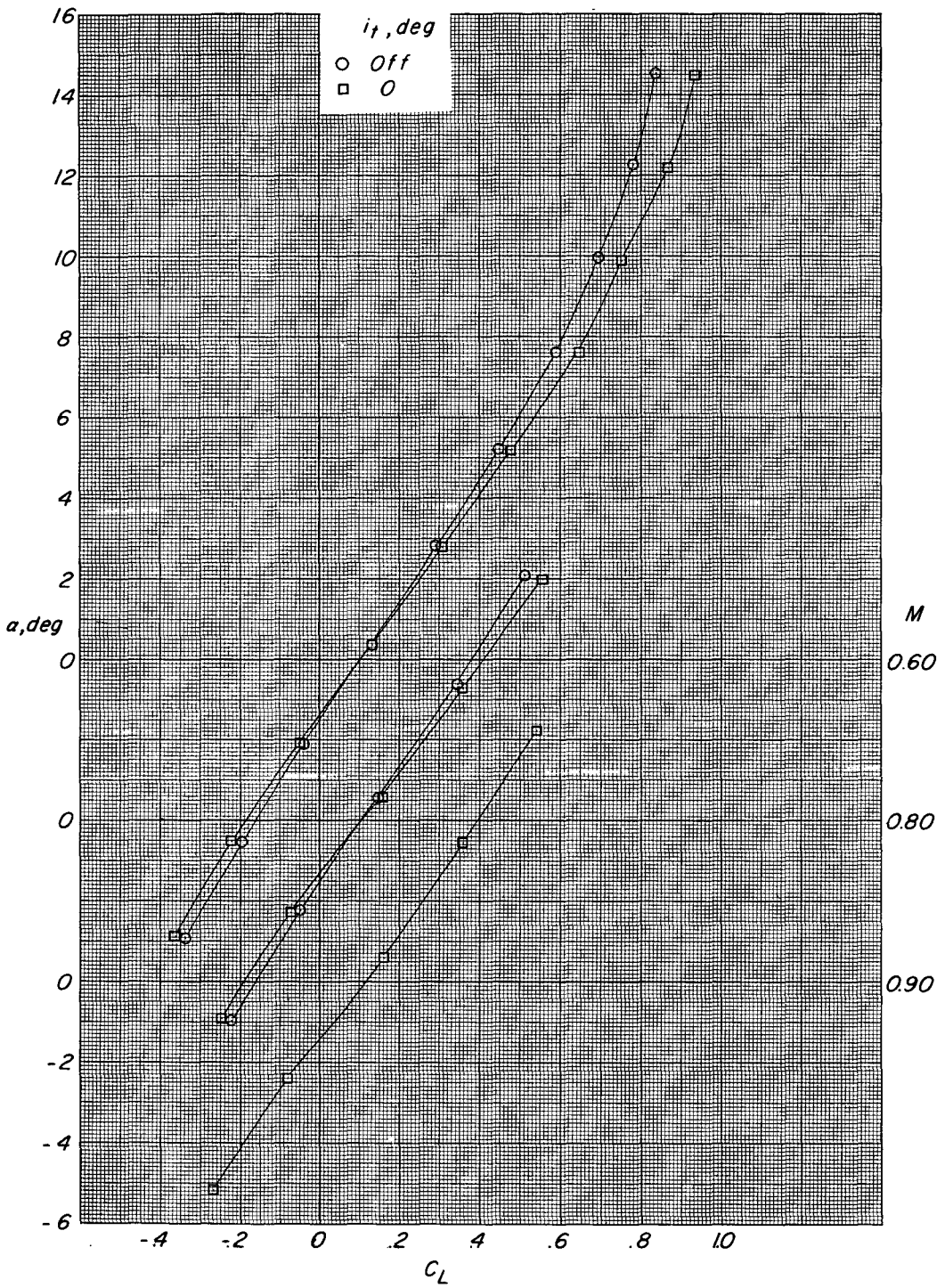

(a) Angle of attack.

Figure 9.- Aerodynamic characteristics for configuration BW_1VH_1N at $\Lambda_{LE} = 35^{\circ}$.

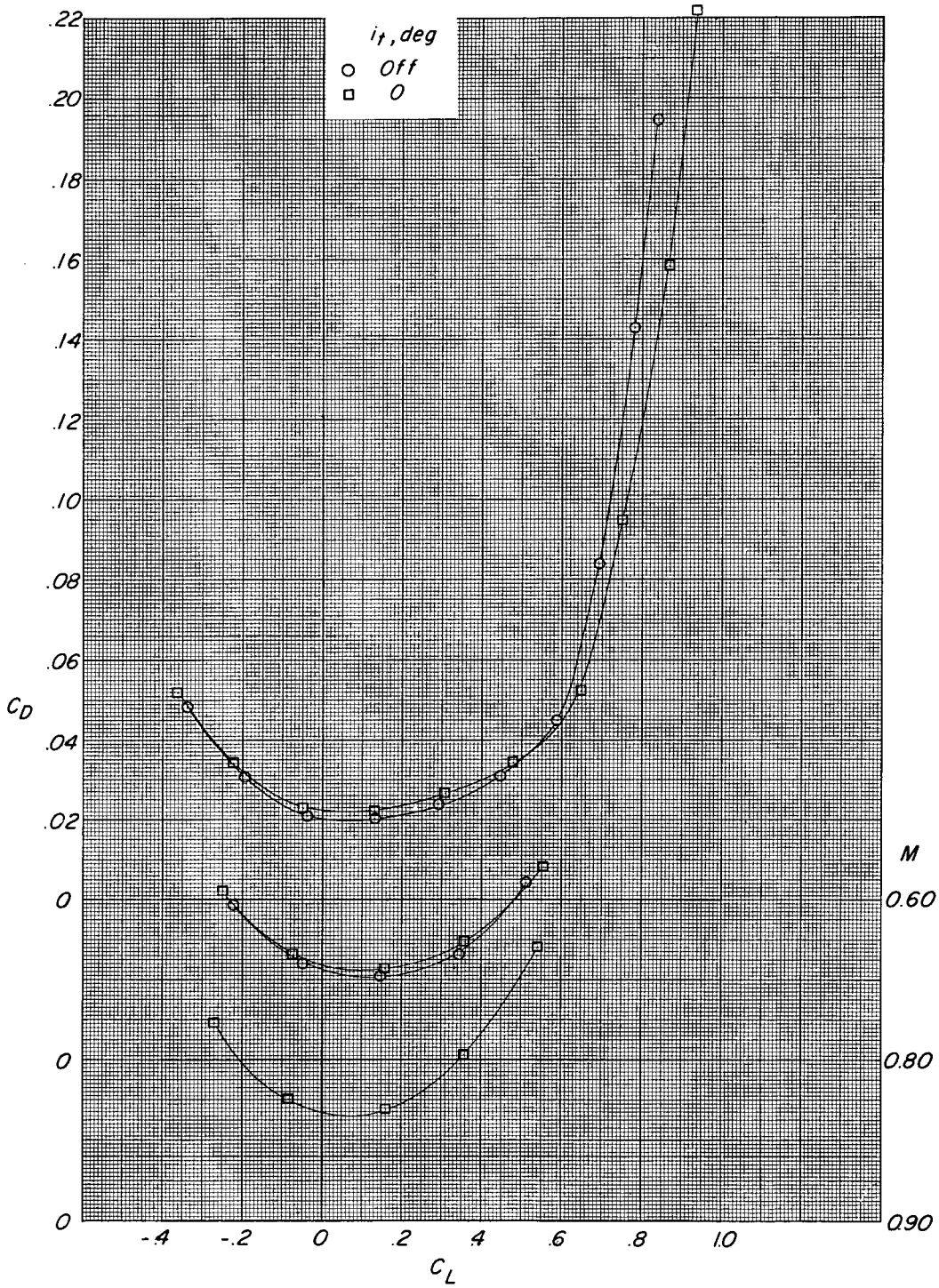

(b) Drag coefficient.

Figure 9.- Continued.

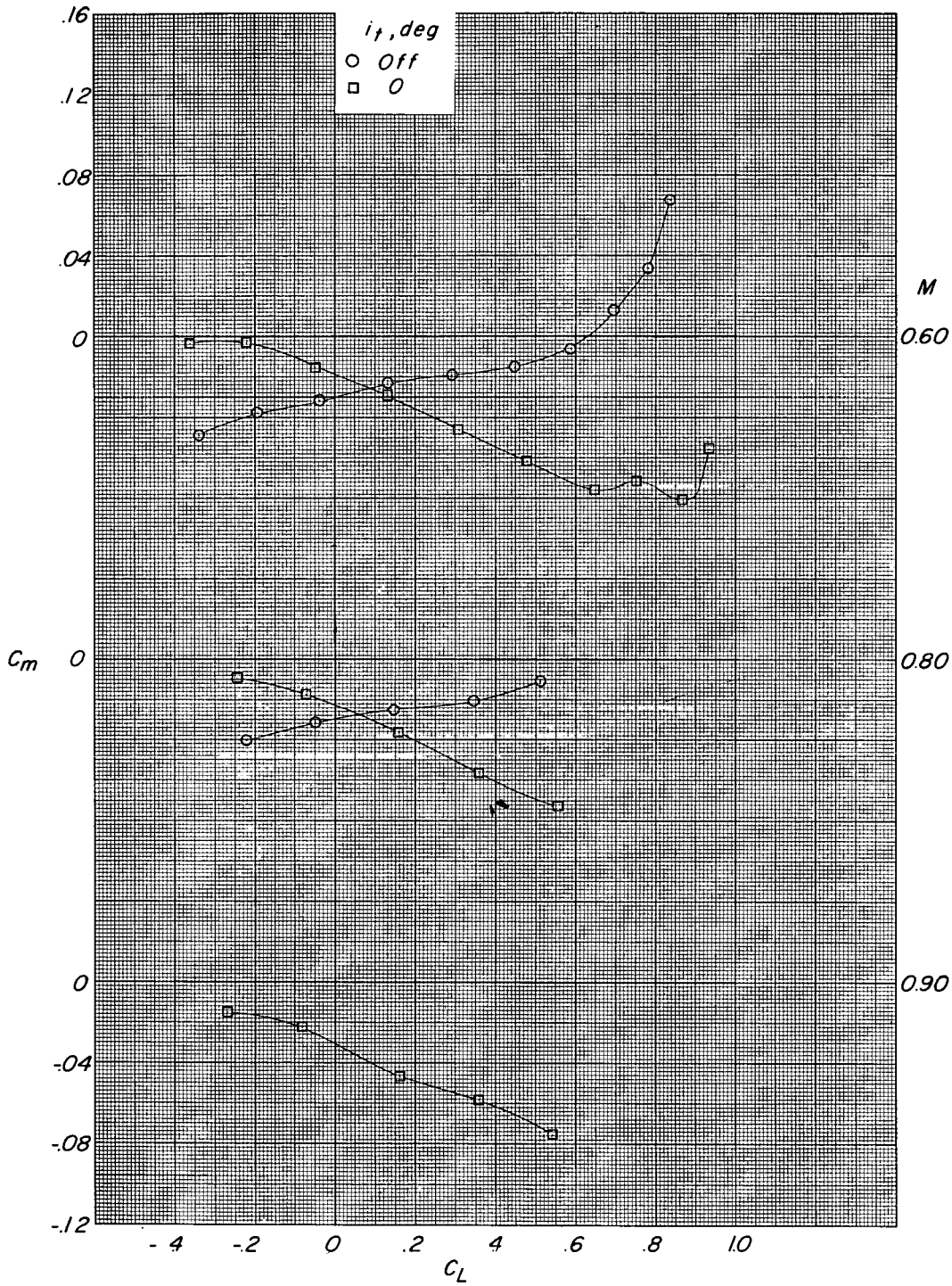

(c) Pitching-moment coefficient.

Figure 9.- Concluded.

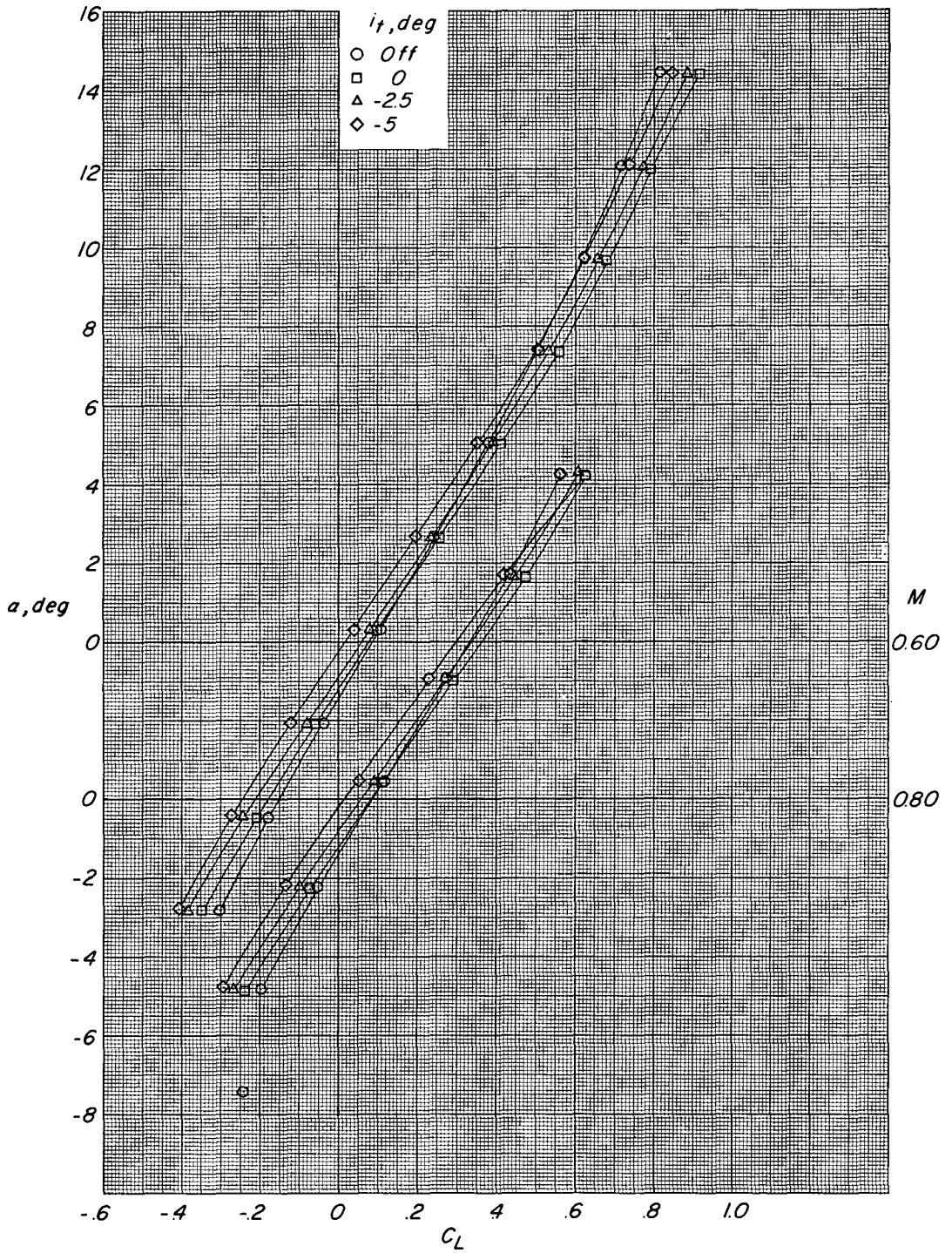

(a) Angle of attack.

Figure 10.- Aerodynamic characteristics for configuration $B_1W_1VH_1N$ at $\Lambda_{LE} = 45^{\circ}$.

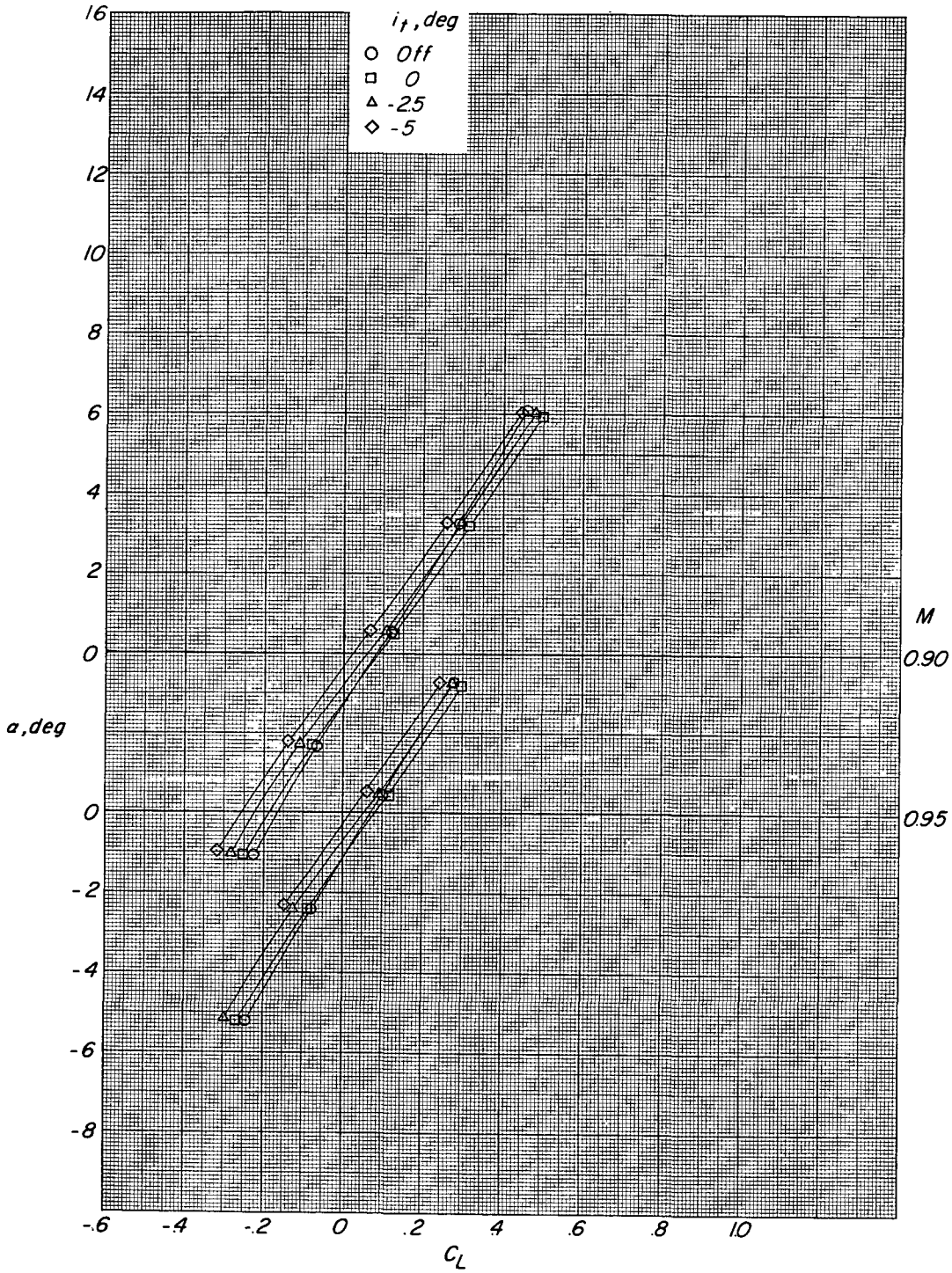

(a) Concluded.

Figure 10.- Continued.

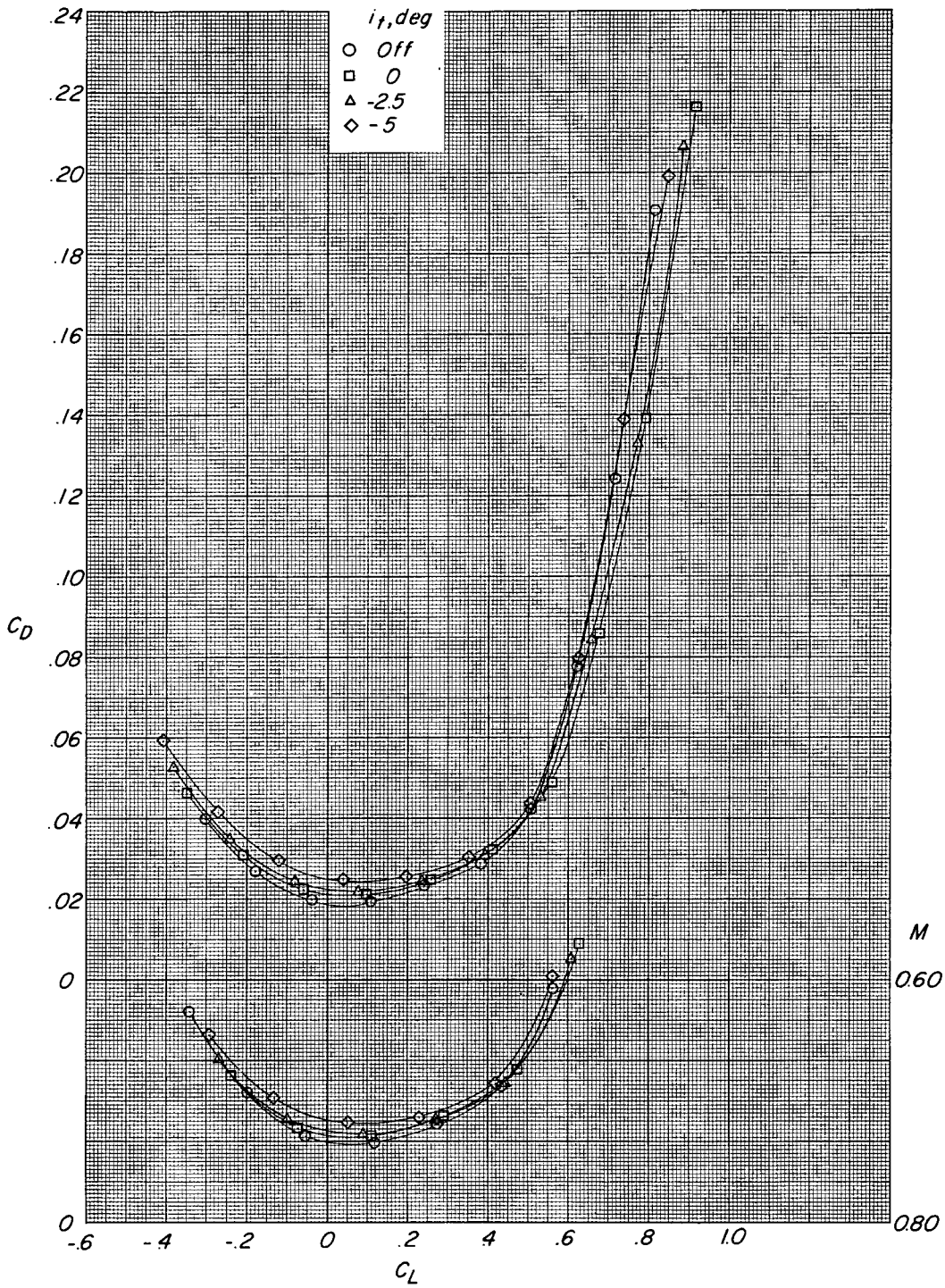

(b) Drag coefficient.

Figure 10.- Continued.

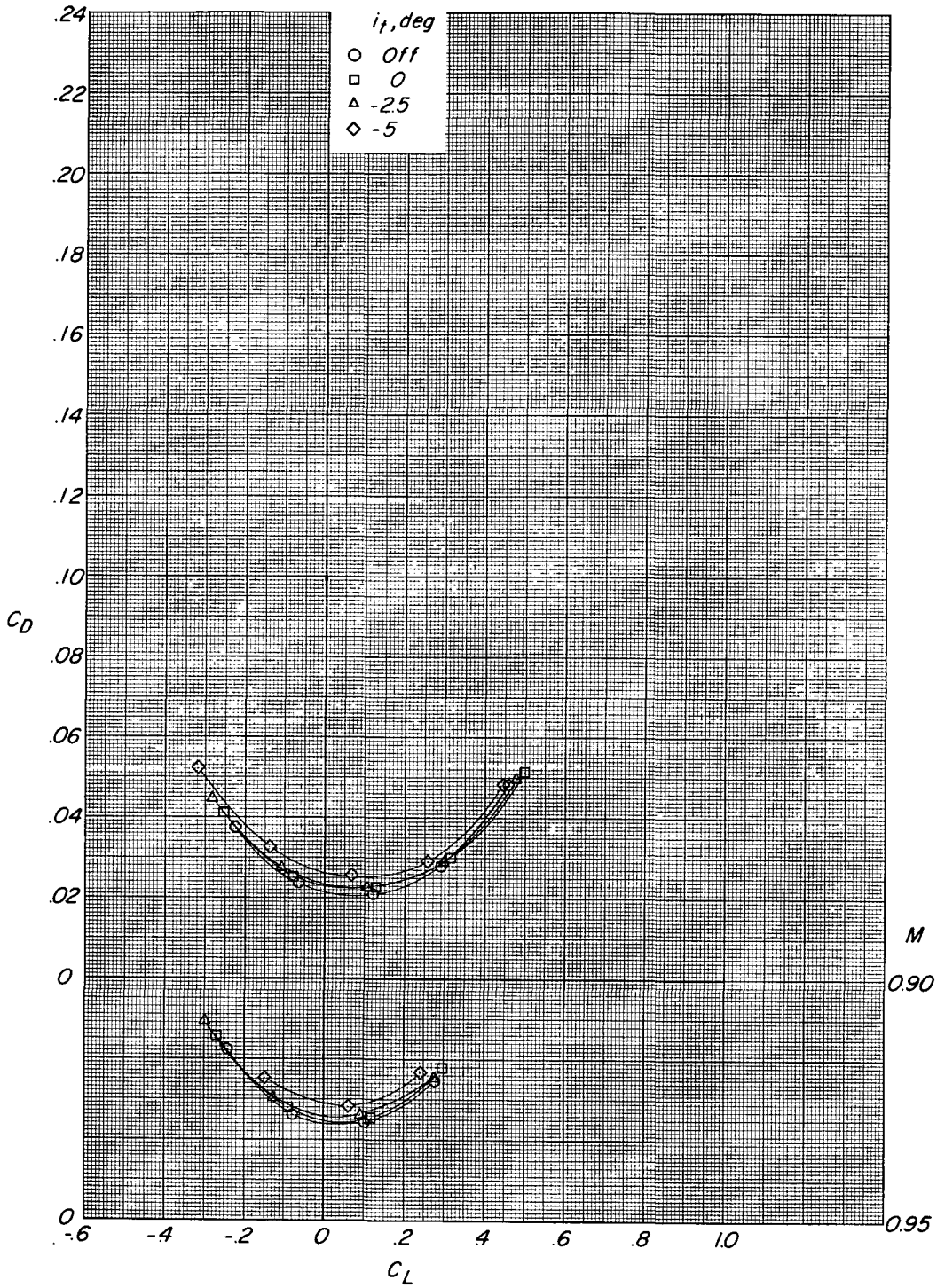

(b) Concluded.

Figure 10.- Continued.

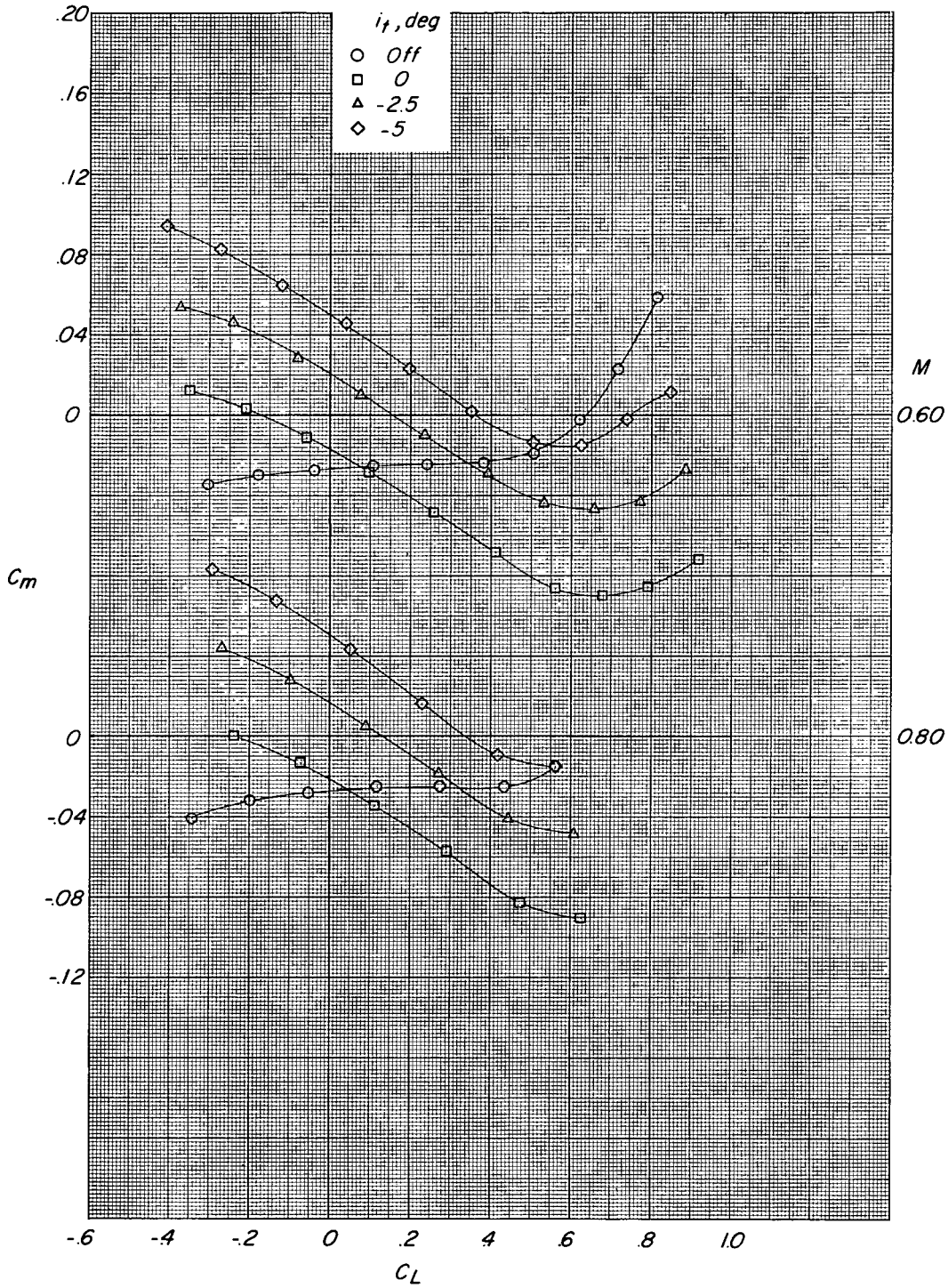

(c) Pitching-moment coefficient.

Figure 10.- Continued.

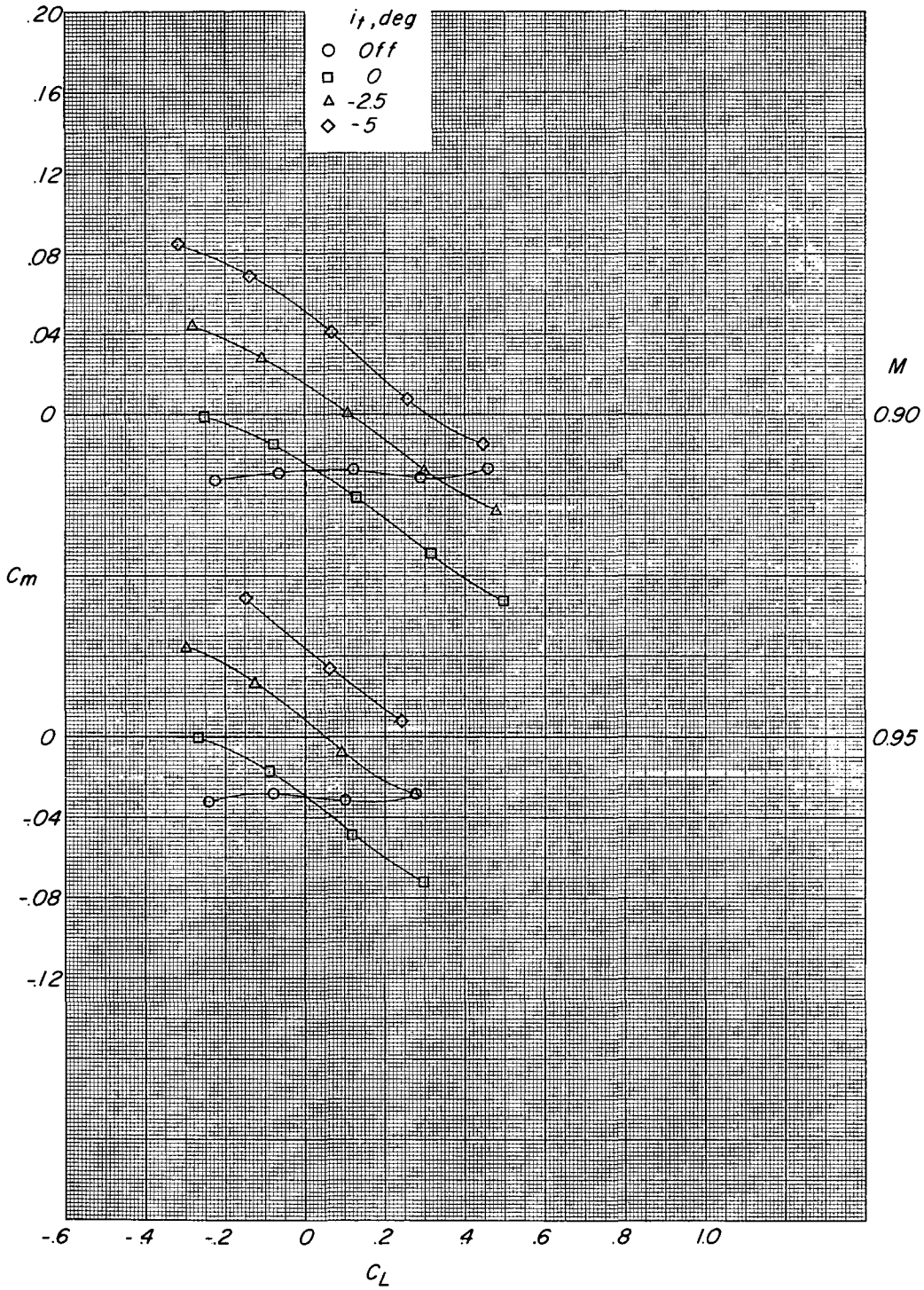

(c) Concluded.

Figure 10.- Concluded.

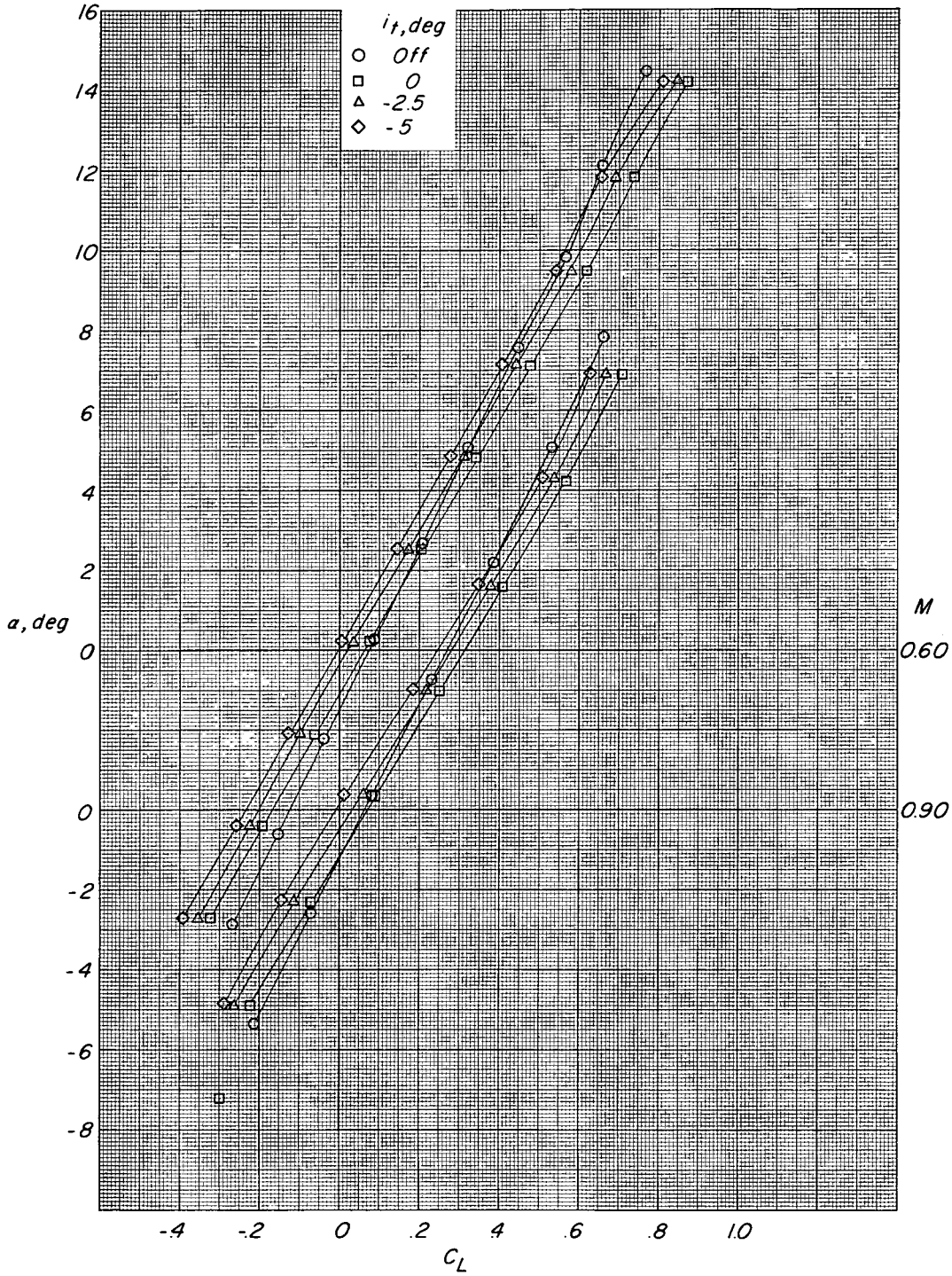

(a) Angle of attack.

Figure 11.- Aerodynamic characteristics for configuration BW_1VH_1N at $\Lambda_{LE} = 55^{\circ}$.

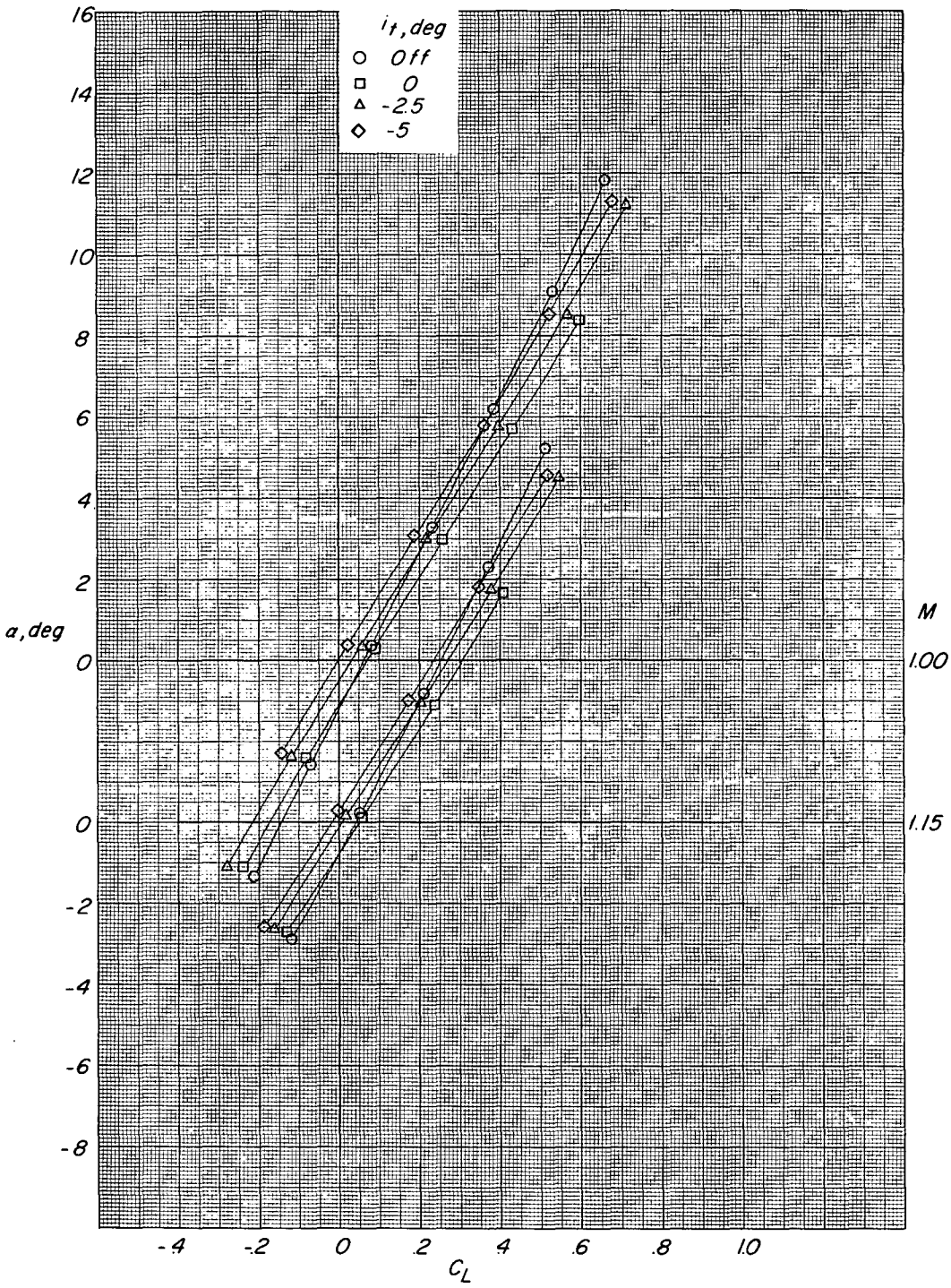

(a) Concluded.

Figure 11.- Continued.

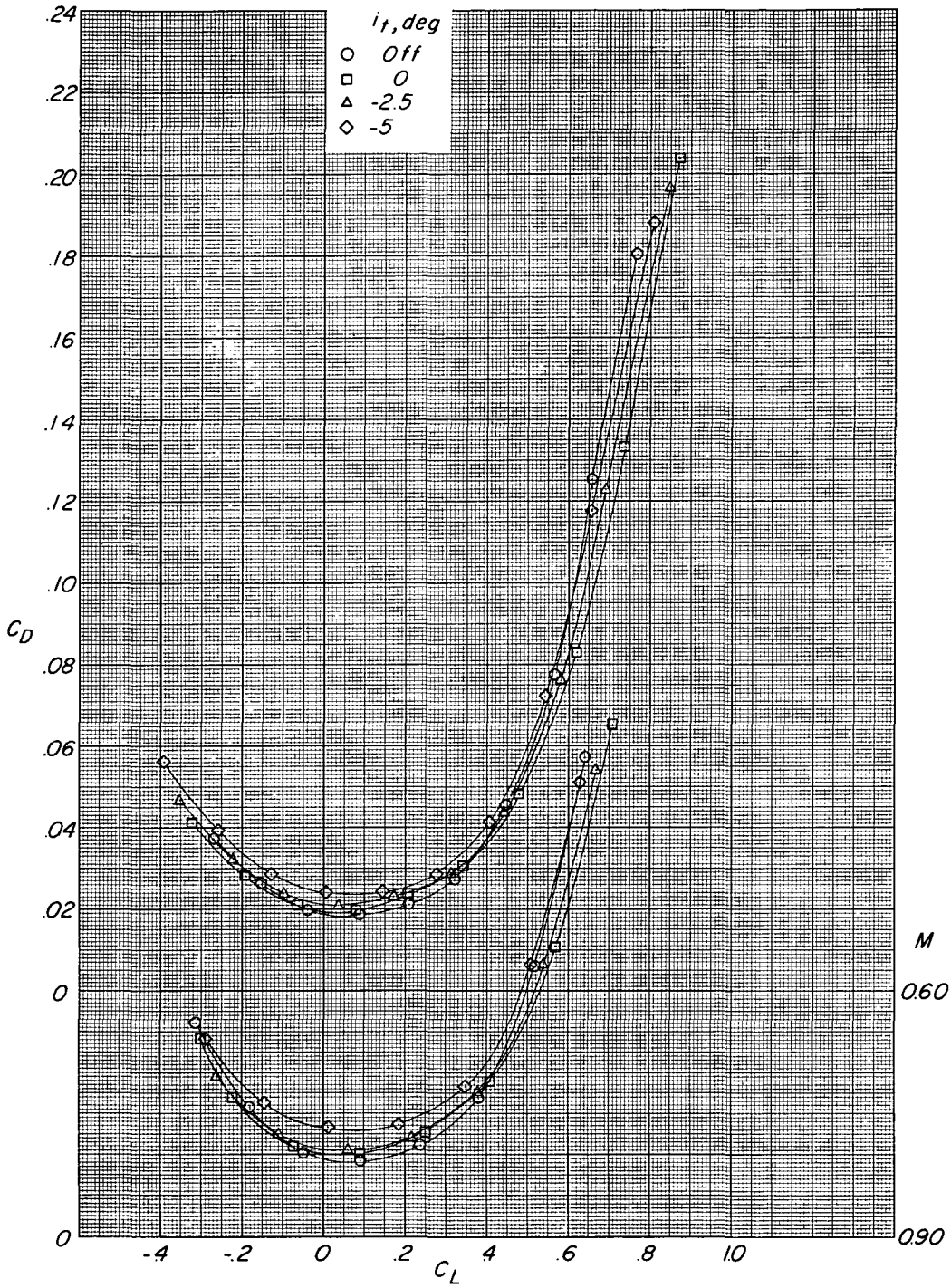

(b) Drag coefficient.

Figure 11.- Continued.

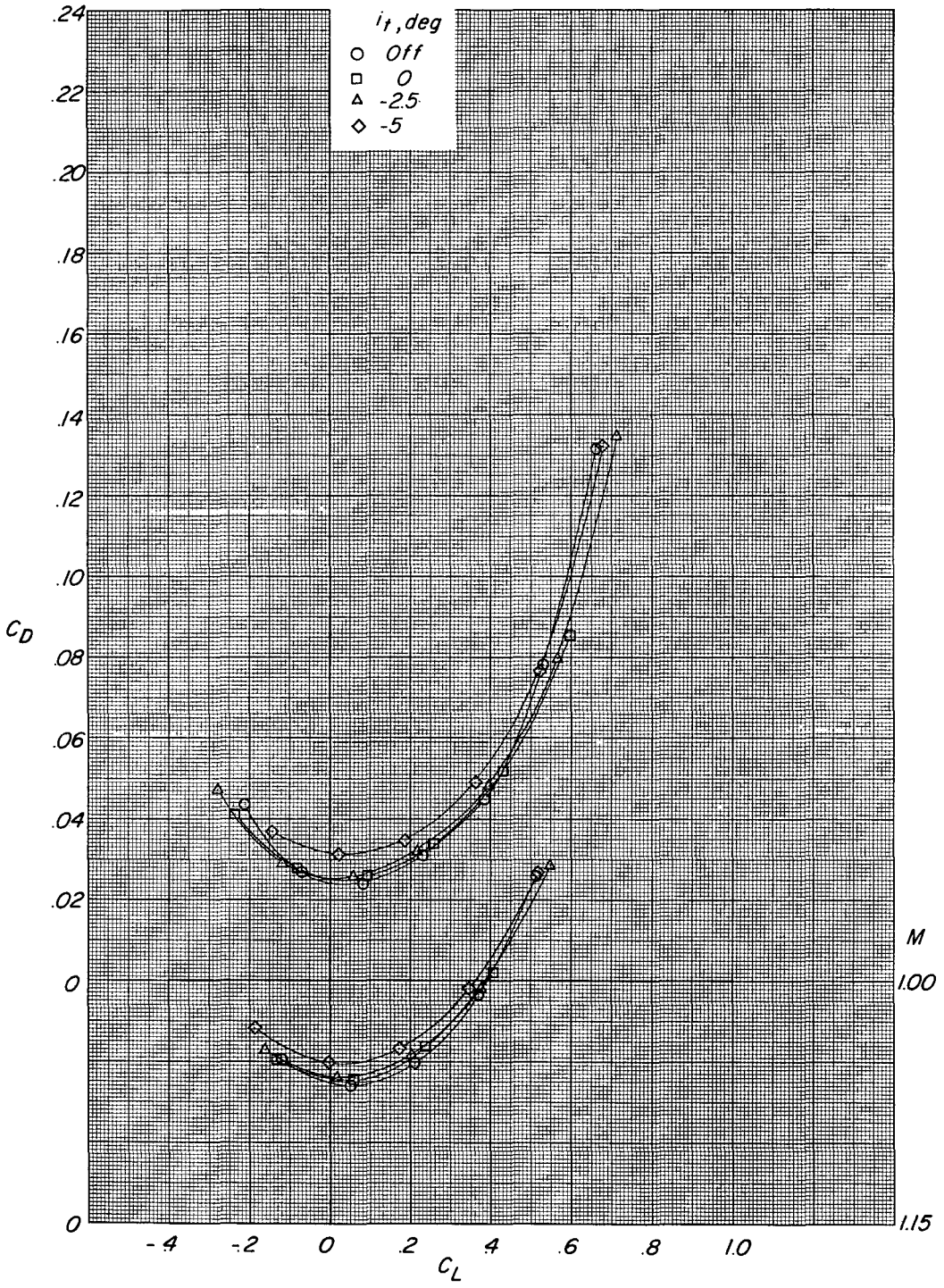

(b) Concluded.

Figure 11.- Continued.

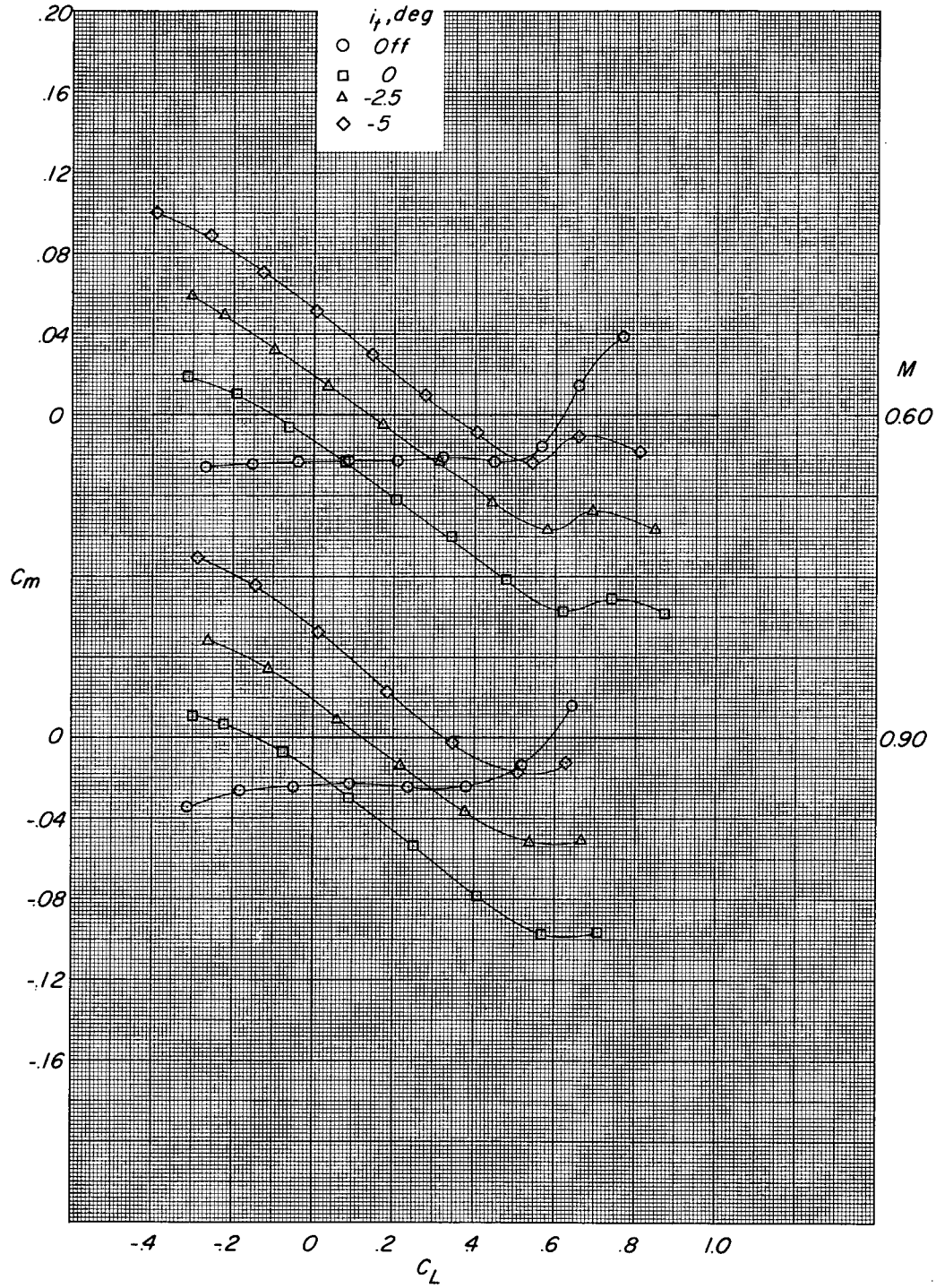

(c) Pitching-moment coefficient.

Figure 11.- Continued.

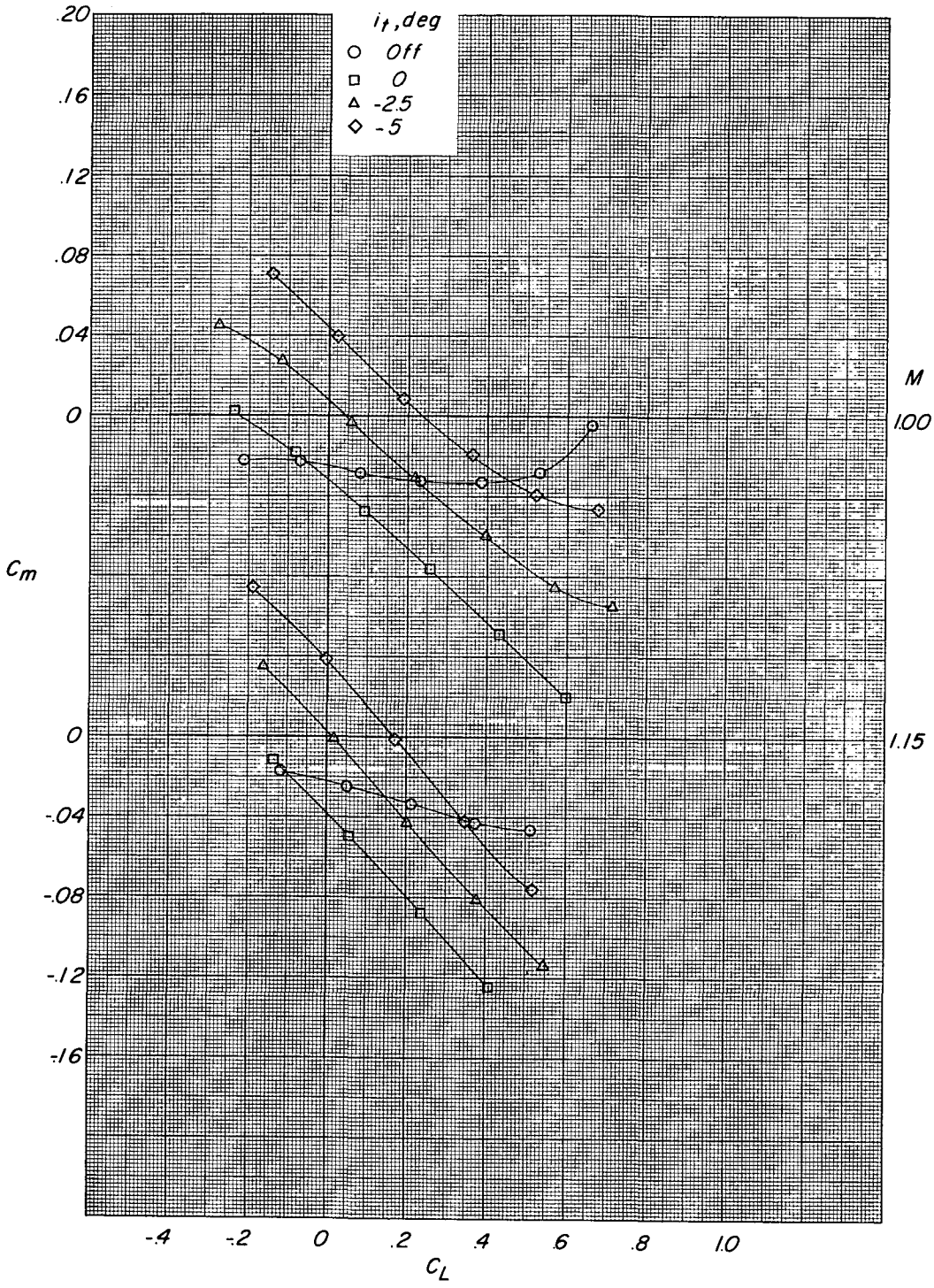

(c) Concluded.

Figure 11.- Concluded.

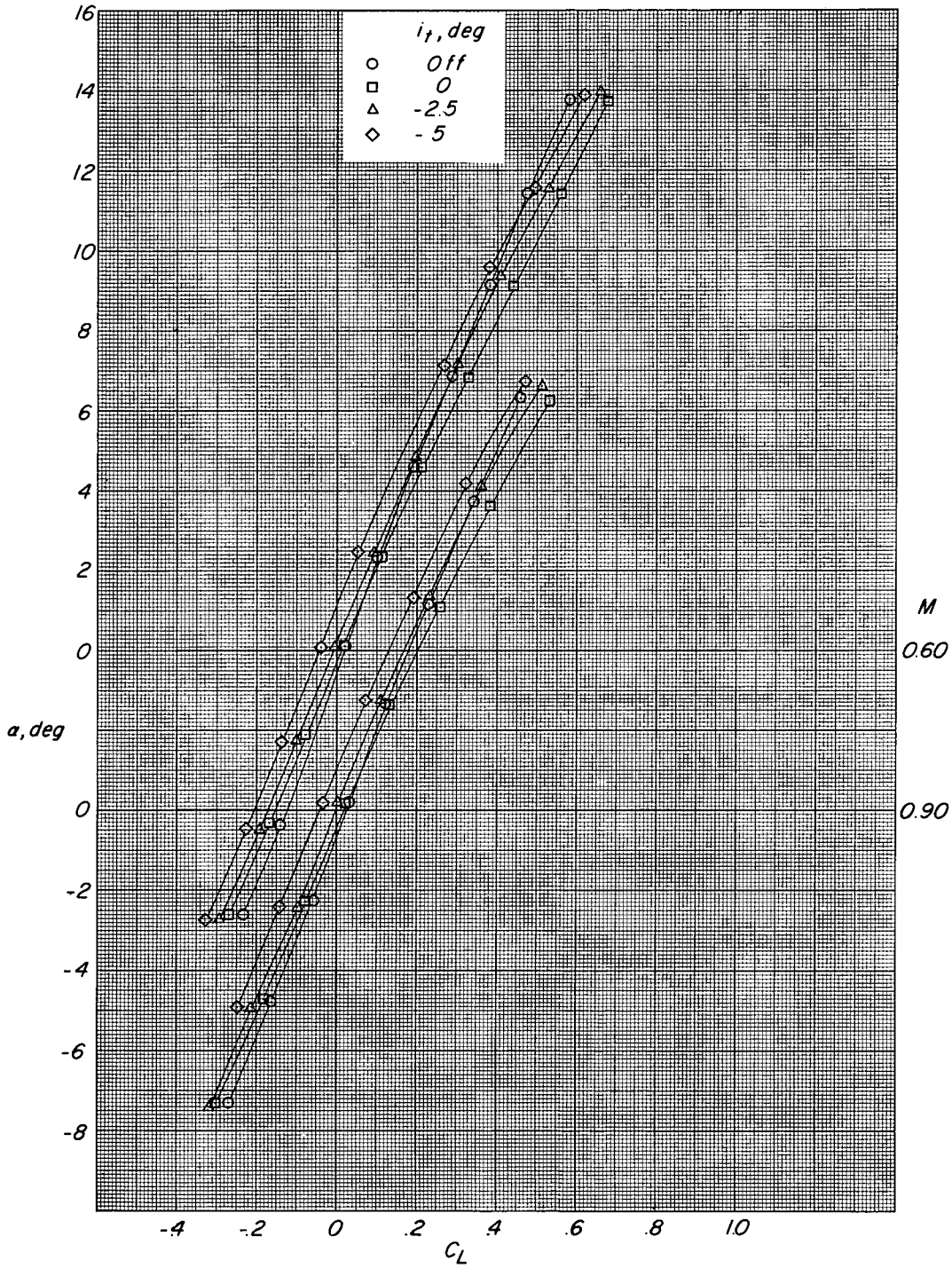

(a) Angle of attack.

Figure 12.- Aerodynamic characteristics for configuration BW_1VH_1N at $\Lambda_{LE} = 75^{\circ}$.

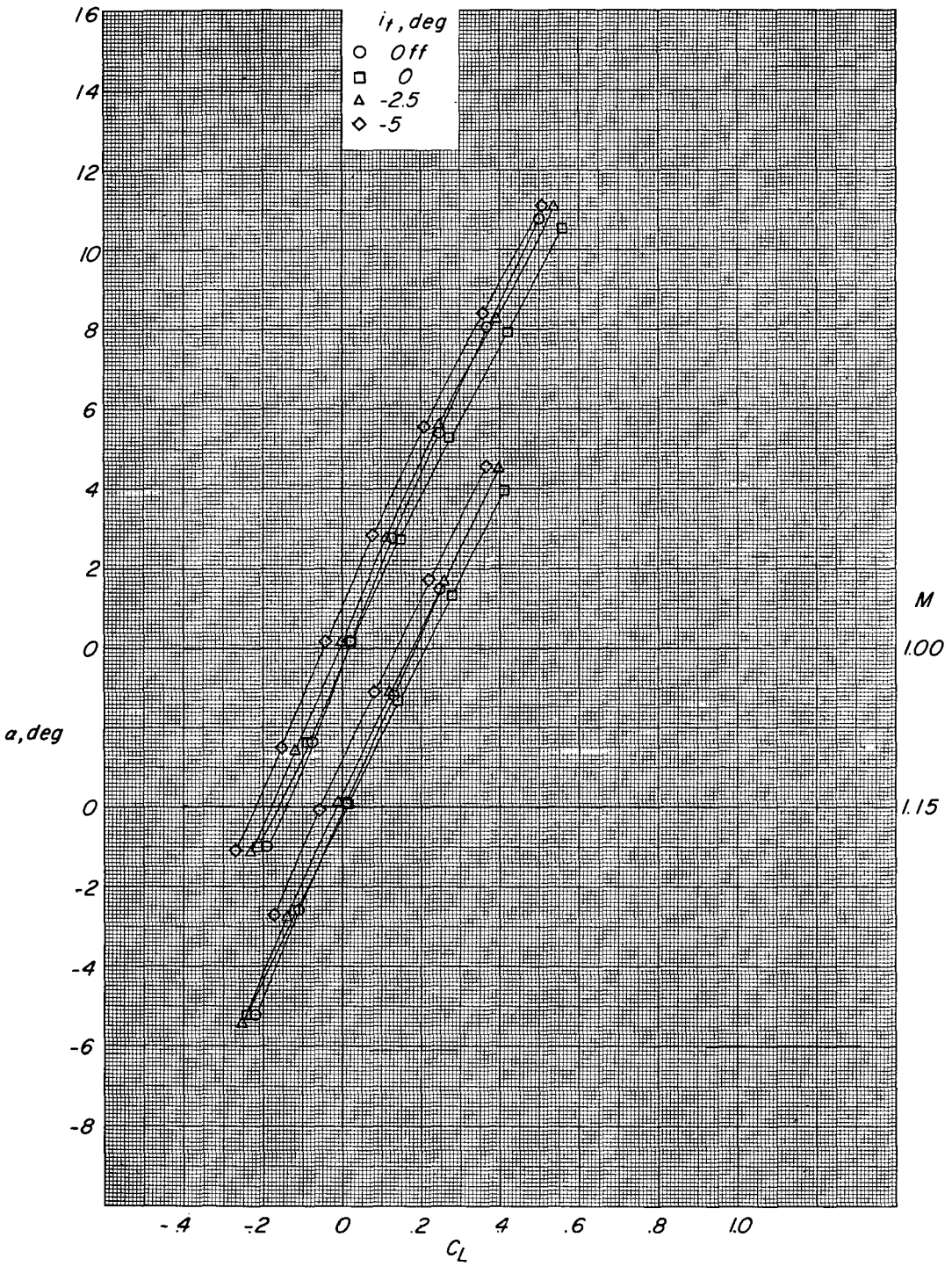

(a) Concluded.

Figure 12.- Continued.

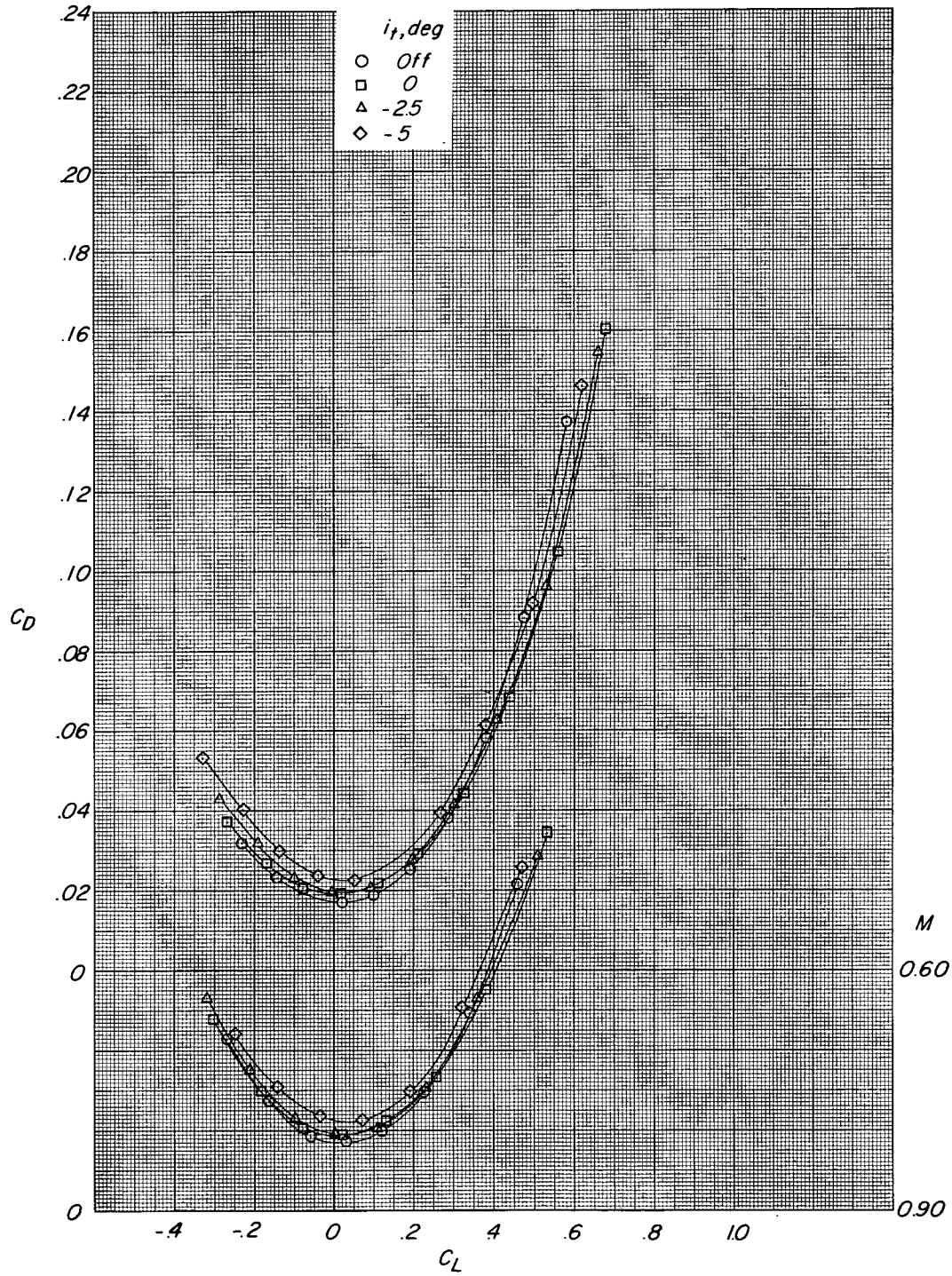

(b) Drag coefficient.

Figure 12.- Continued.

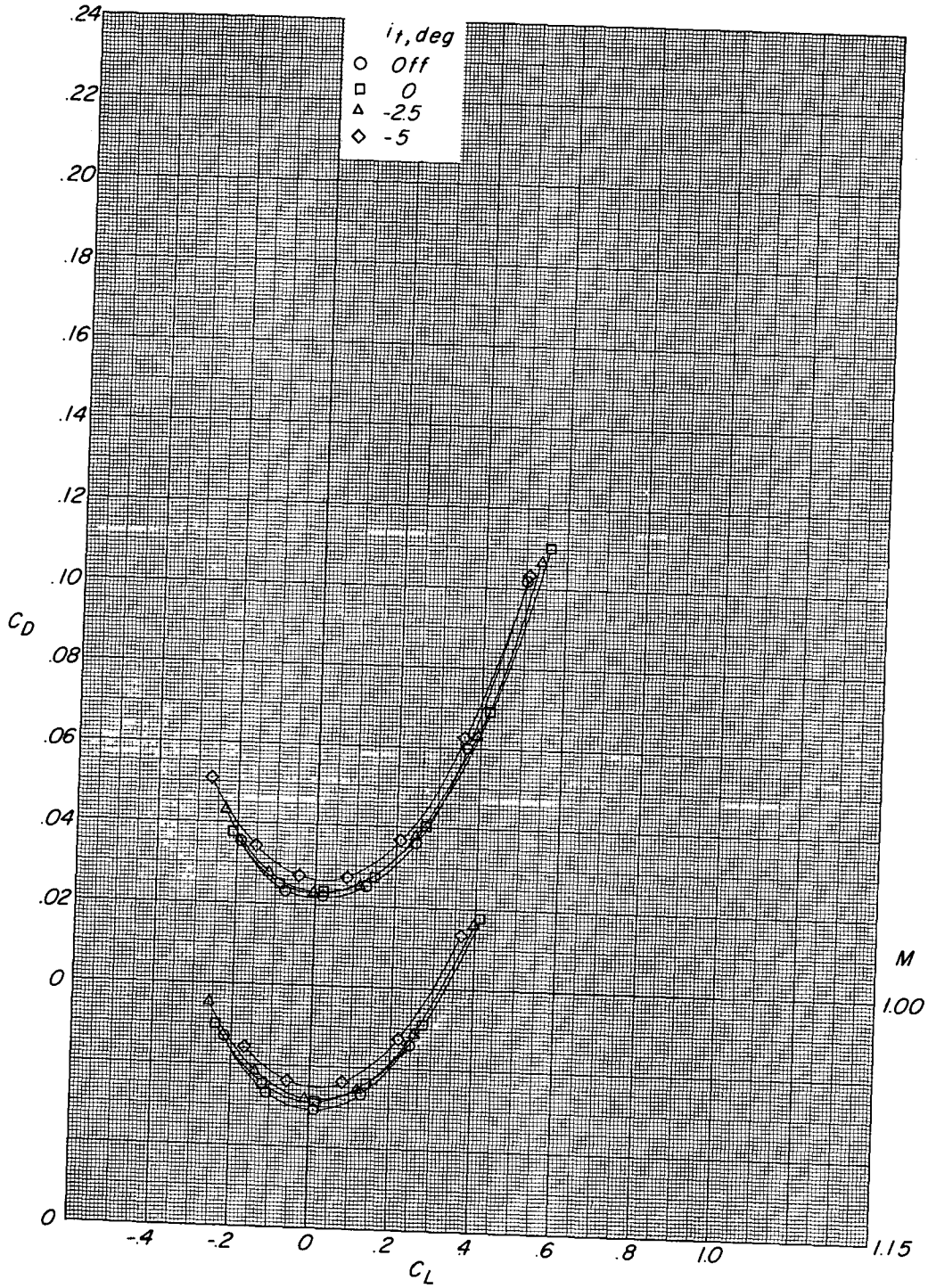

(b) Concluded.

Figure 12.- Continued.

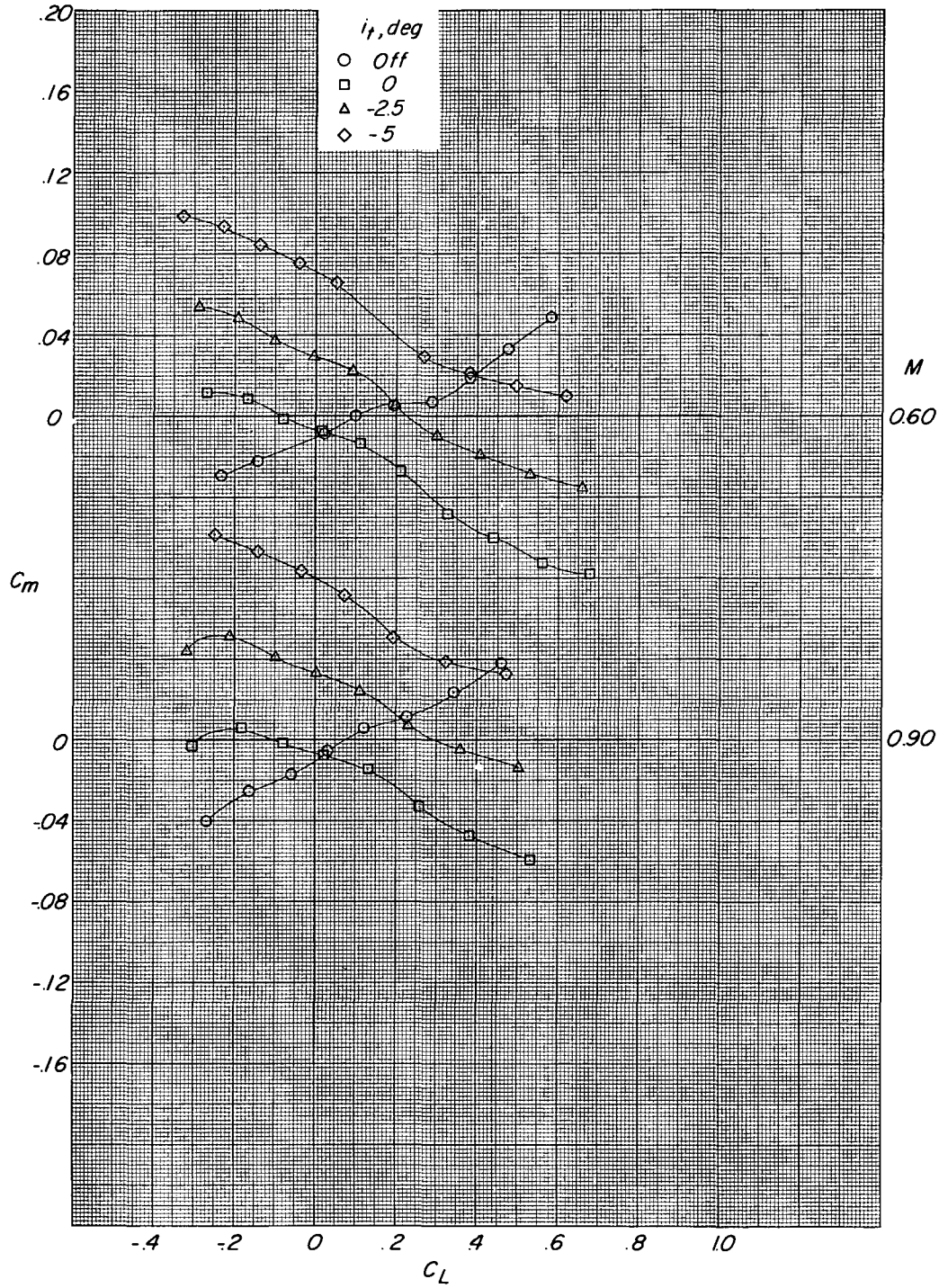

(c) Pitching-moment coefficient.

Figure 12.- Continued.

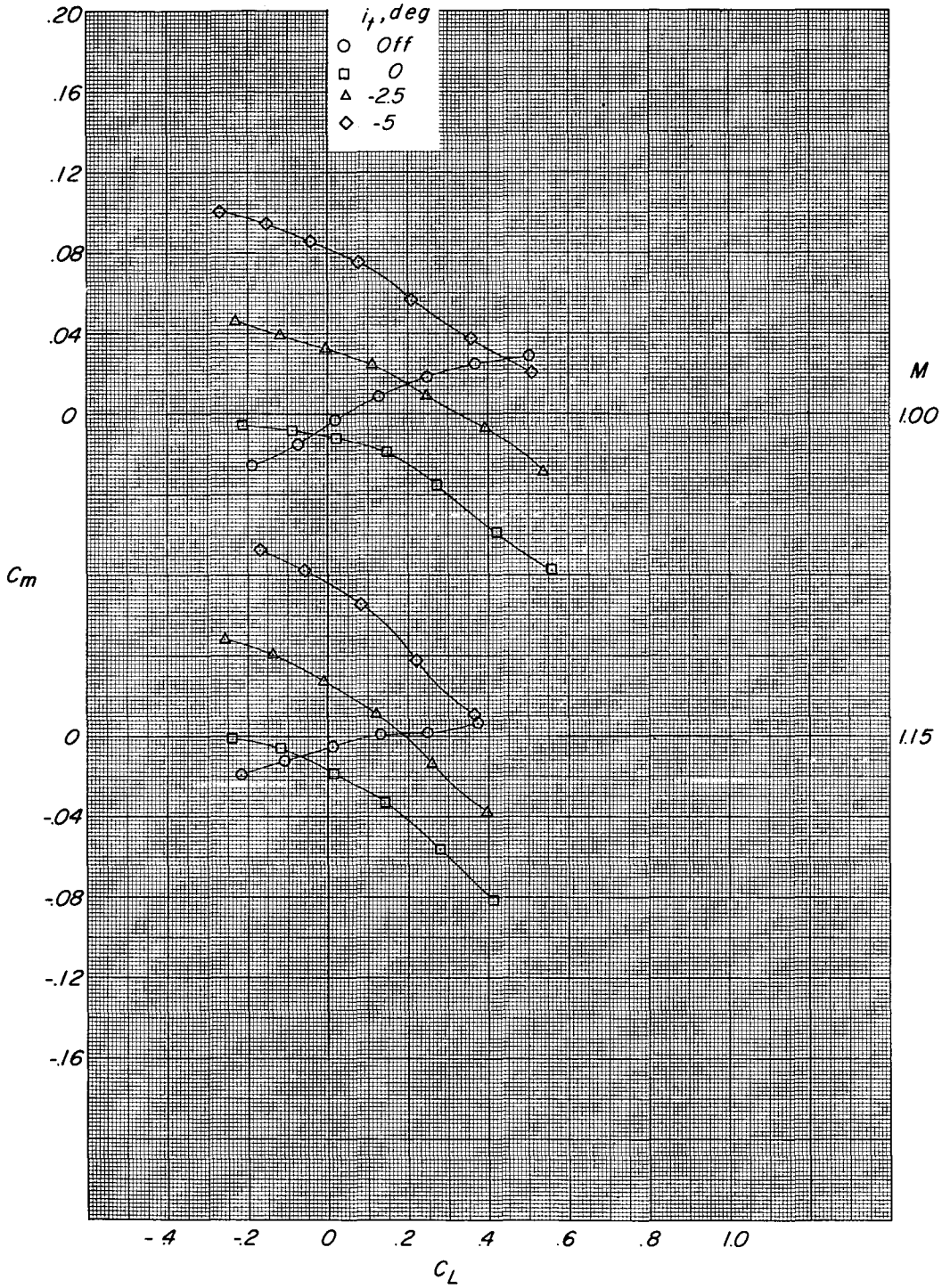

(c) Concluded.

Figure 12.- Concluded.

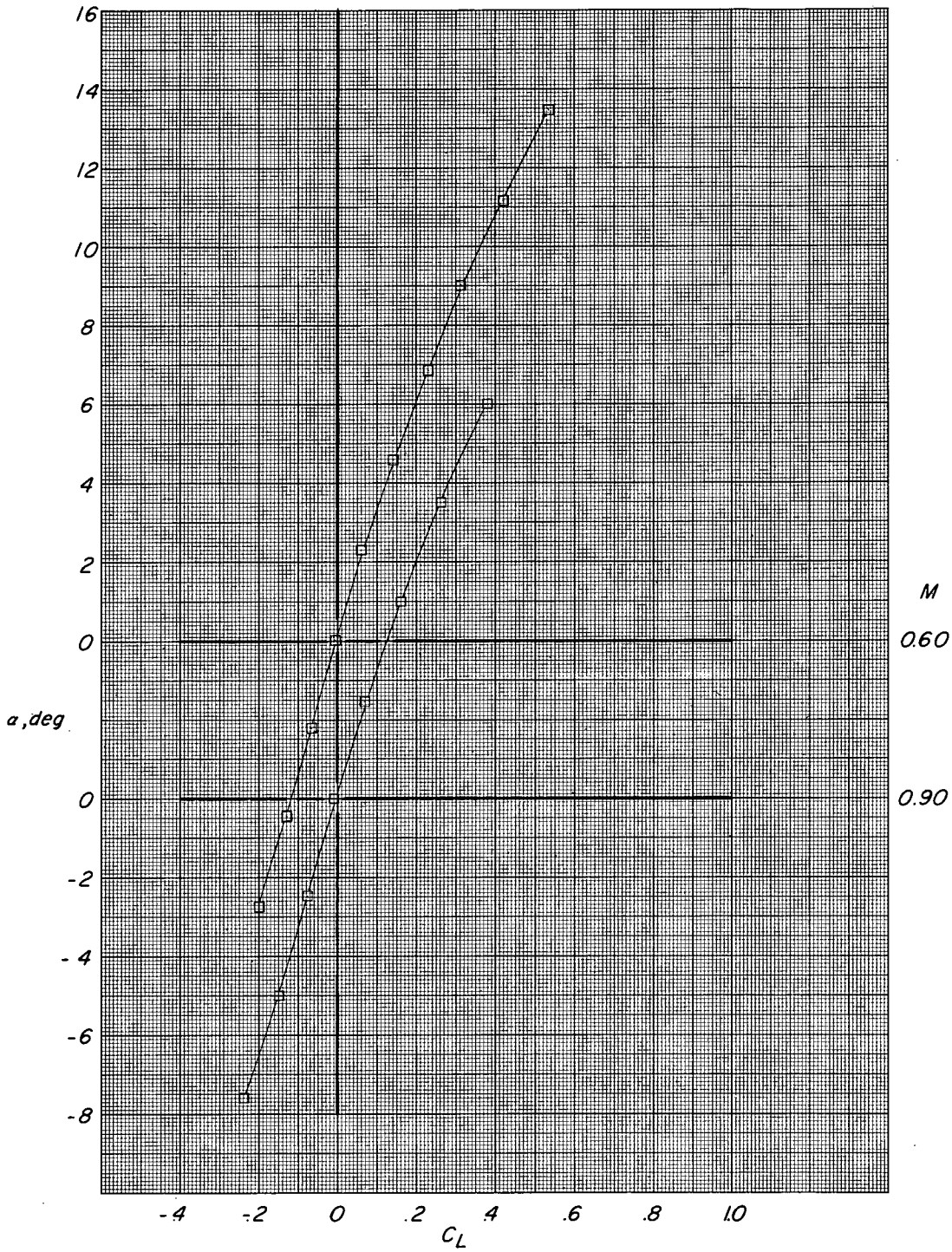

(a) Angle of attack.

Figure 13.- Aerodynamic characteristics for configuration BW_1VH_1N at $\Lambda_{LE} = 90^{\circ}$.

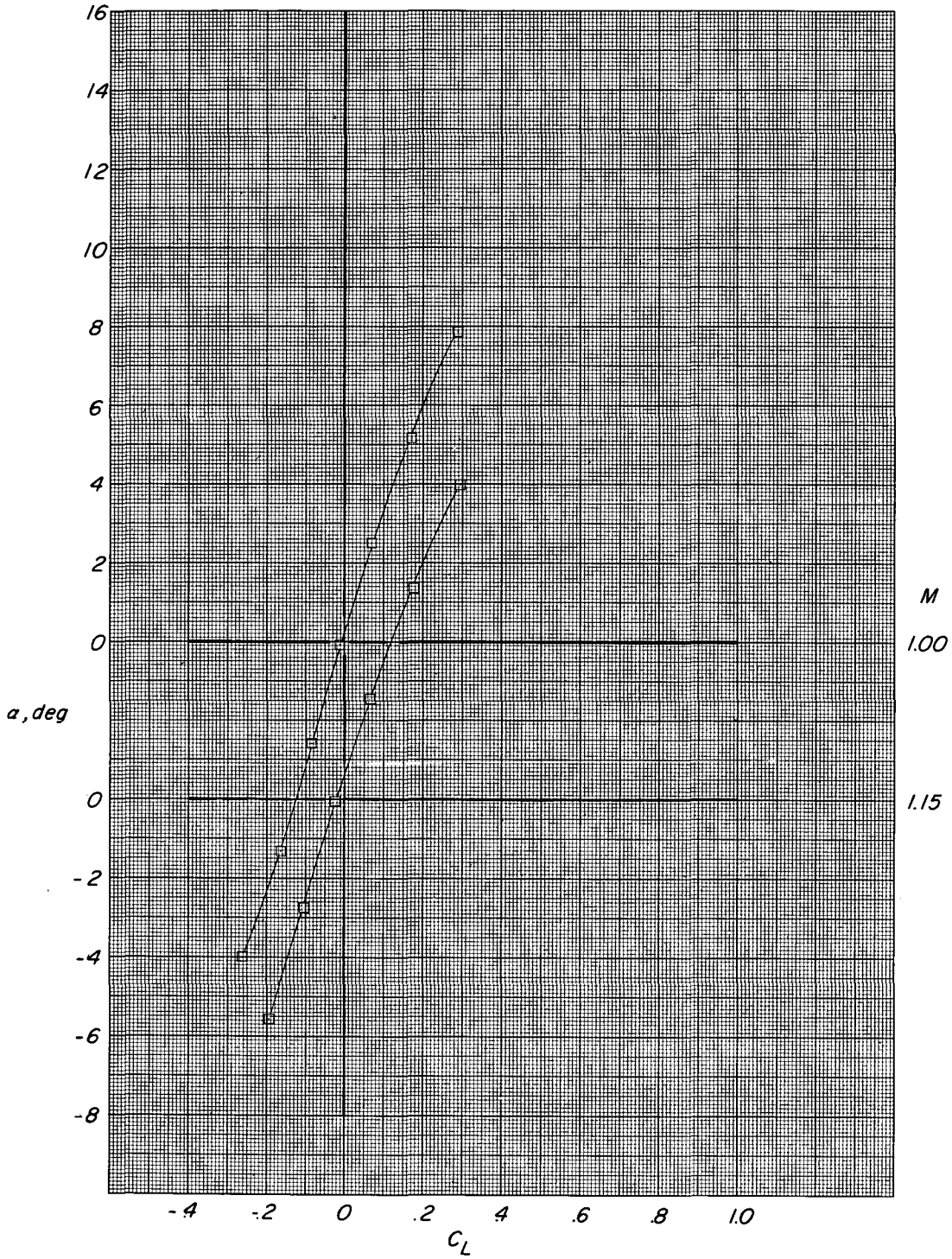

(a) Concluded.

Figure 13.- Continued.

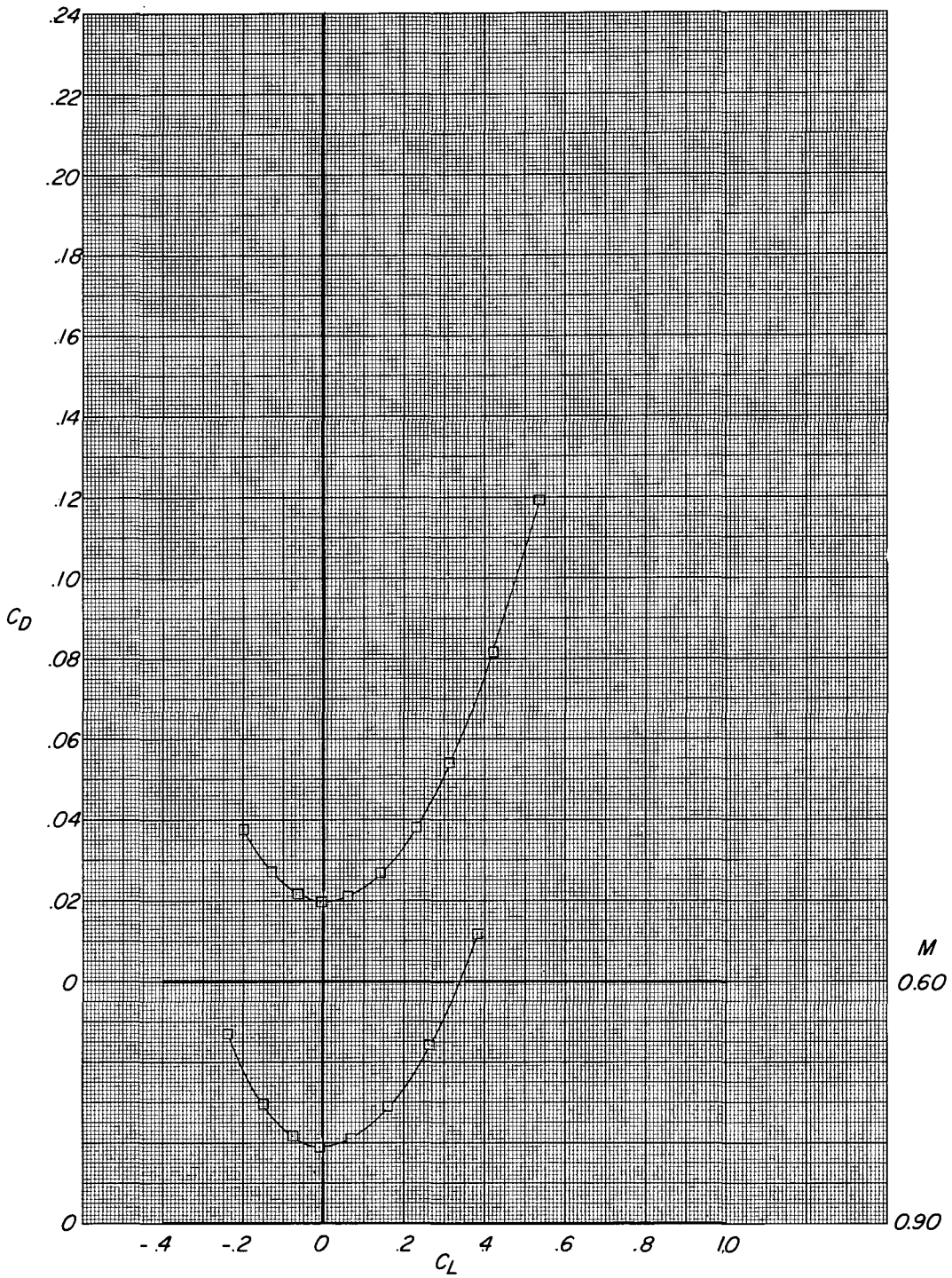

(b) Drag coefficient.

Figure 13.- Continued.

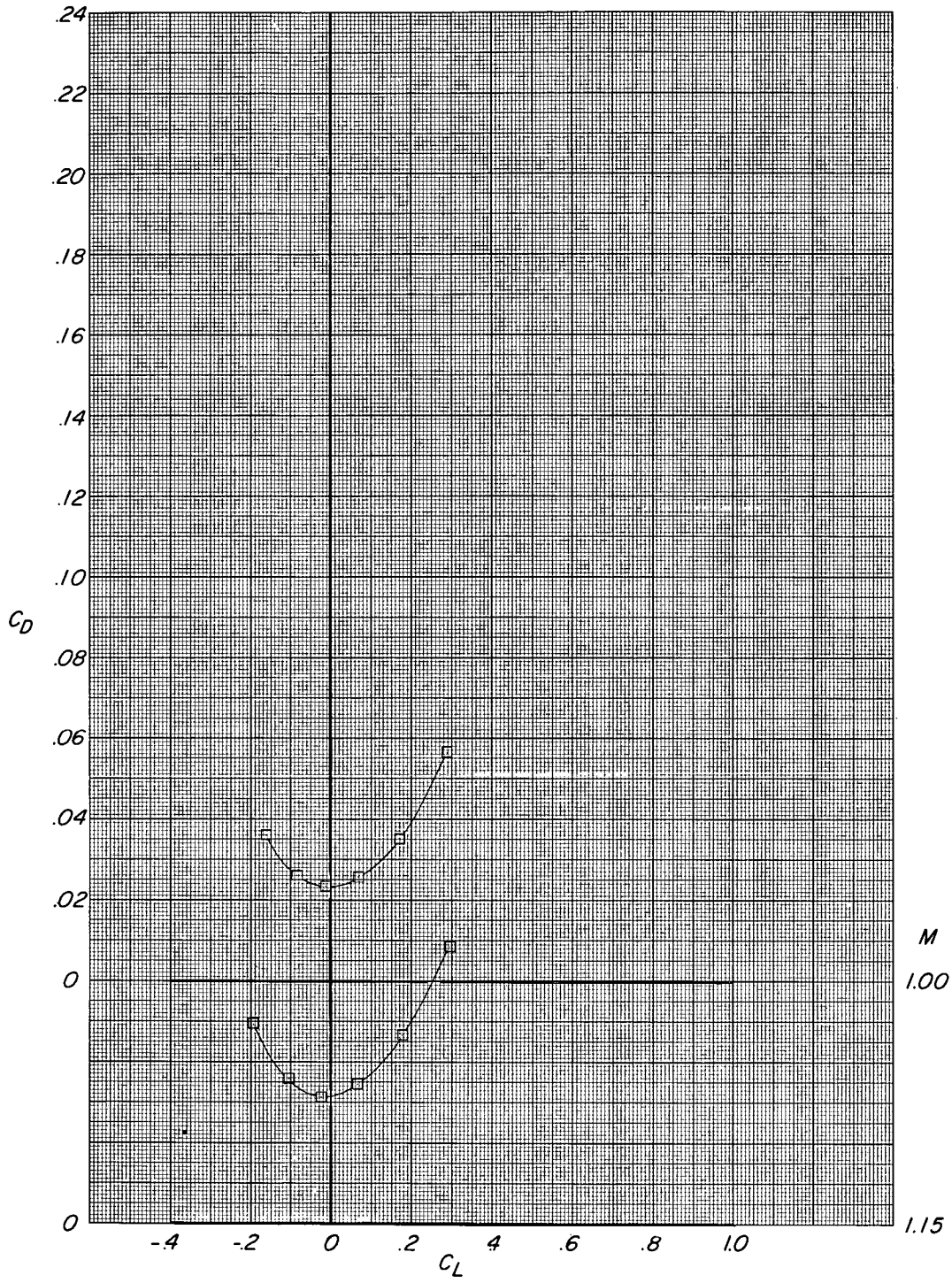

(b) Concluded.

Figure 13.- Continued.

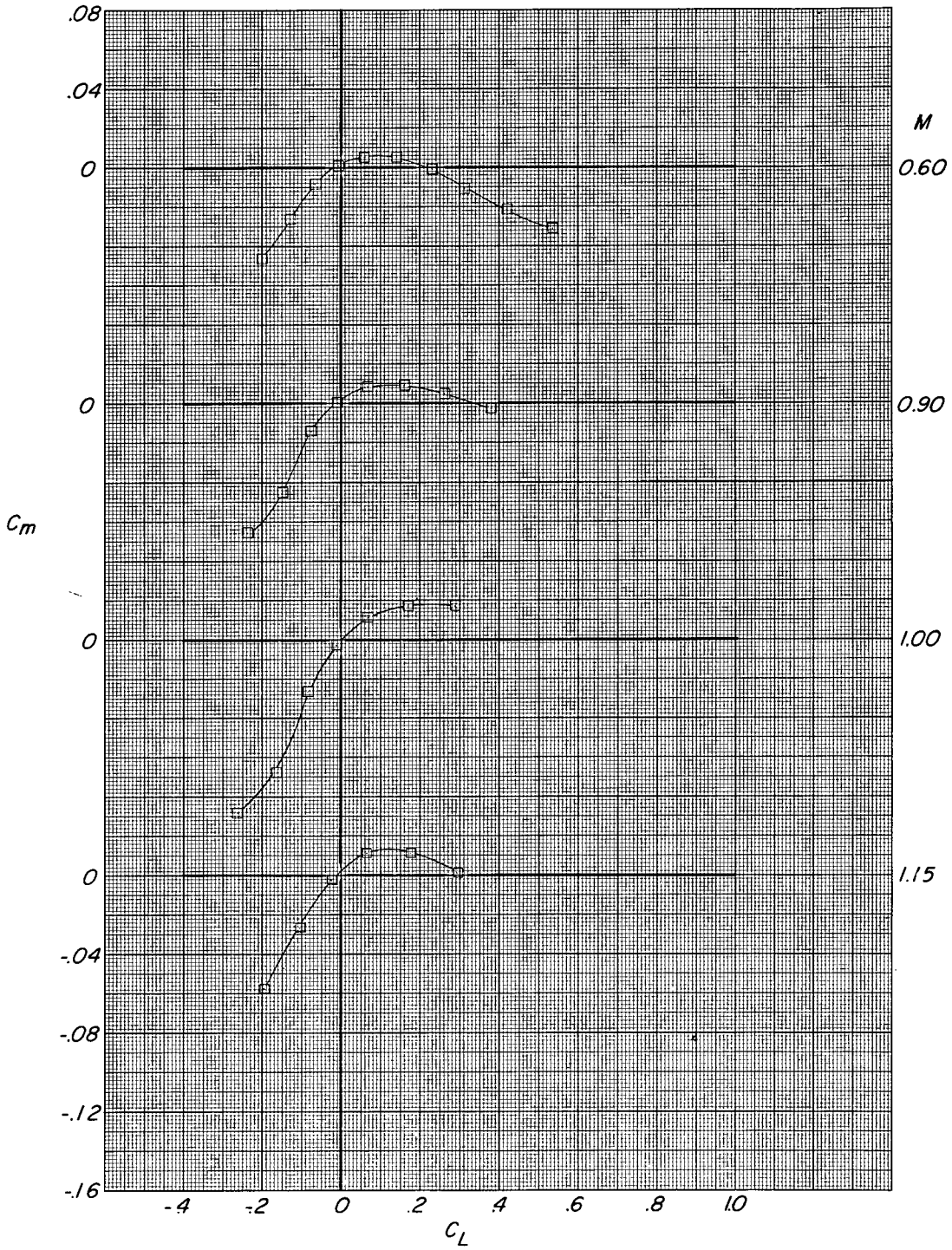

(c) Pitching-moment coefficient.

Figure 13.- Concluded.

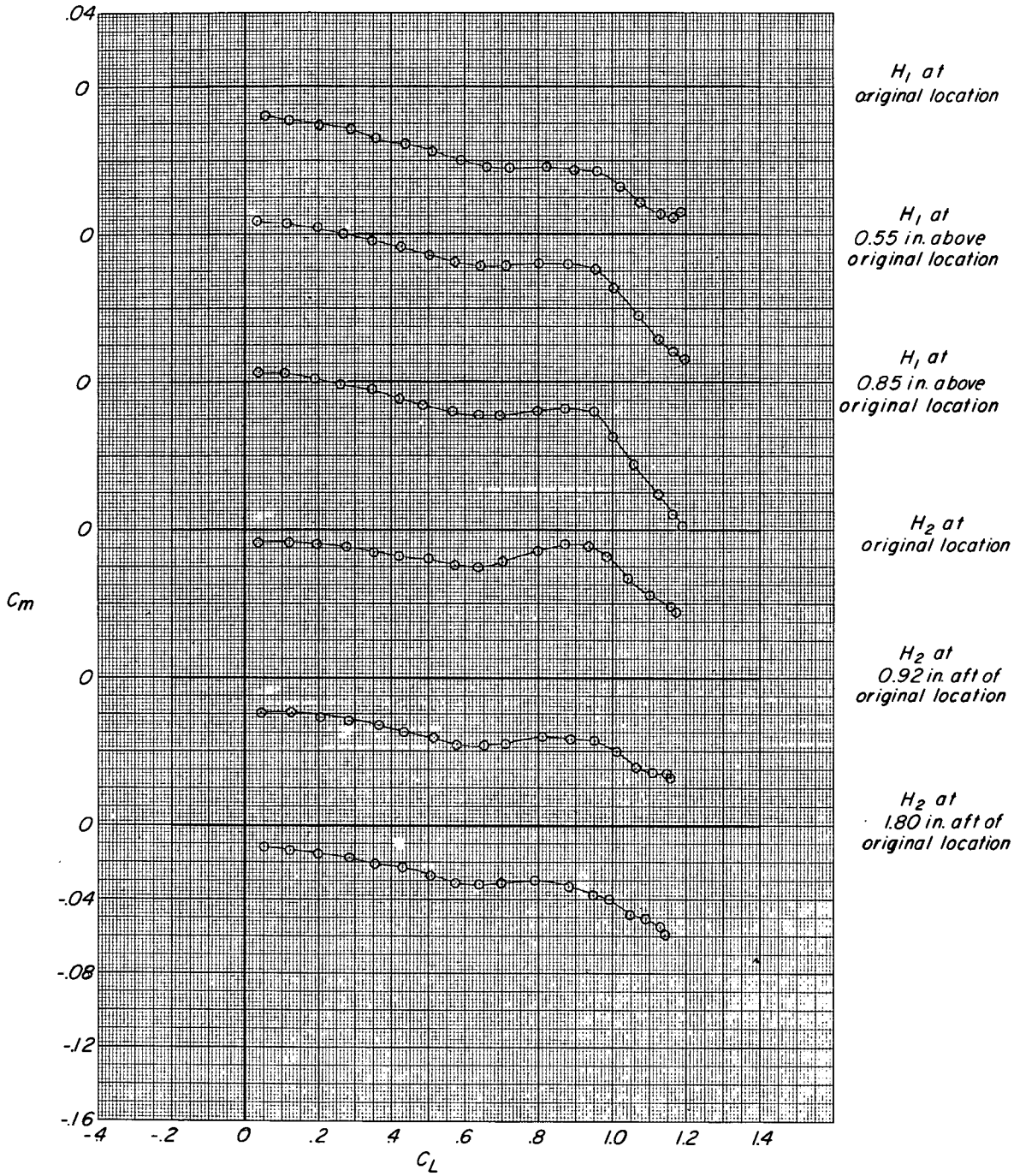

(a) $\Lambda_{LE} = 25^{\circ}$.

Figure 14.- The effect of horizontal-tail orientation and size for configuration BW_2VH_1N and BW_2VH_2N at $M = 0.38$ and $i_t = 0^{\circ}$.

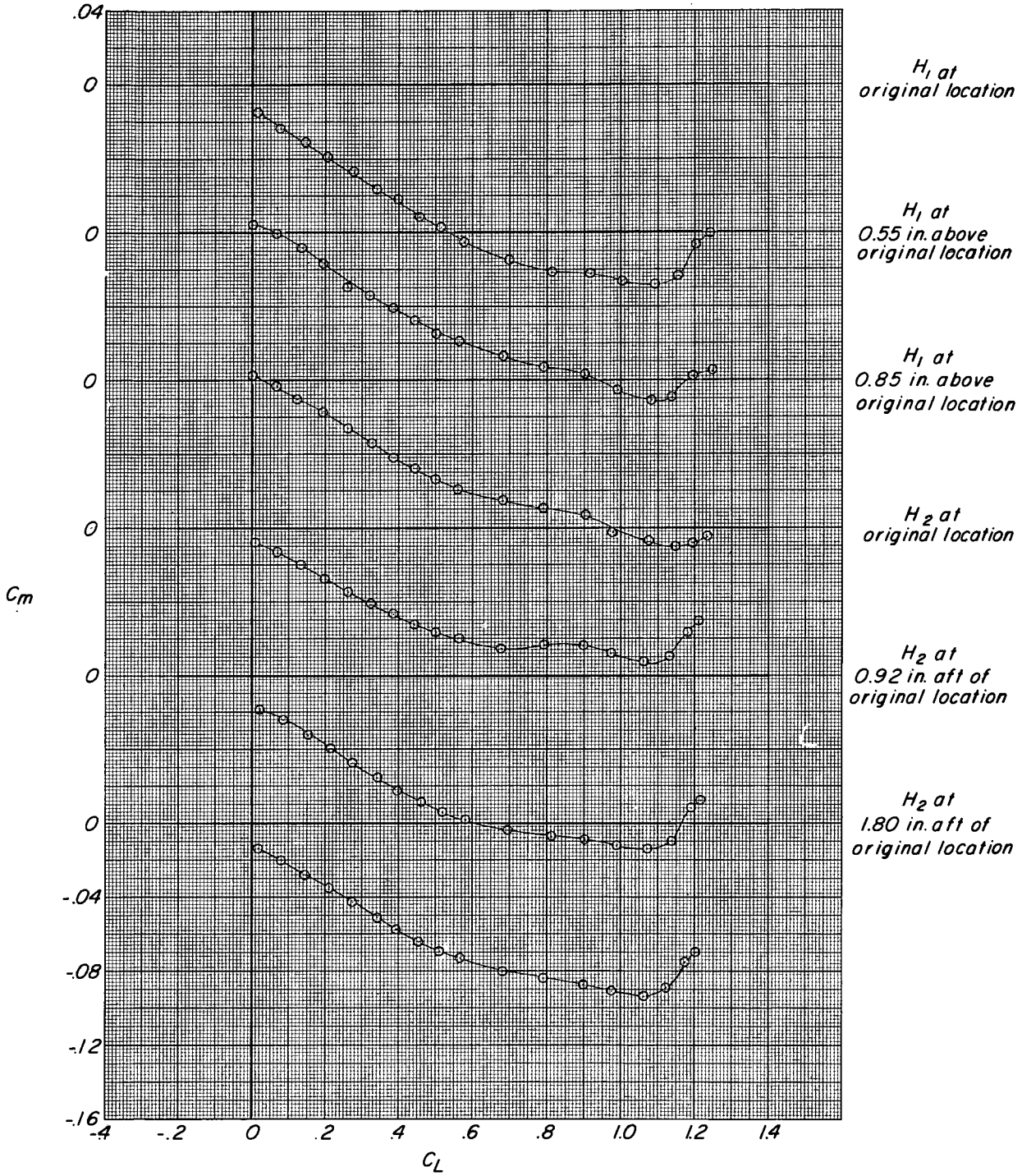

(b) $\Lambda_{LE} = 45^{\circ}$.

Figure 14.- Continued.

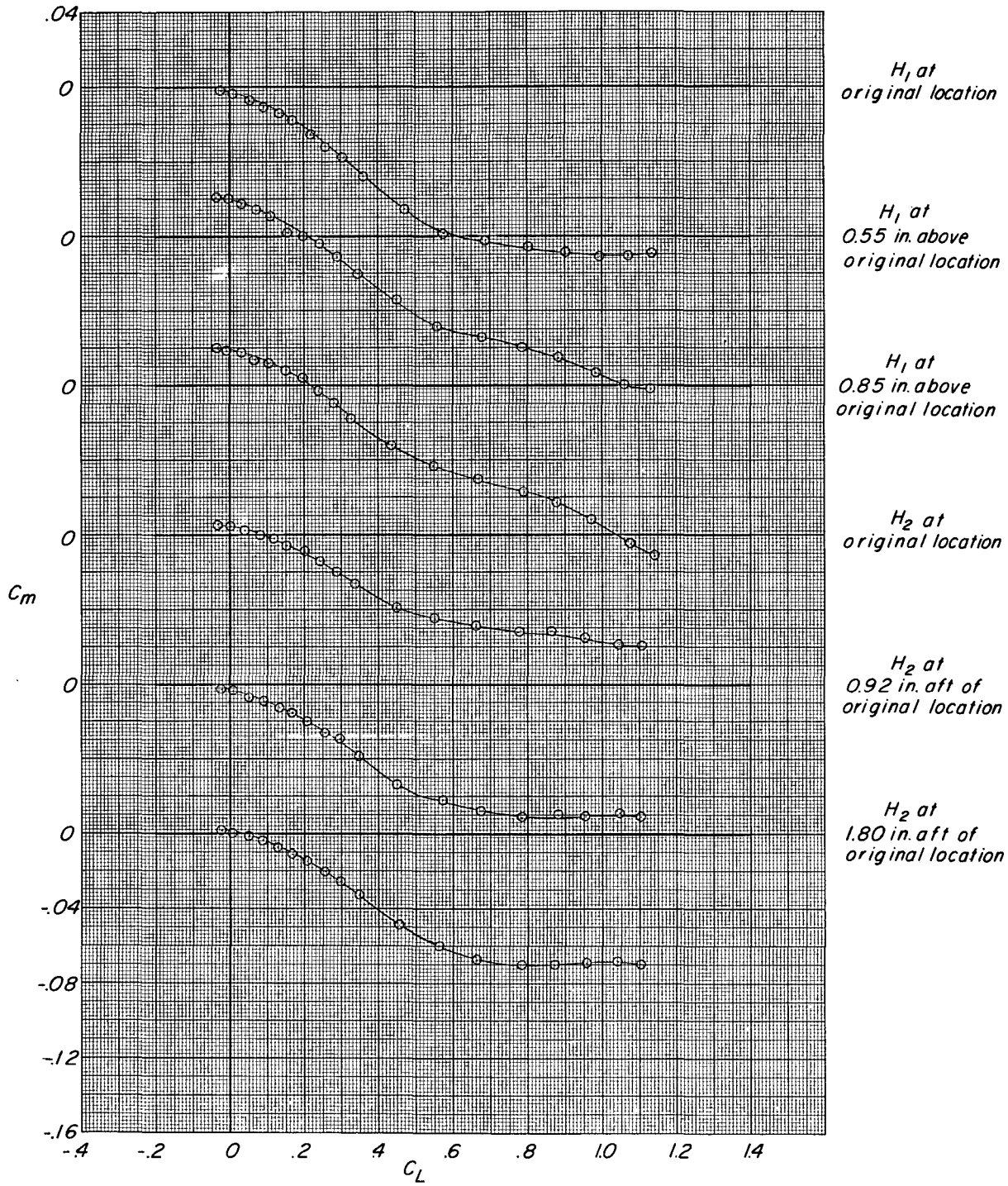

(c) $\Lambda_{LE} = 75^{\circ}$.

Figure 14.- Continued.

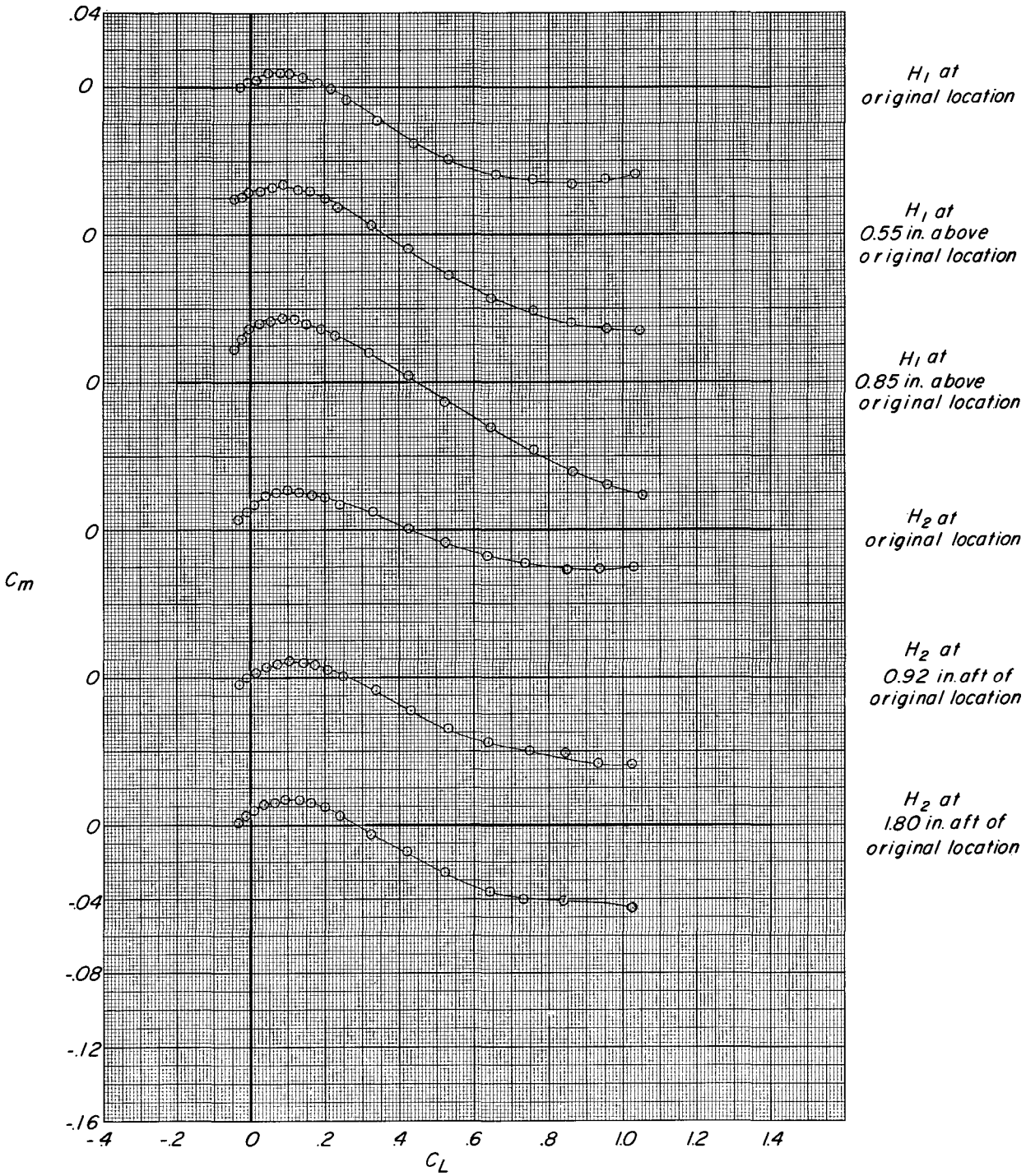

(d) $\Lambda_{LE} = 90^{\circ}$.

Figure 14.- Concluded.

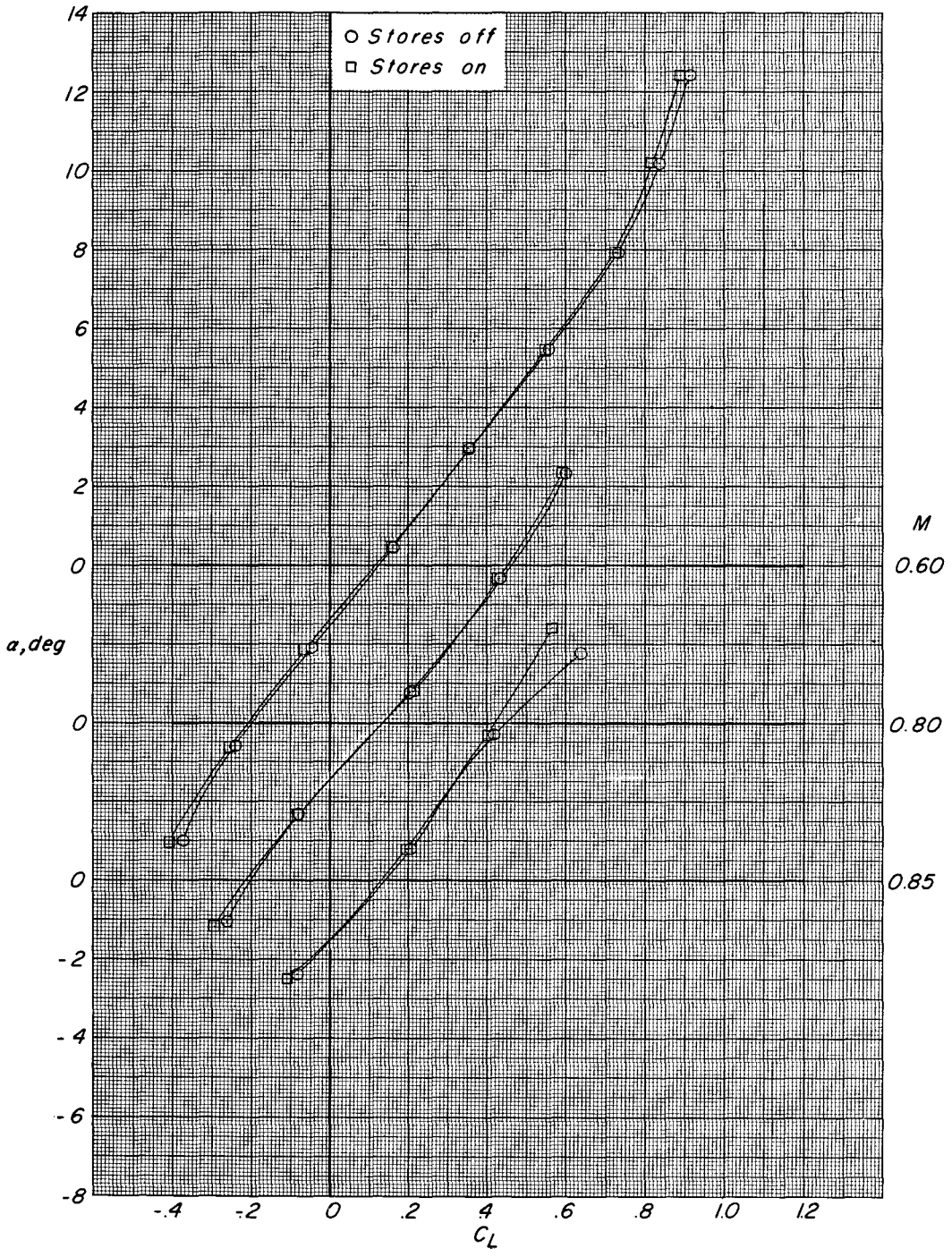

(a) Angle of attack.

Figure 15.- Effect of the addition of one ASM-N-7B store at each wing-pivot point on the aerodynamic characteristics for configuration BW_1VH_1N at $\Lambda_{LE} = 25^\circ$ and $i_t = 0^\circ$.

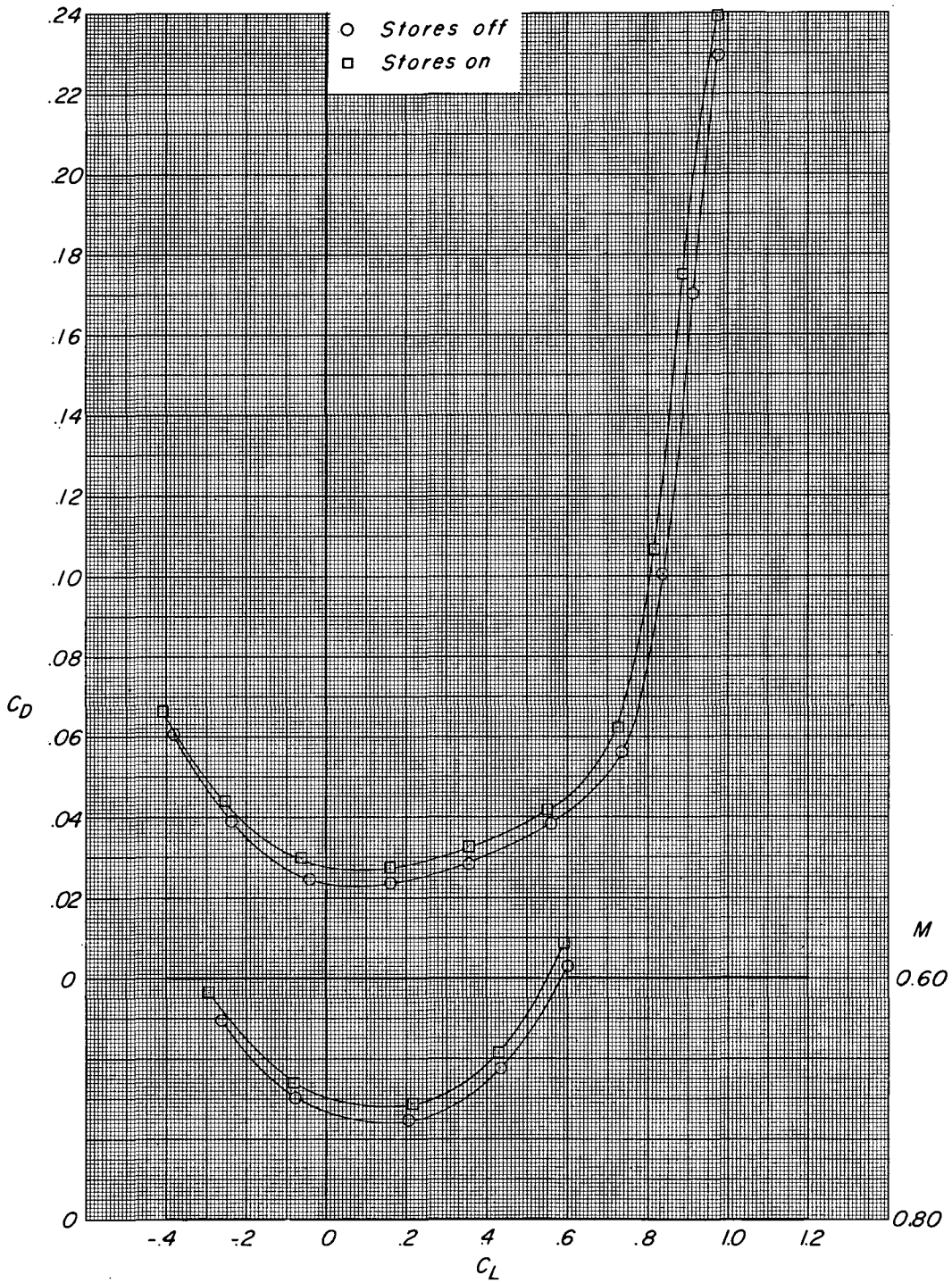

(b) Drag coefficient.

Figure 15.- Continued.

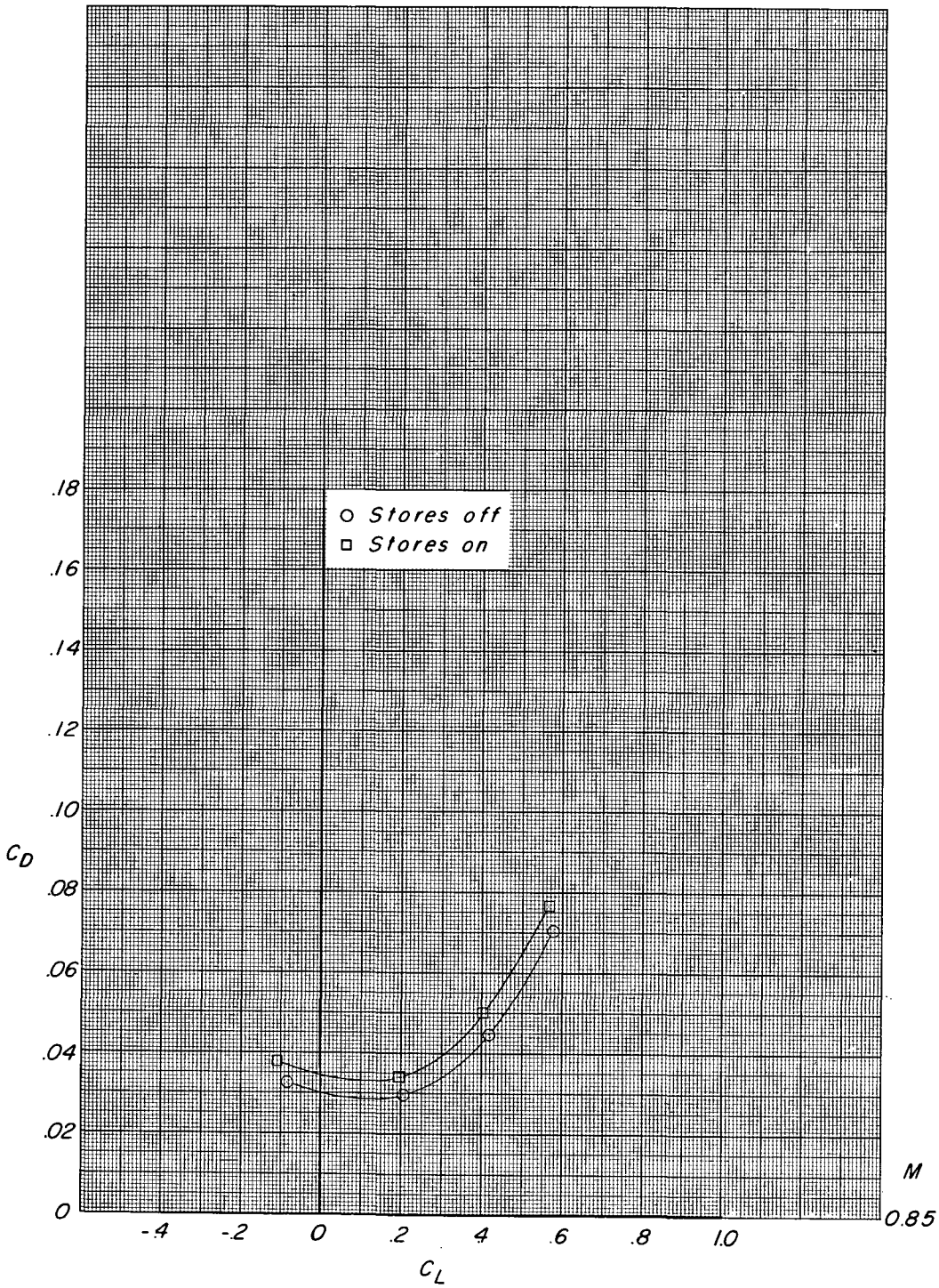

(b) Concluded.

Figure 15.- Continued.

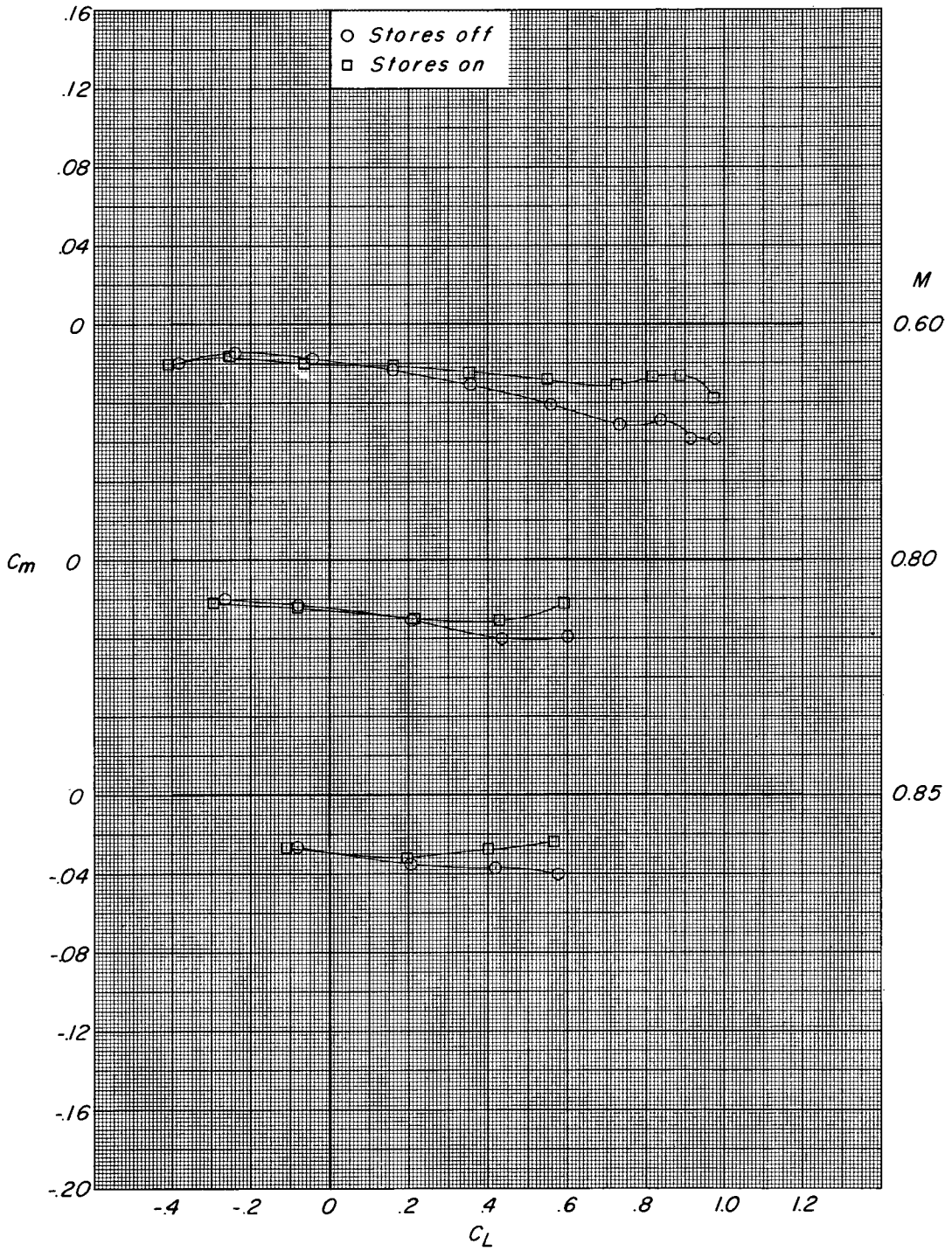

(c) Pitching-moment coefficient.

Figure 15.- Concluded.

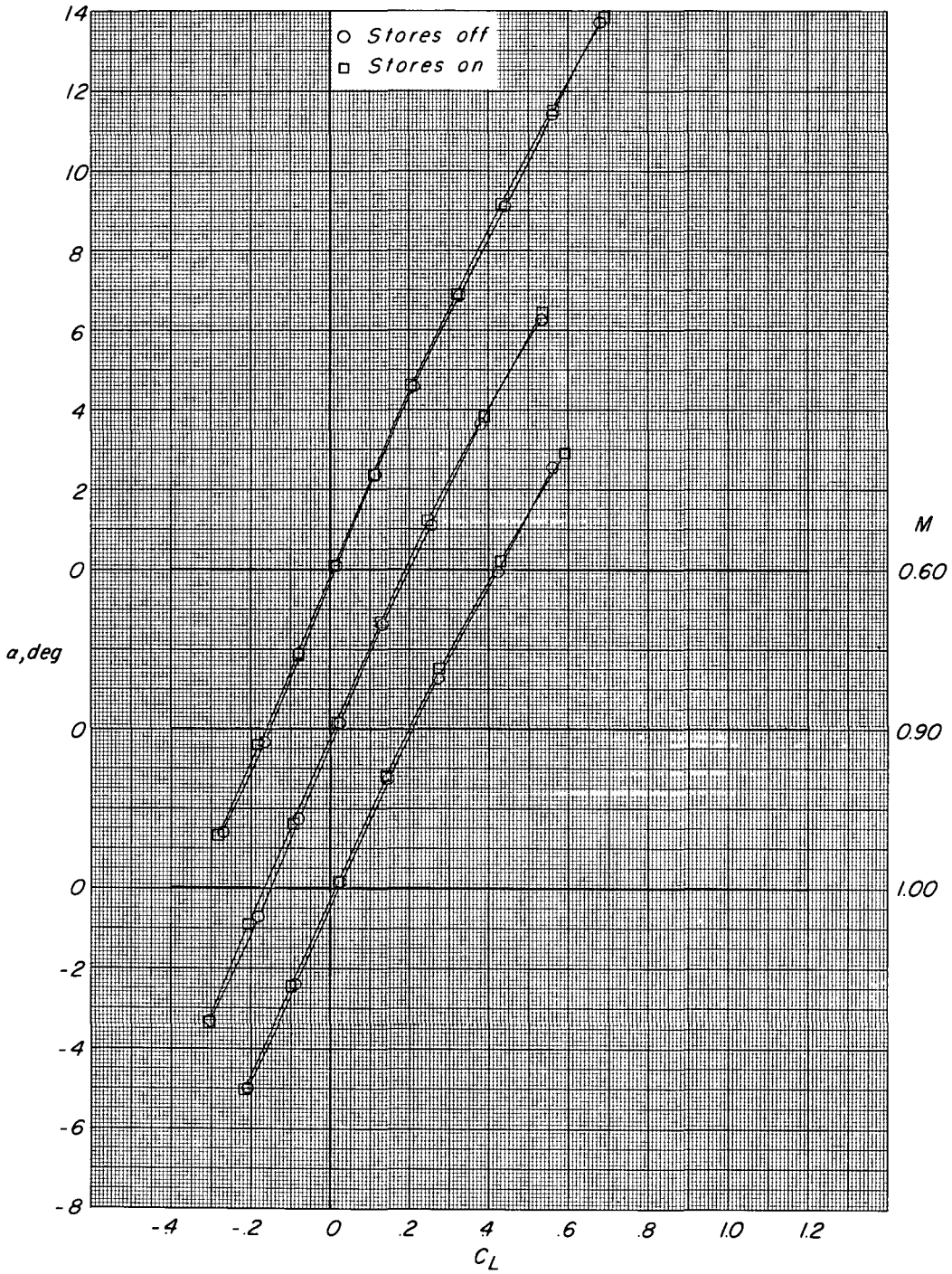

(a) Angle of attack.

Figure 16.- Effect of the addition of one ASM-N-7B store at each wing-pivot point on the aerodynamic characteristics for configuration BW_1VH_1N at $\Lambda_{LE} = 75^{\circ}$ and $i_t = 0^{\circ}$.

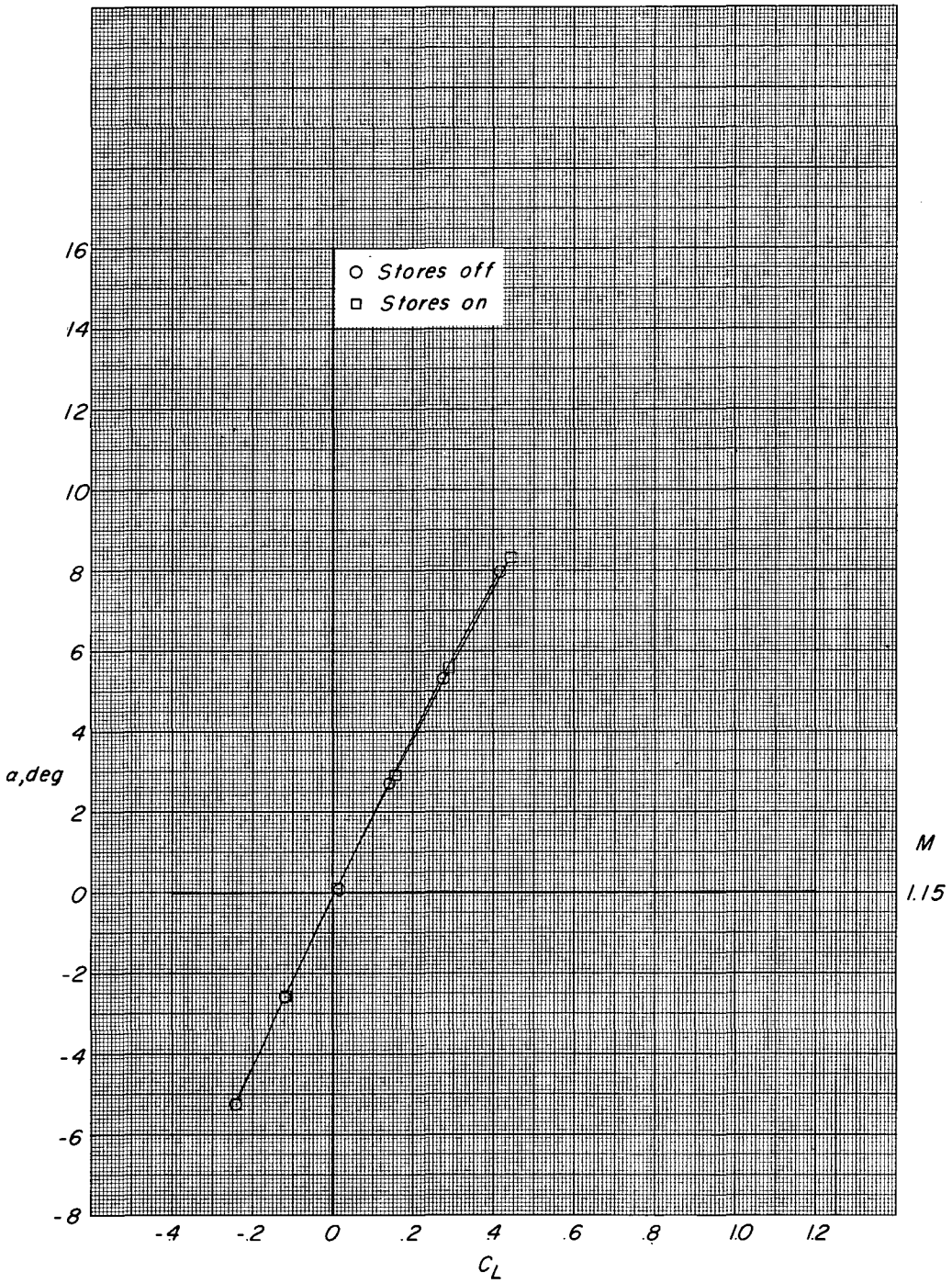

(a) Concluded.

Figure 16.- Continued.

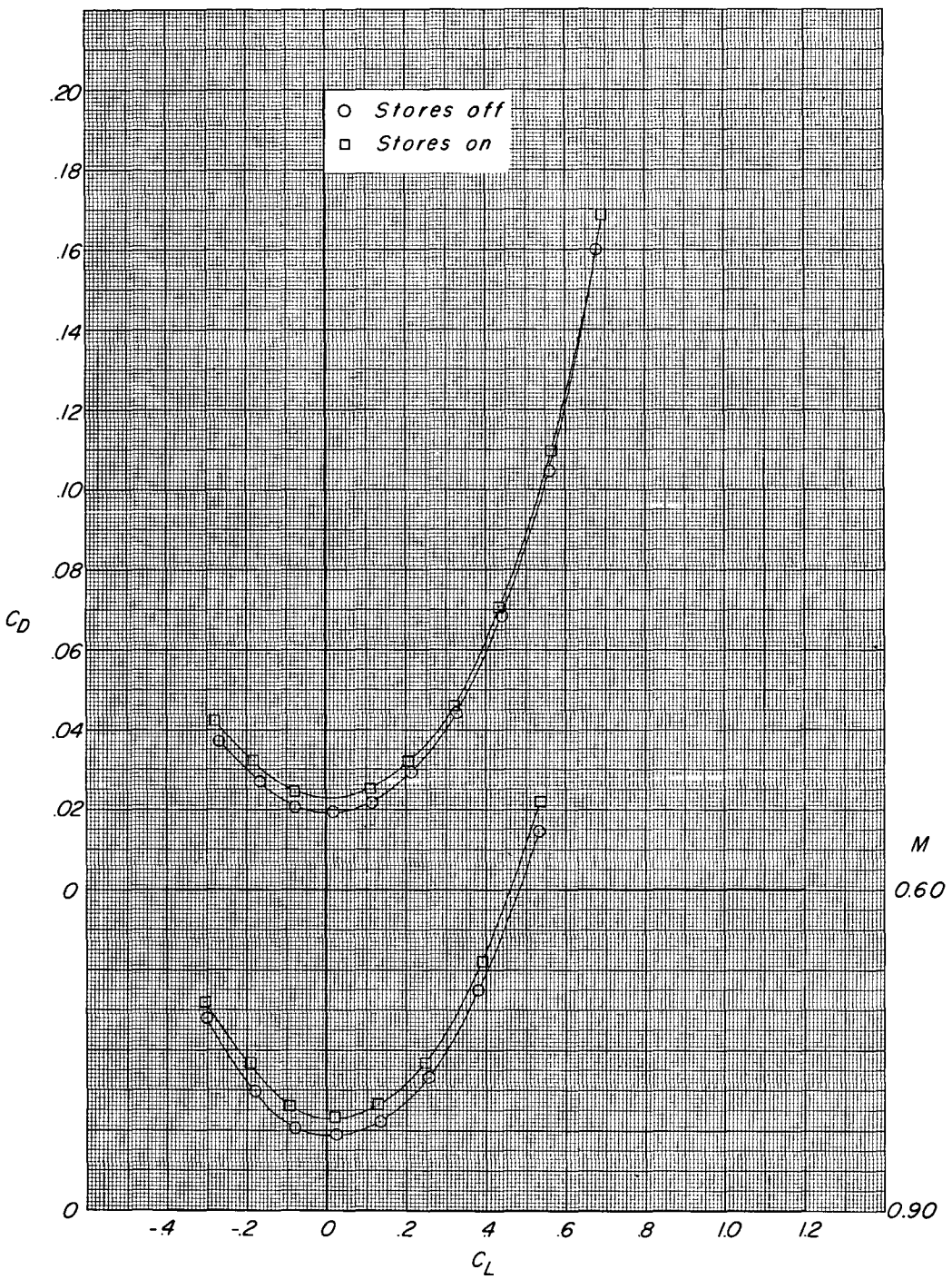

(b) Drag coefficient.

Figure 16.- Continued.

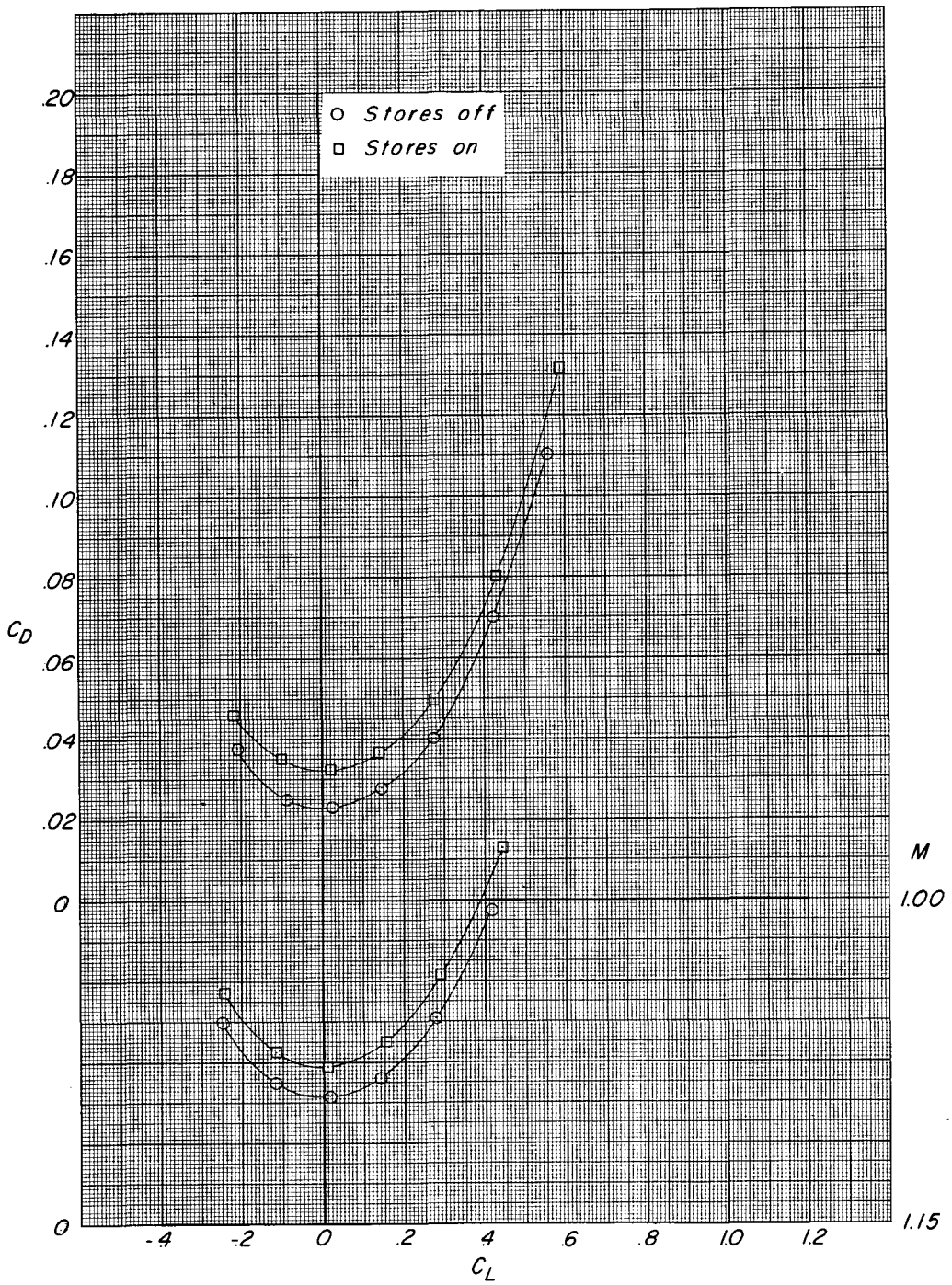

(b) Concluded.

Figure 16.- Continued.

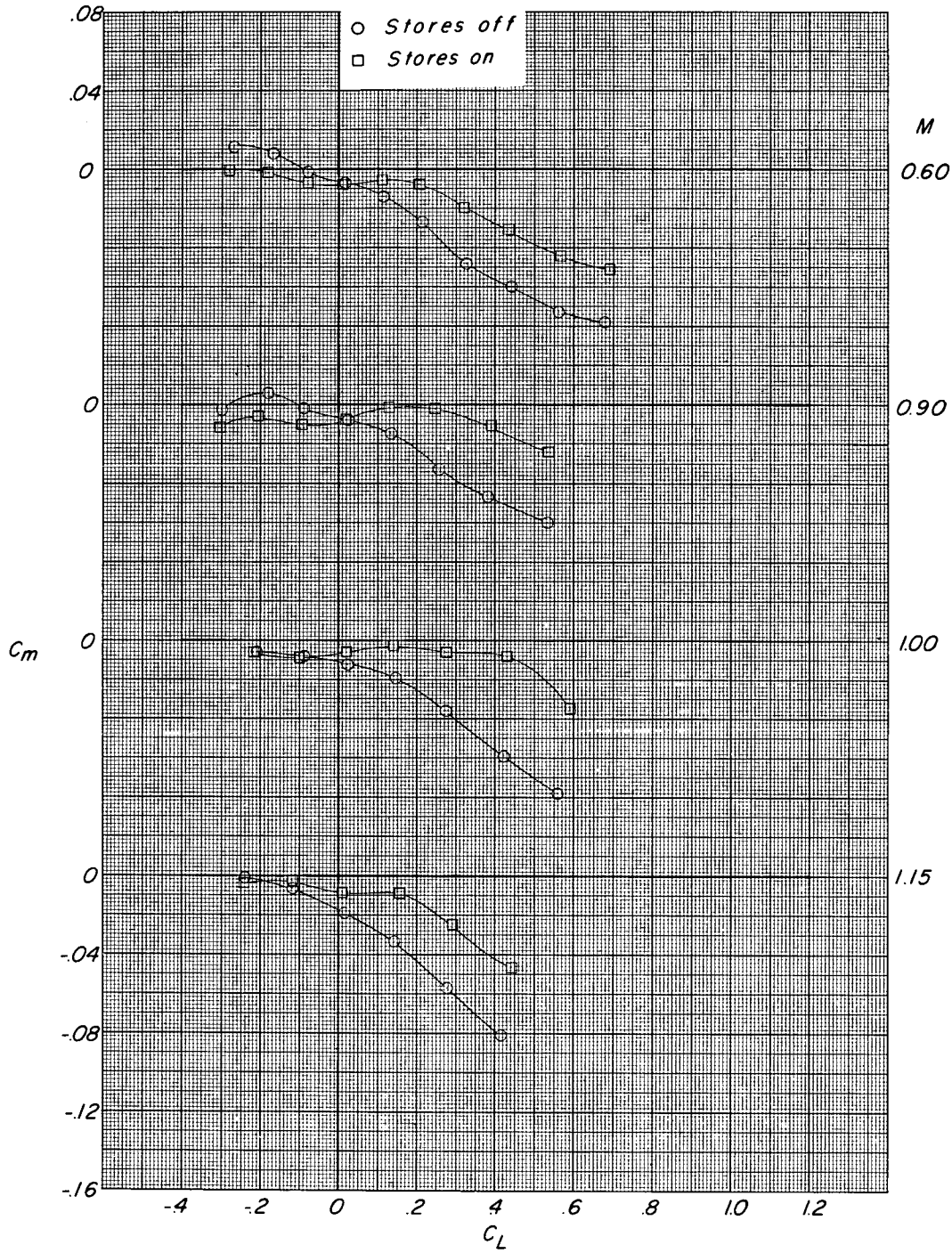

(c) Pitching-moment coefficient.

Figure 16.- Concluded.

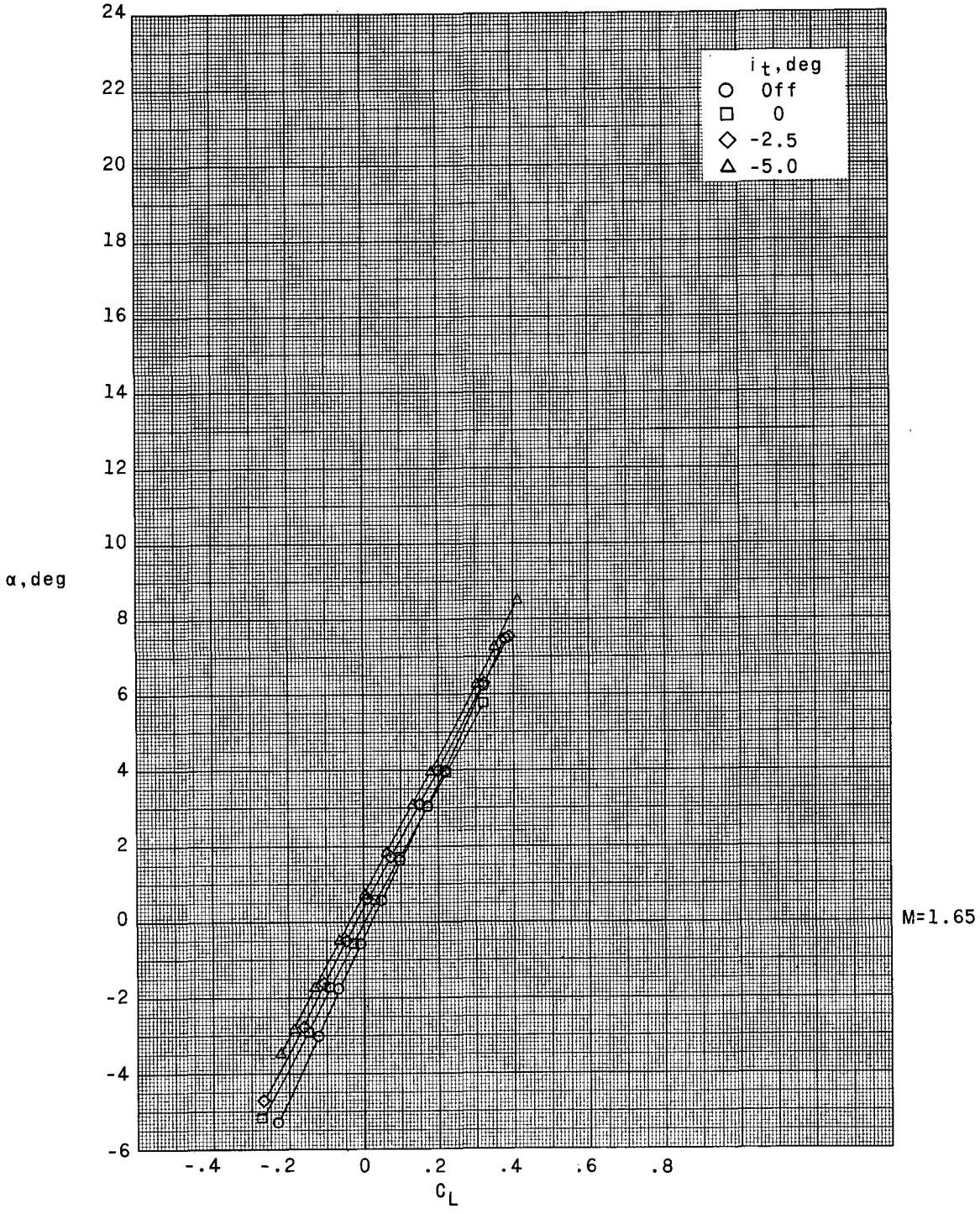

(a) Angle of attack.

Figure 17.- Aerodynamic characteristics for configuration BW_2VH_1N at $\Lambda_{LE} = 55^{\circ}$.

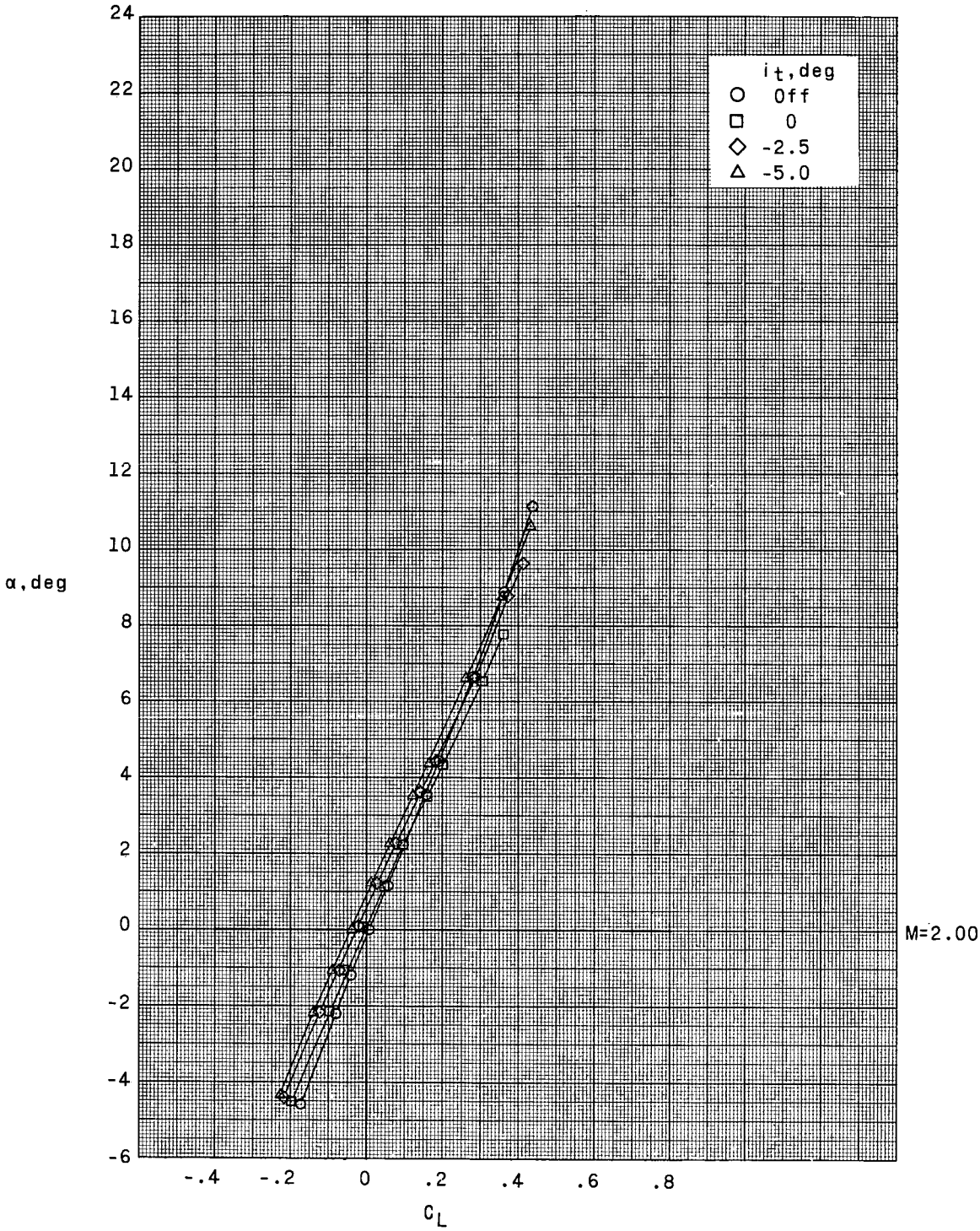

(a) Continued.

Figure 17.- Continued.

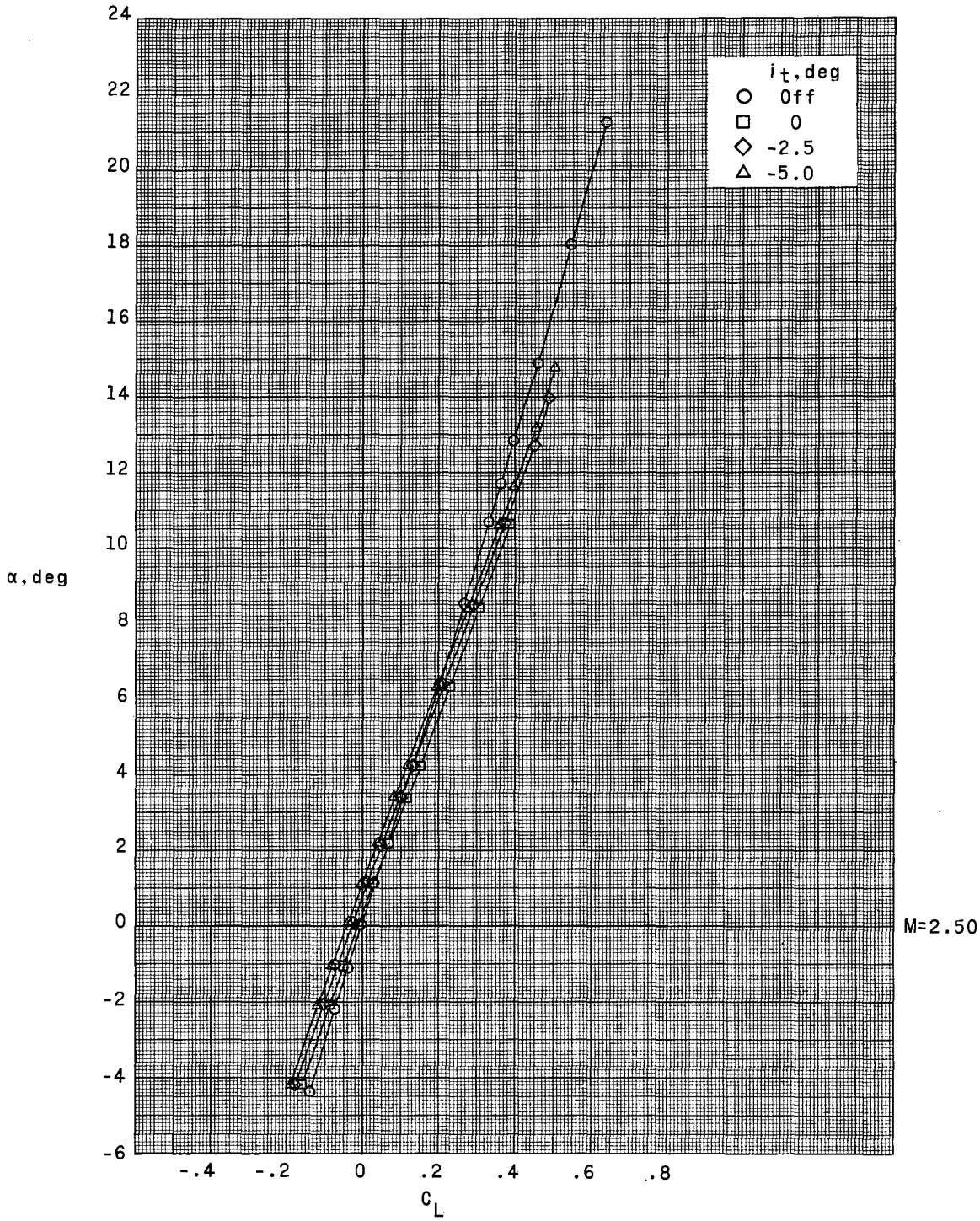

(a) Concluded.

Figure 17.- Continued.

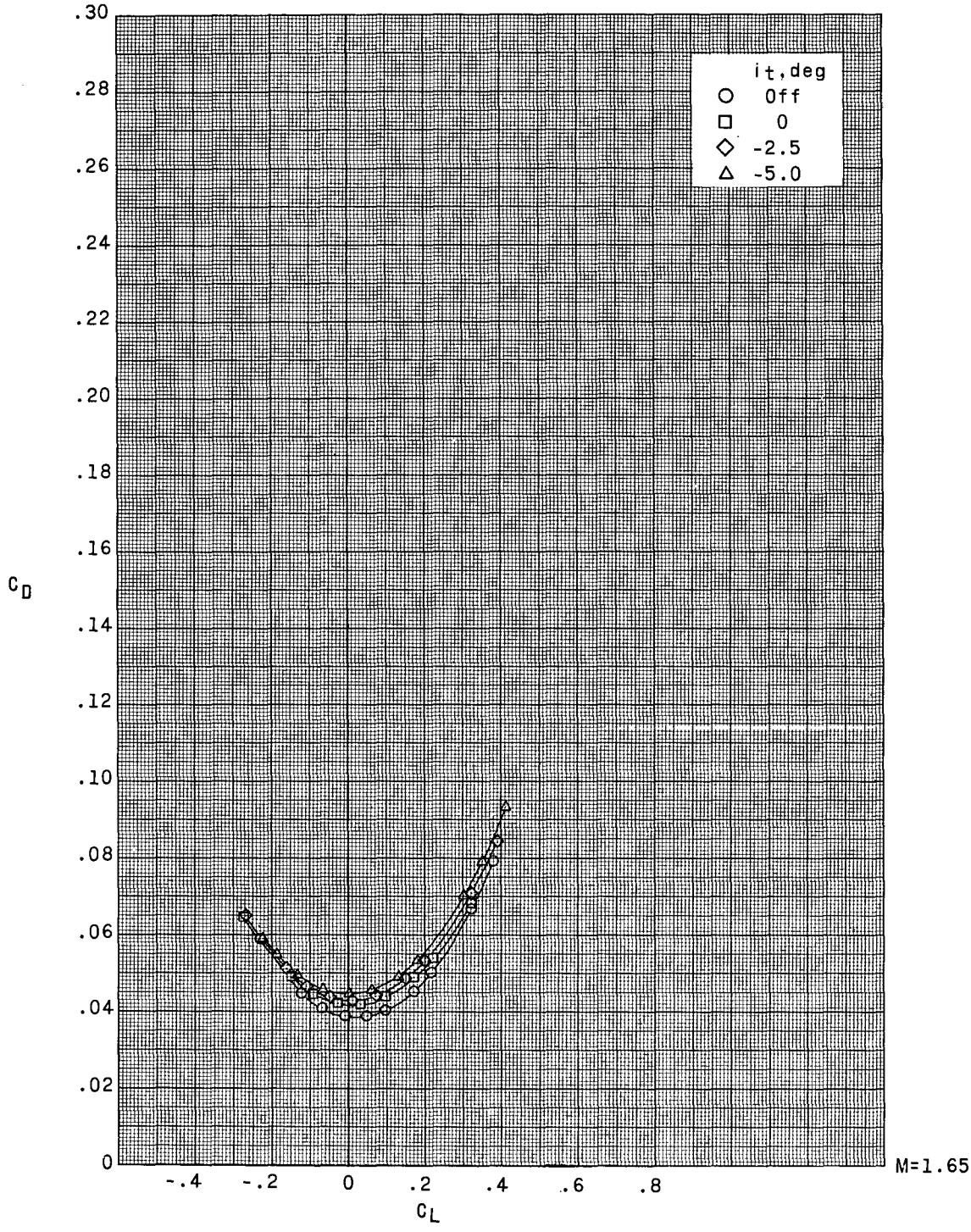

(b) Drag coefficient.

Figure 17.- Continued.

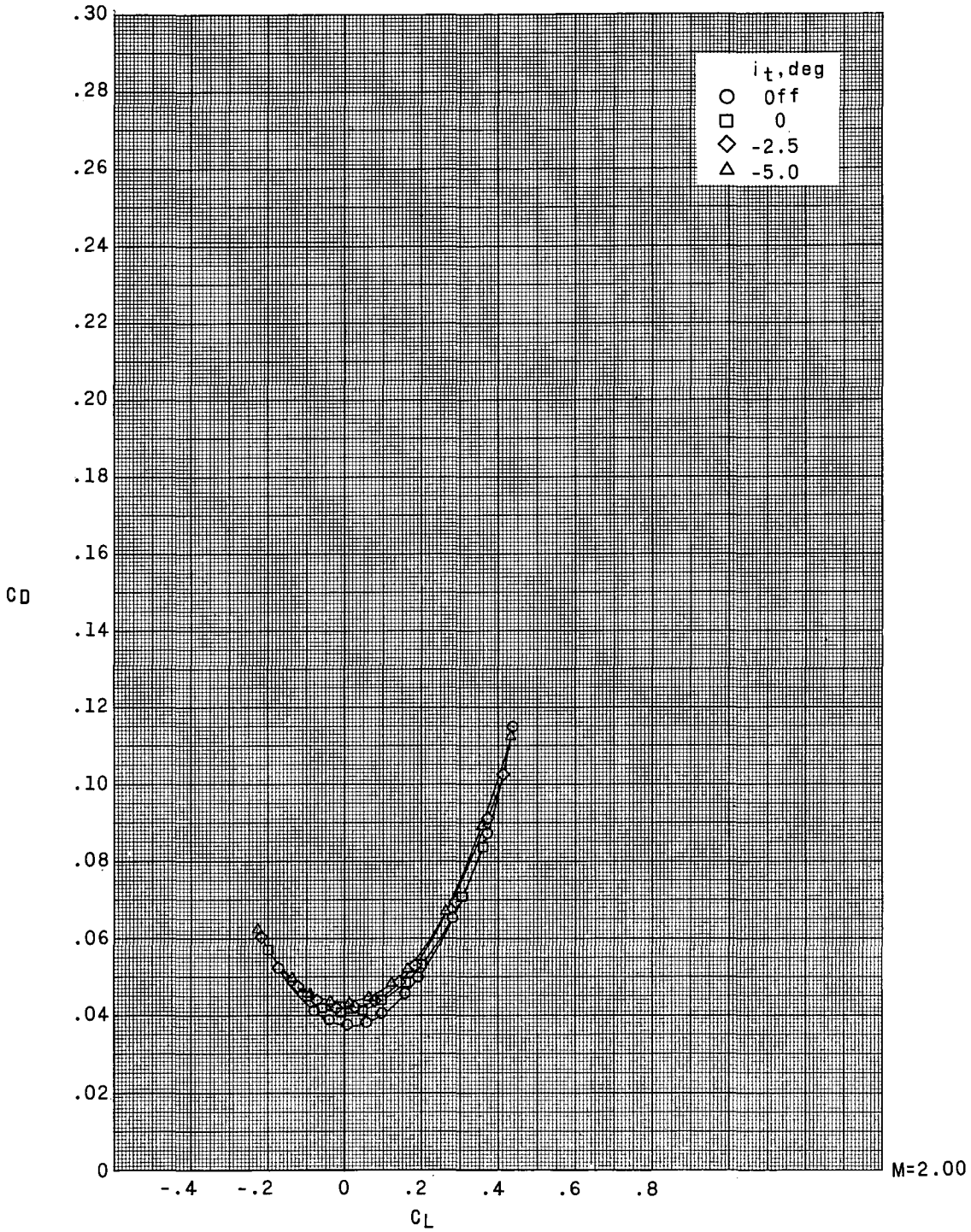

(b) Continued.

Figure 17.- Continued.

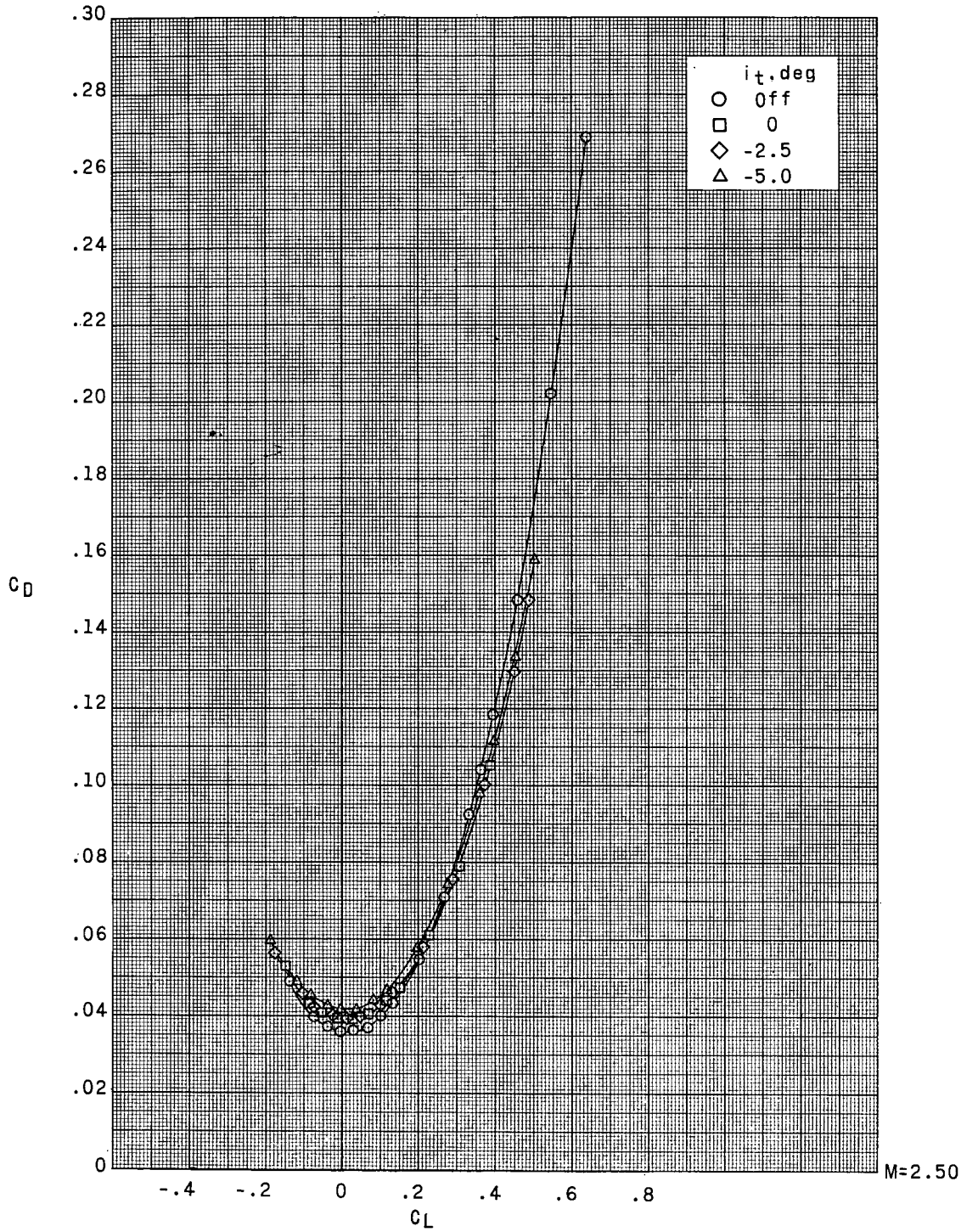

(b) Concluded.

Figure 17.- Continued.

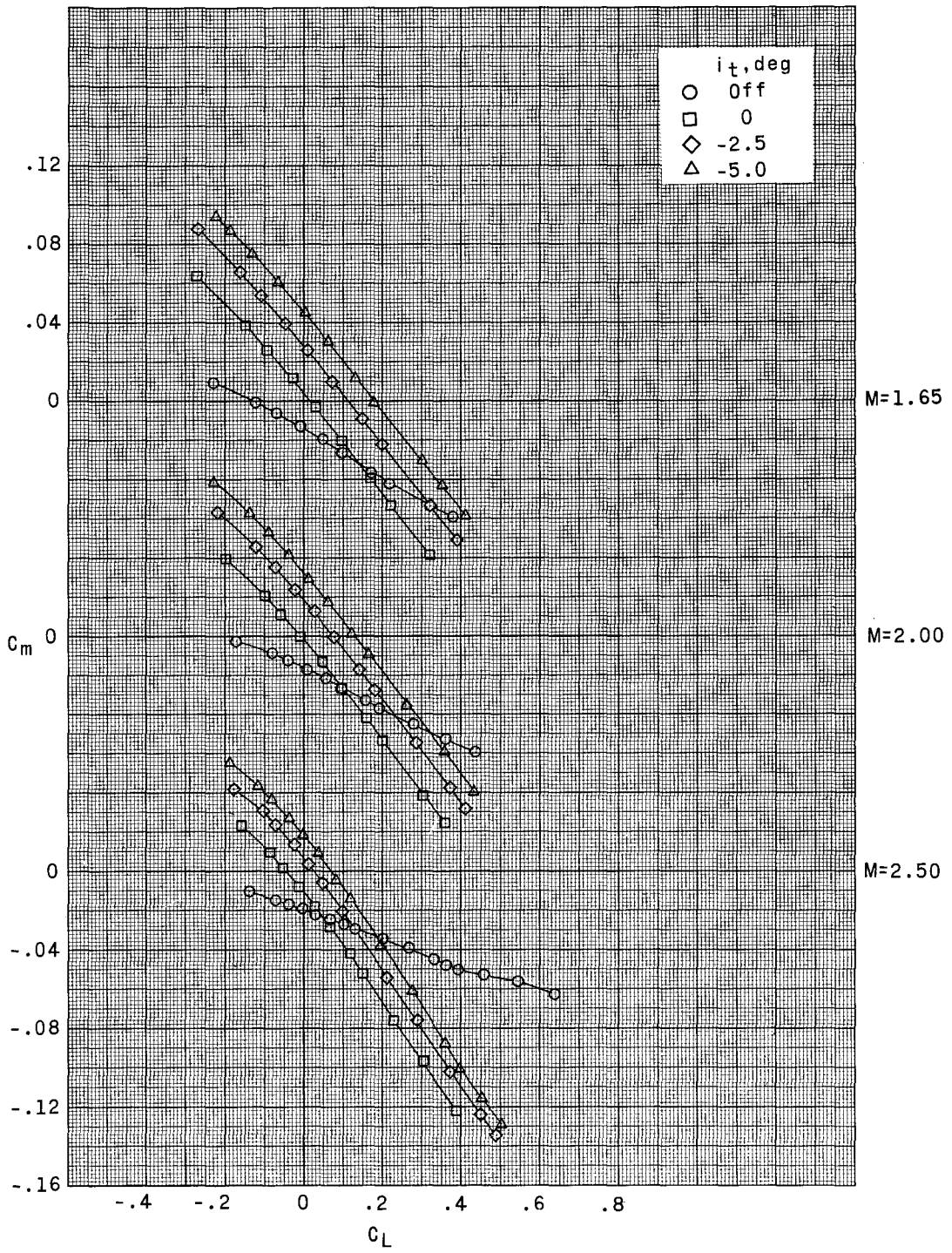

(c) Pitching-moment coefficient.

Figure 17.- Concluded.

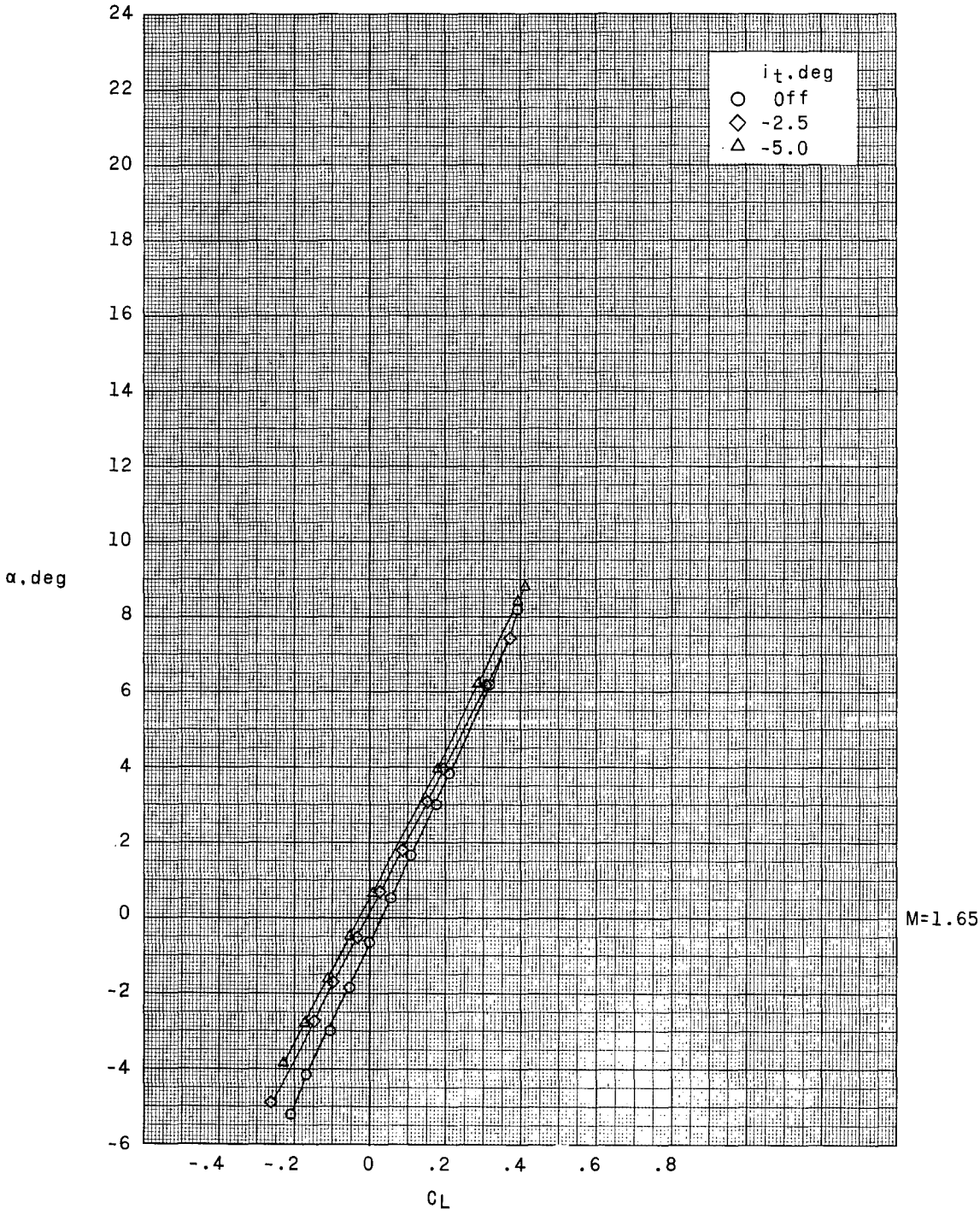

(a) Angle of attack.

Figure 18.- Aerodynamic characteristics for configuration BW_2VH_1N at $\Lambda_{LE} = 65^{\circ}$.

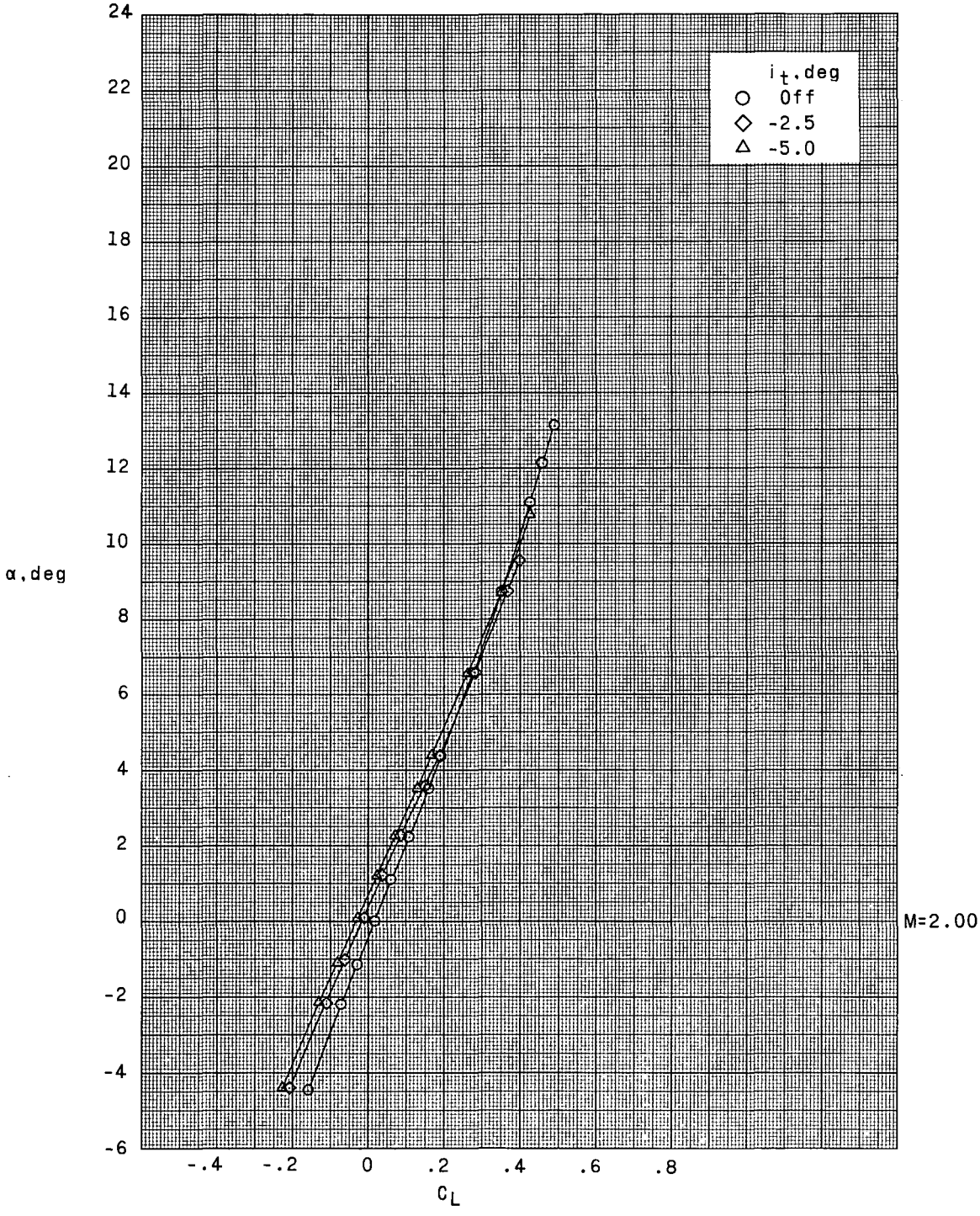

(a) Continued.

Figure 18.- Continued.

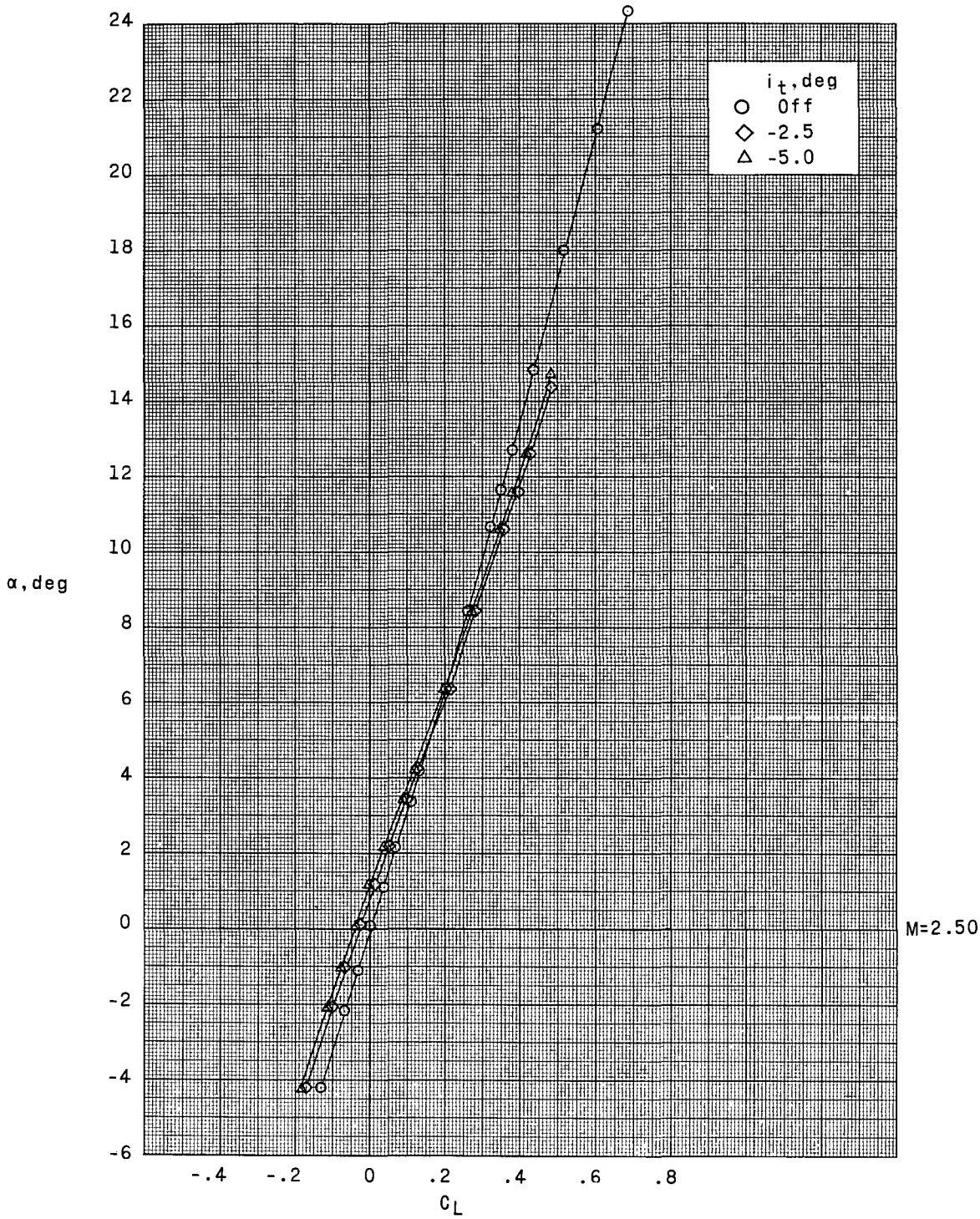

(a) Concluded.

Figure 18.- Continued.

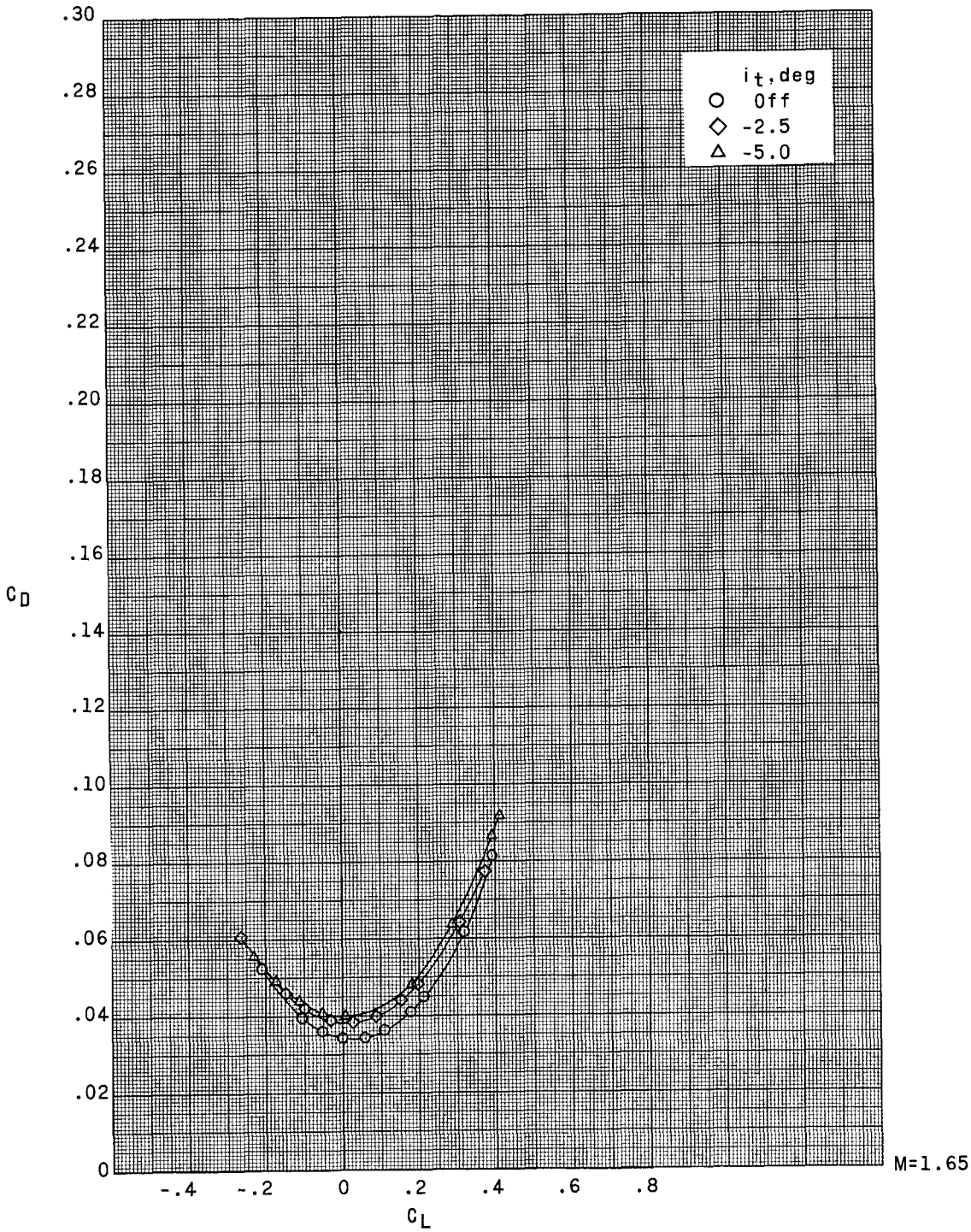

(b) Drag coefficient.

Figure 18.- Continued.

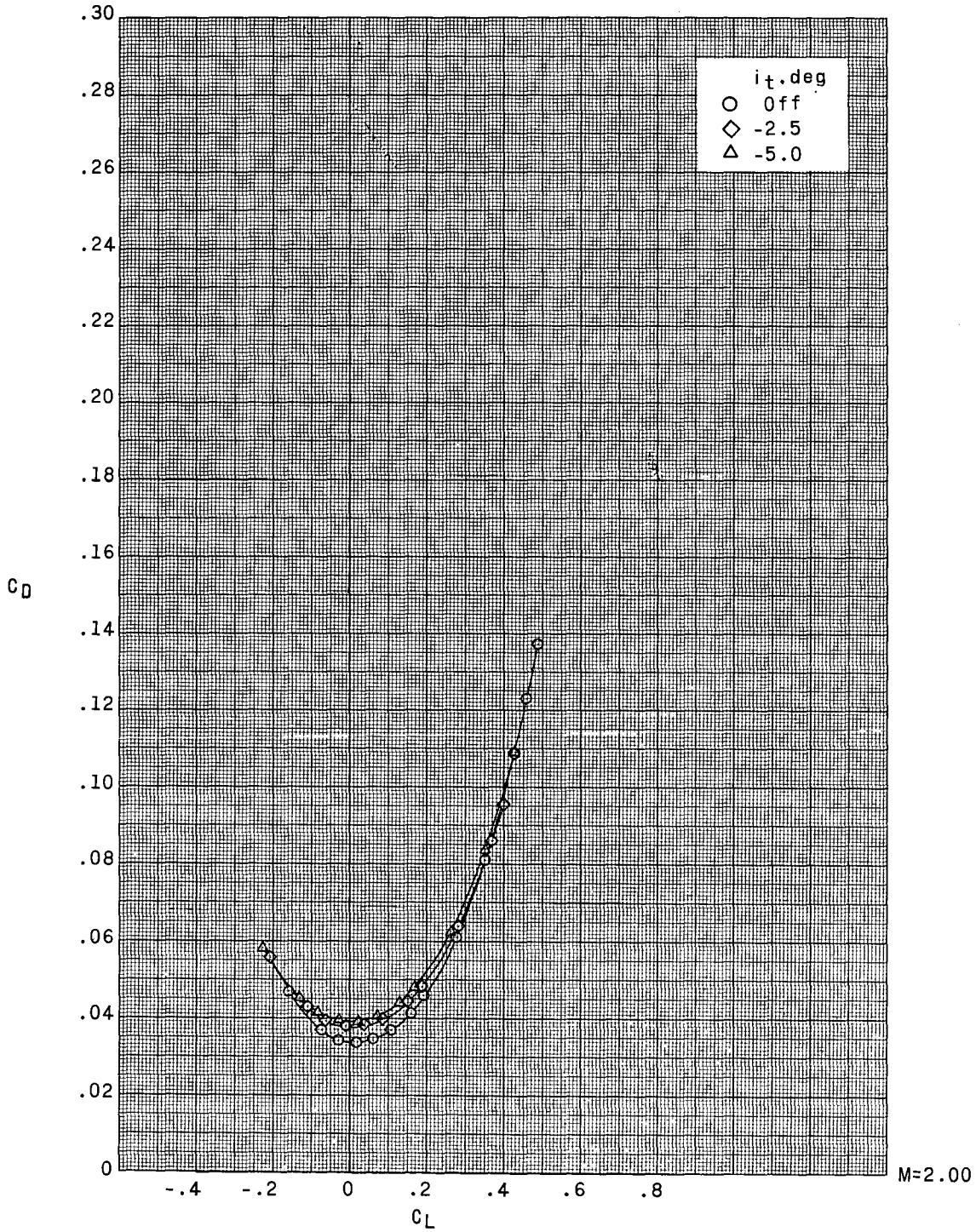

(b) Continued.

Figure 18.- Continued.

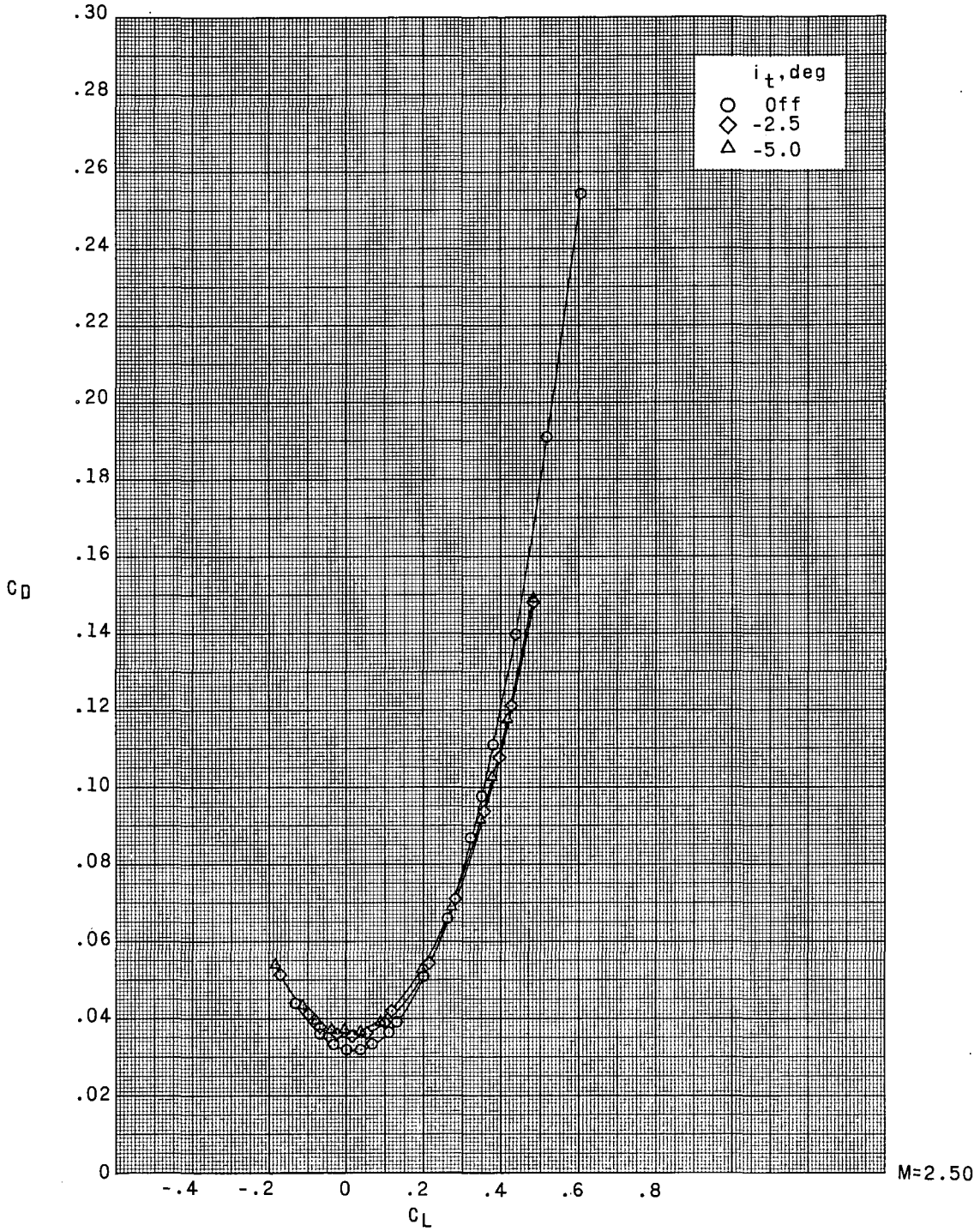

(b) Concluded.

Figure 18.- Continued.

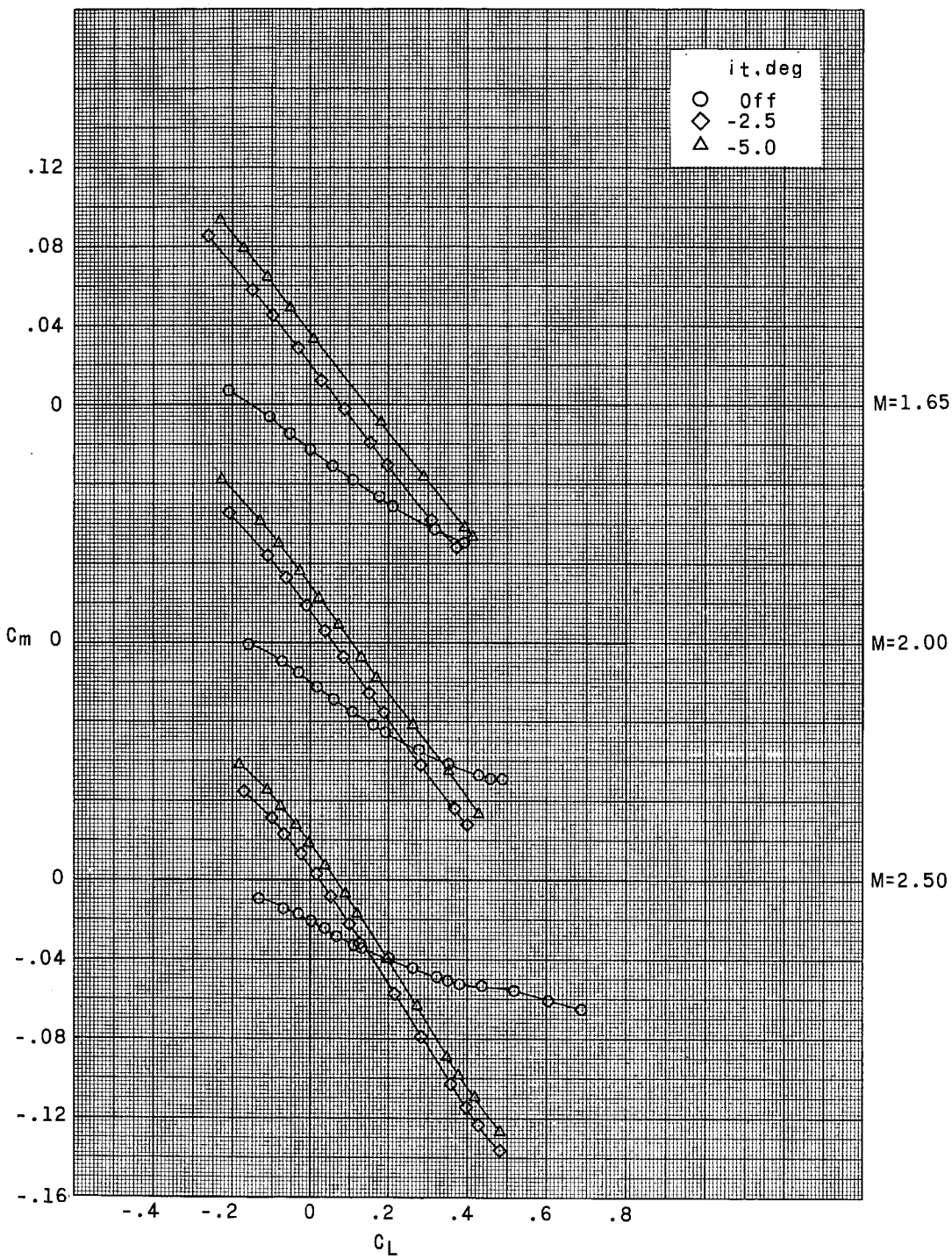

(c) Pitching-moment coefficient.

Figure 18.- Concluded.

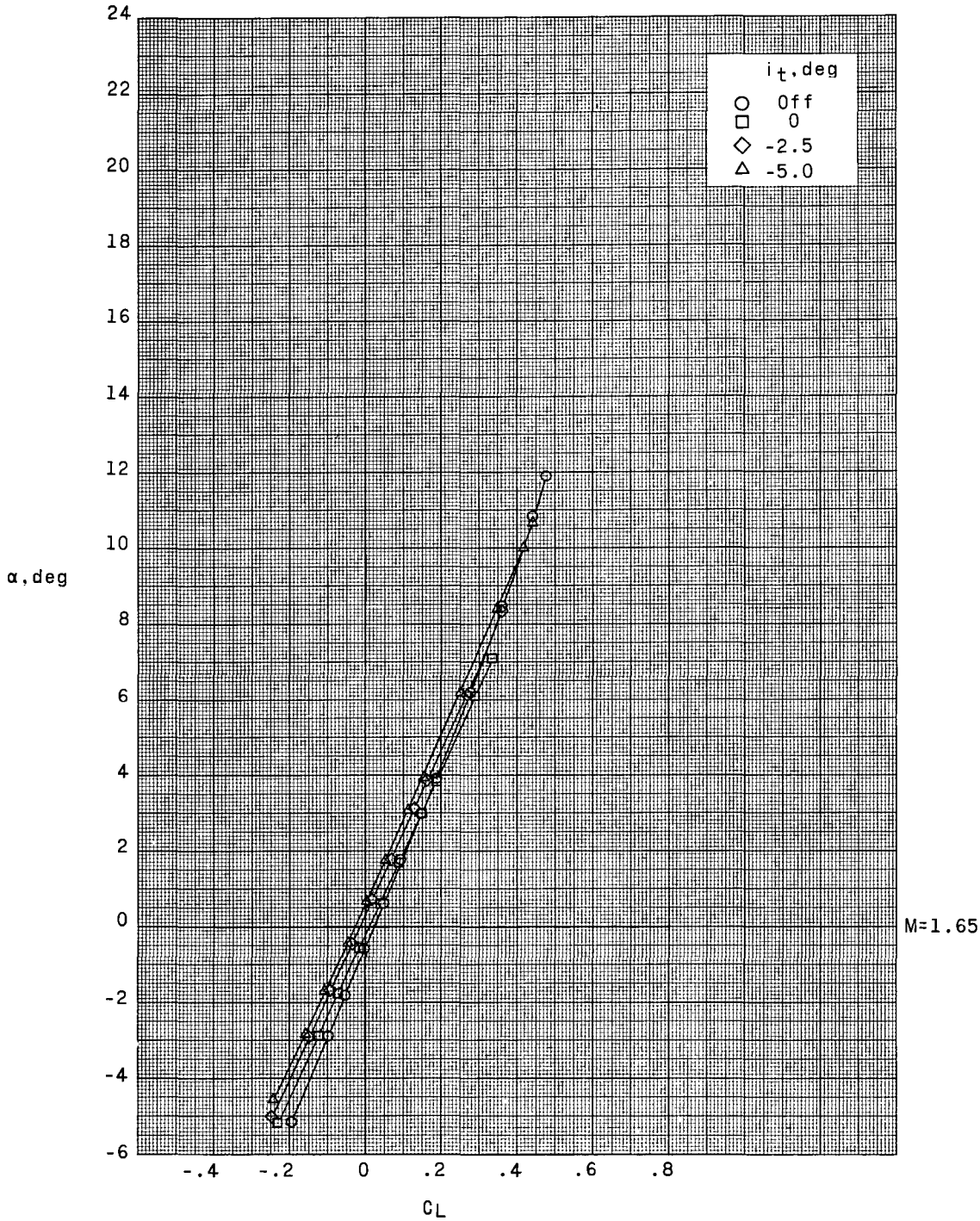

(a) Angle of attack.

Figure 19.- Aerodynamic characteristics for configuration BW_2VH_1N at $\Lambda_{LE} = 75^{\circ}$.

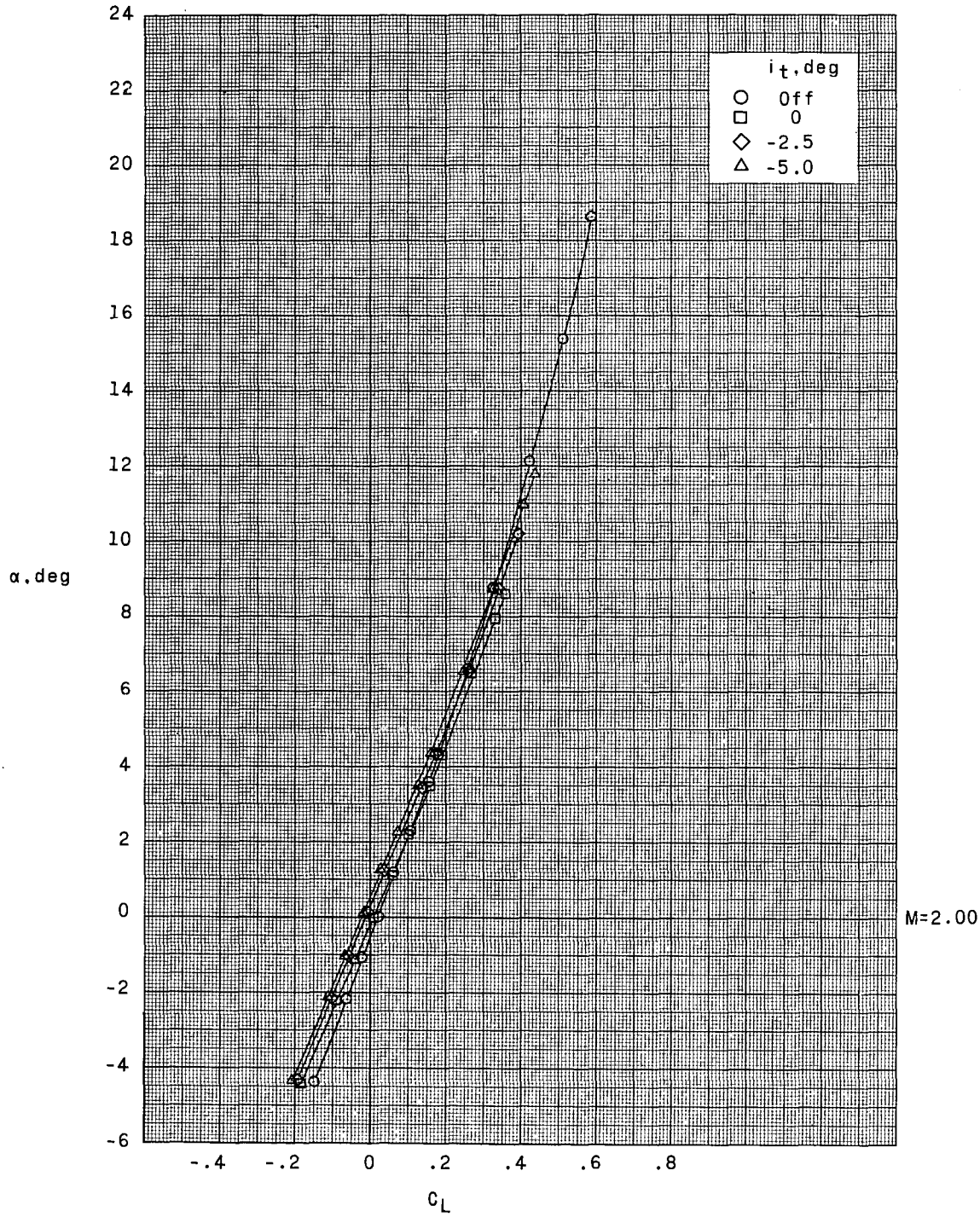

(a) Continued.

Figure 19.- Continued.

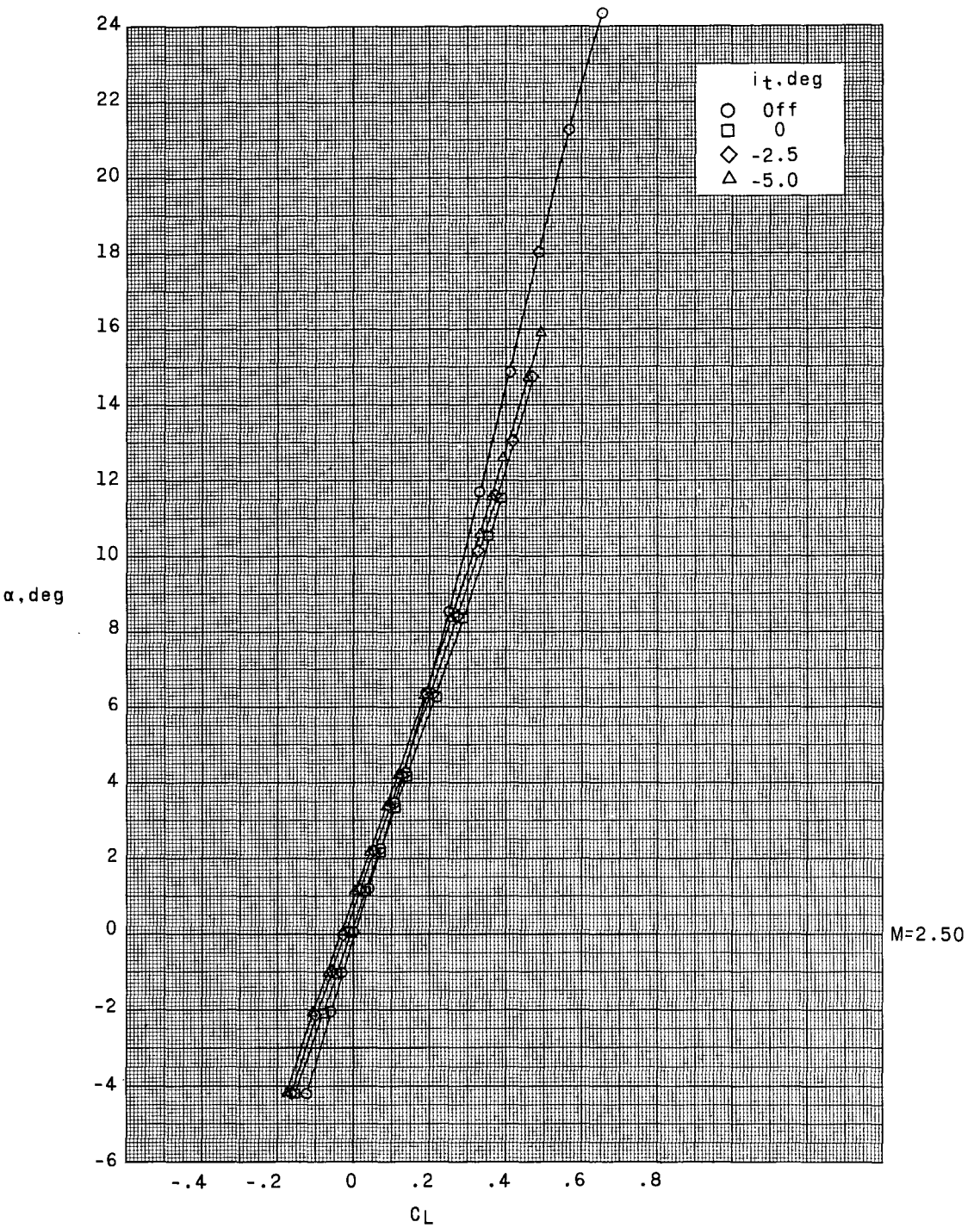

(a) Concluded.

Figure 19.- Continued.

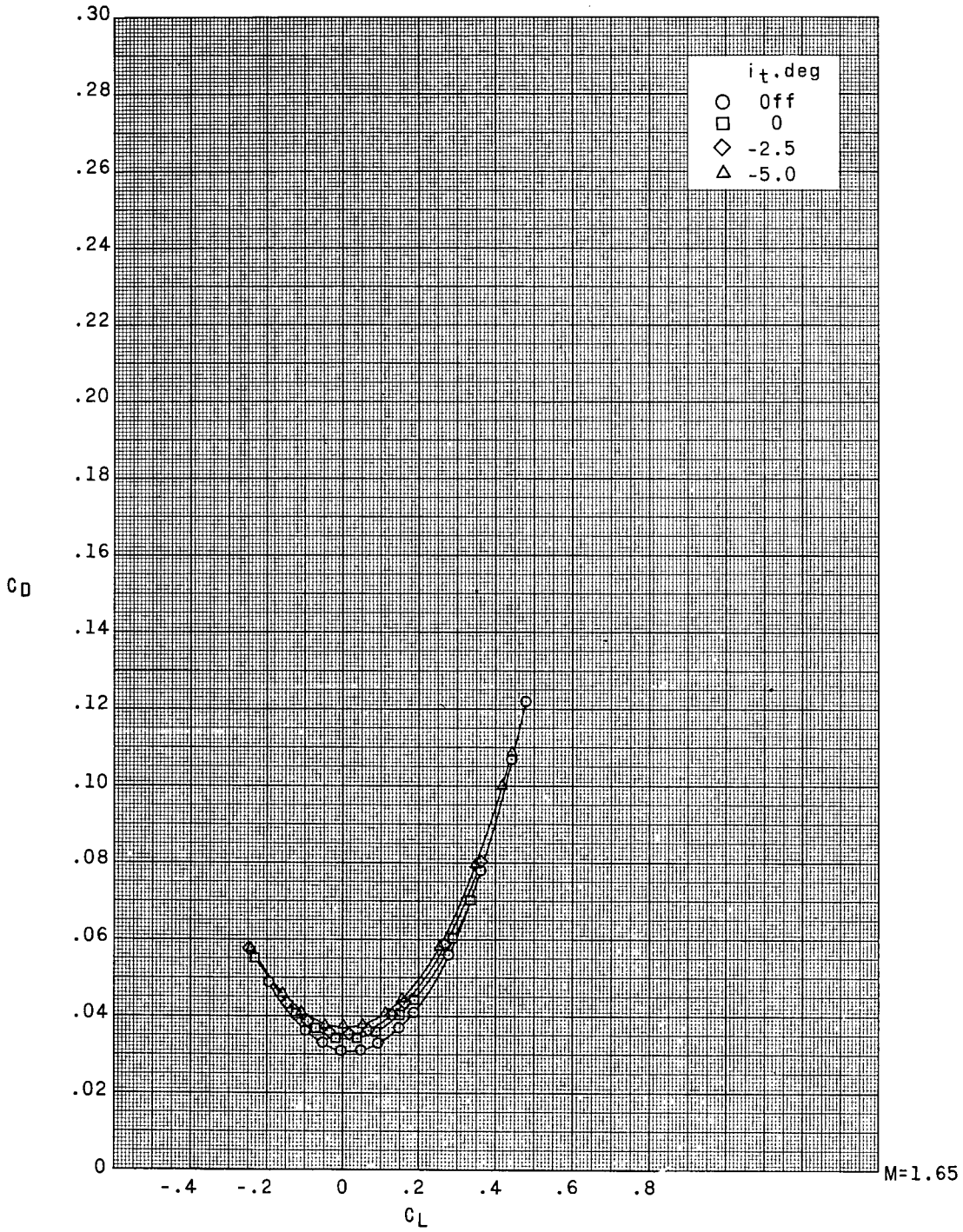

(b) Drag coefficient.

Figure 19.- Continued.

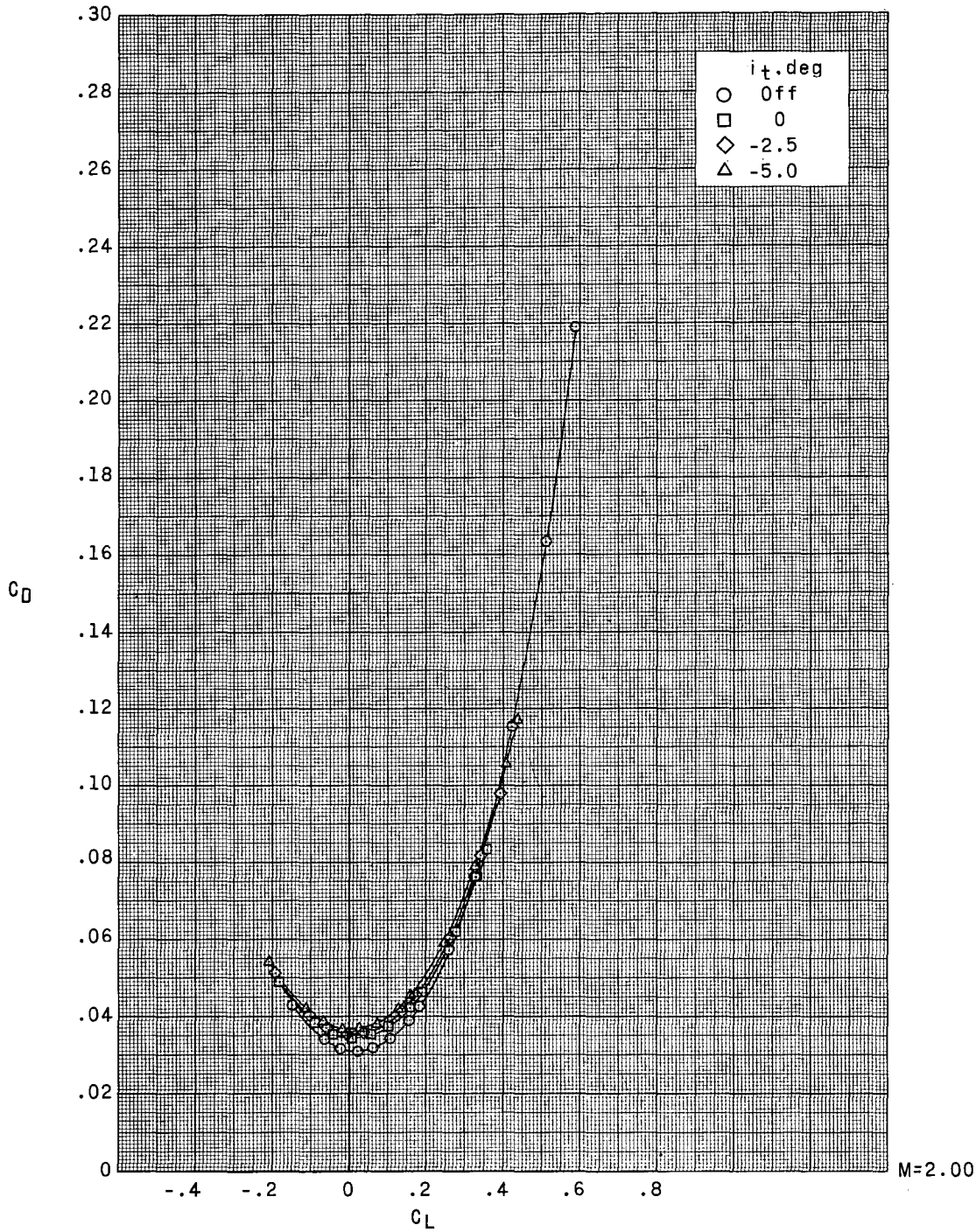

(b) Continued.

Figure 19.- Continued.

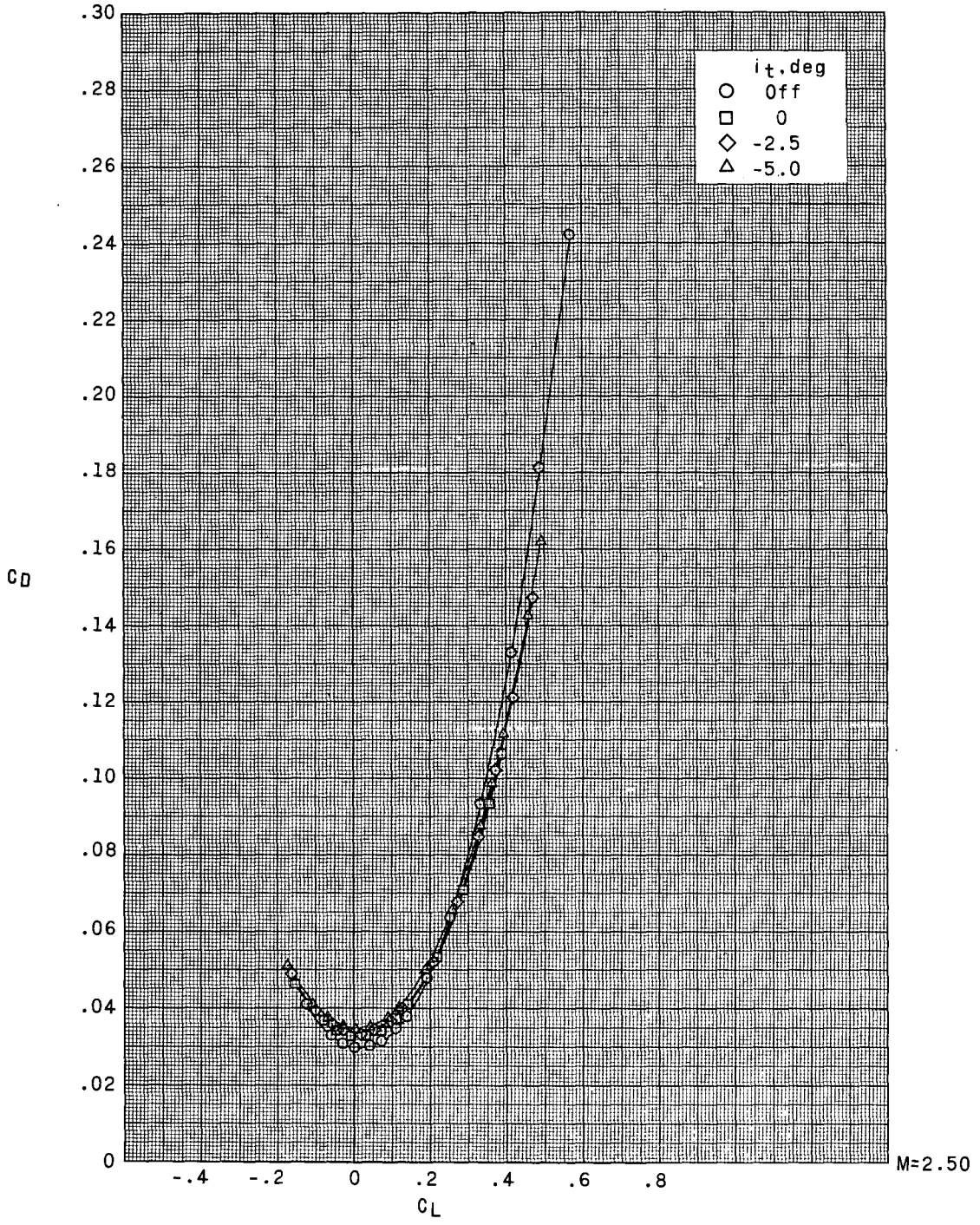

(b) Concluded.

Figure 19.- Continued.

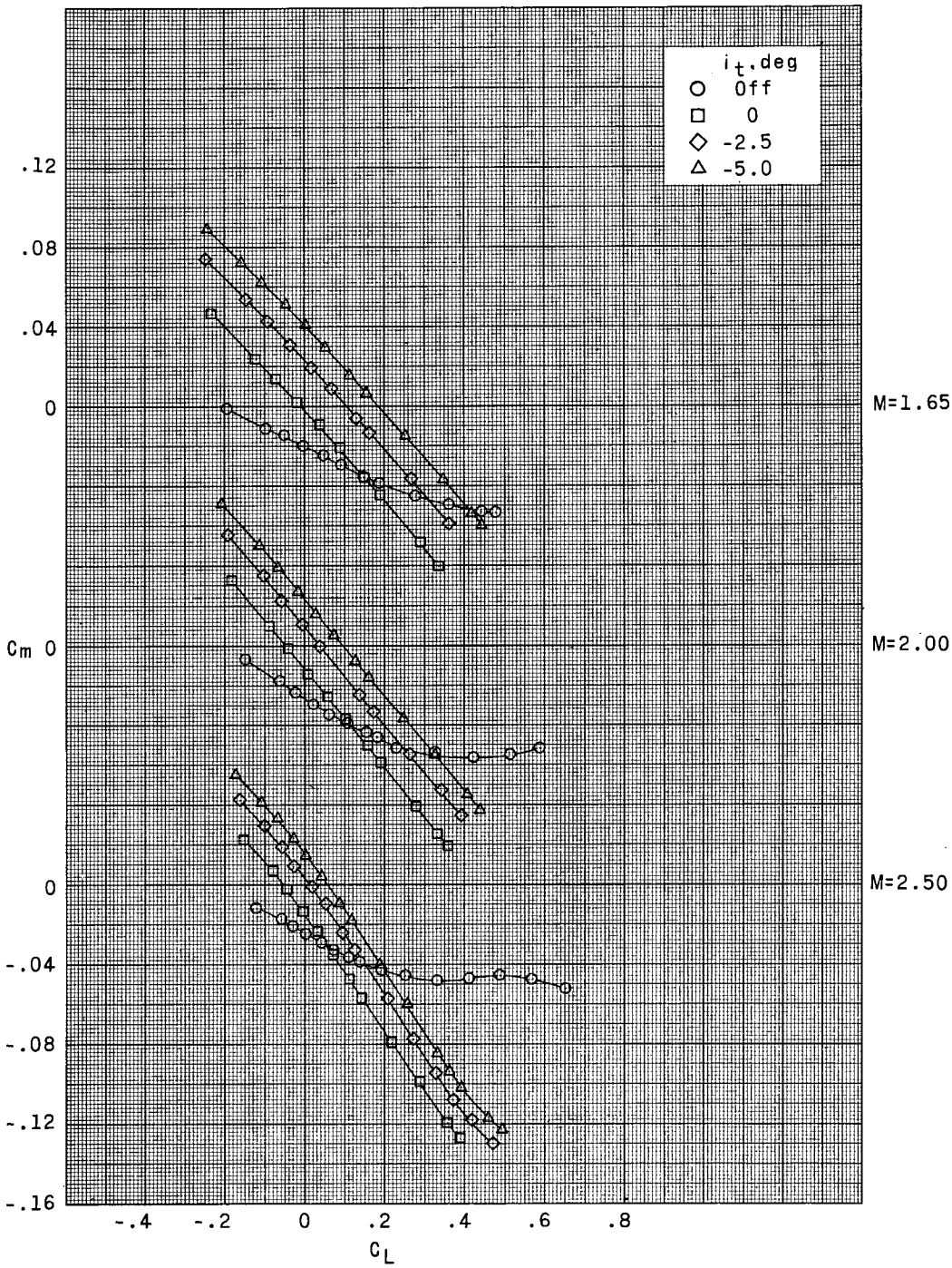

(c) Pitching-moment coefficient.

Figure 19.- Concluded.

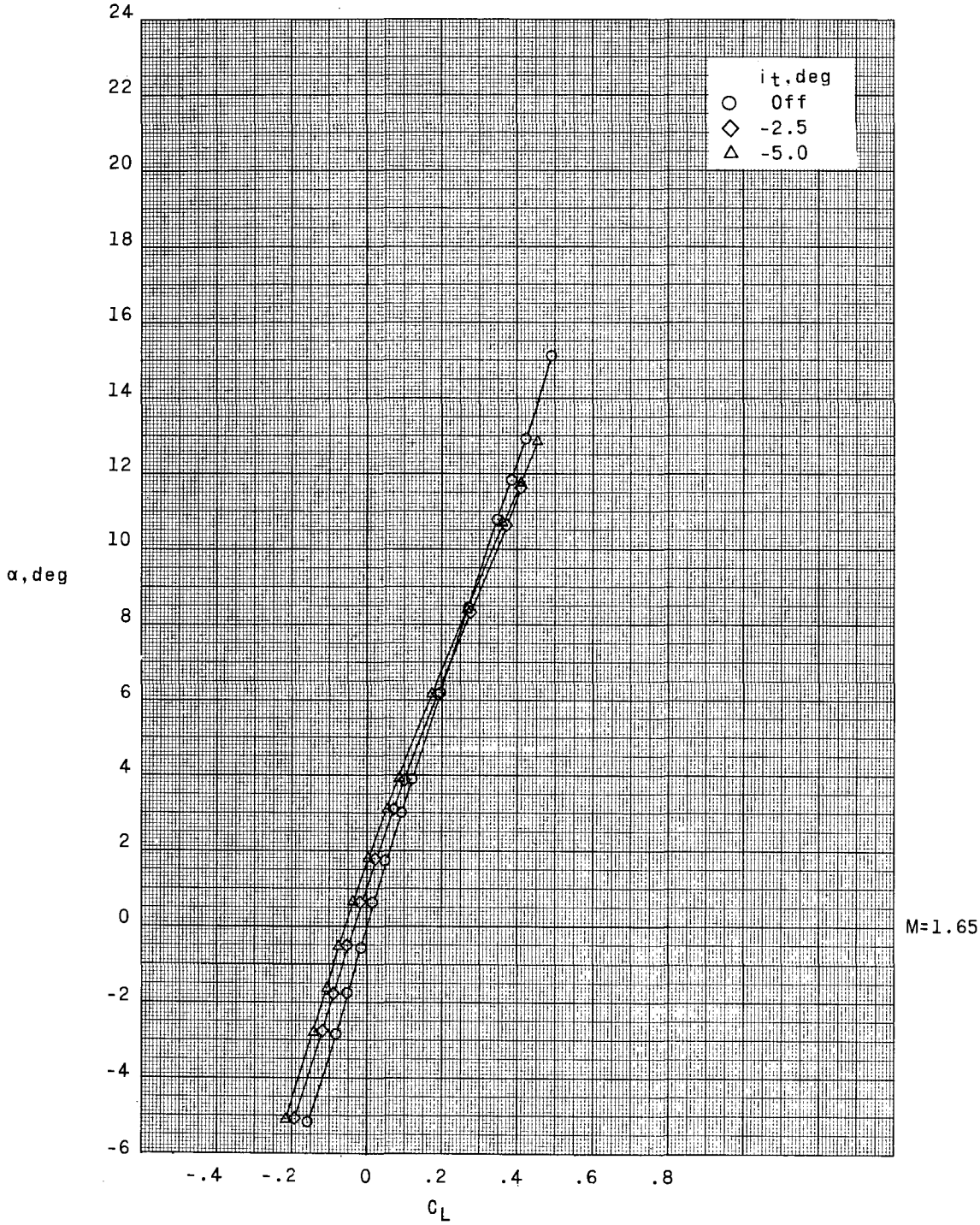

(a) Angle of attack.

Figure 20.- Aerodynamic characteristics for configuration BW_2VH_1N at $\Lambda_{LE} = 90^{\circ}$.

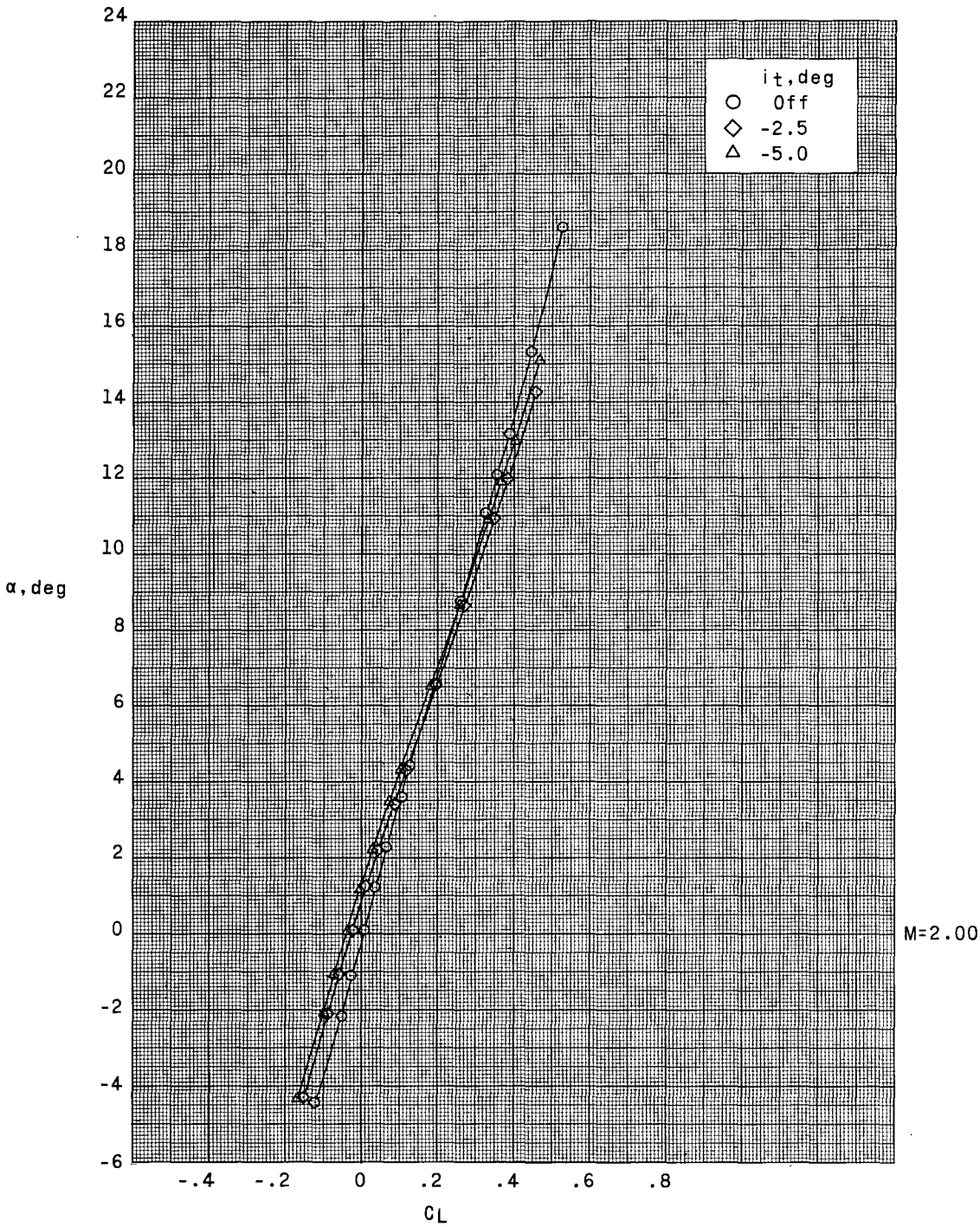

(a) Continued.

Figure 20.- Continued.

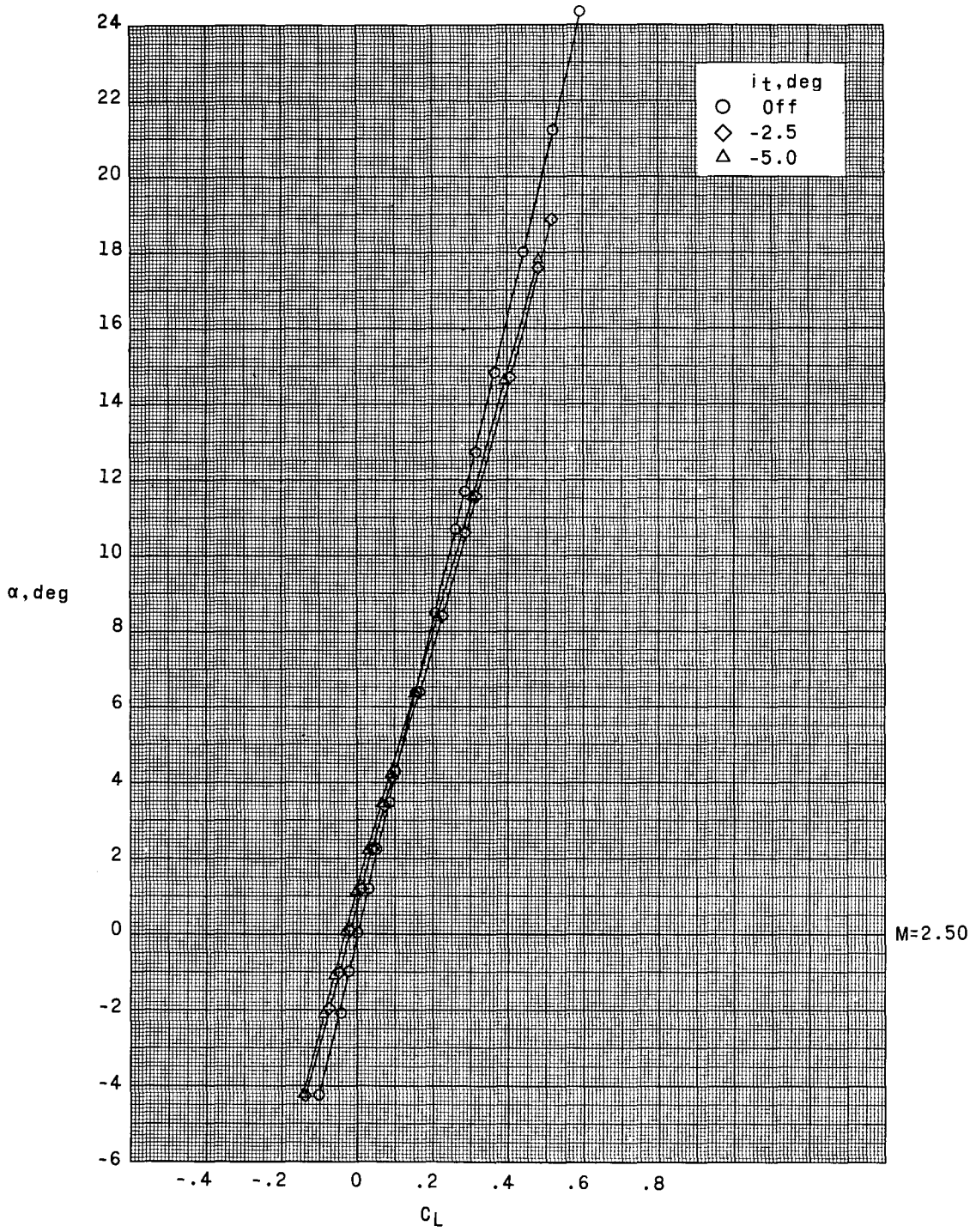

(a) Concluded.

Figure 20.- Continued.

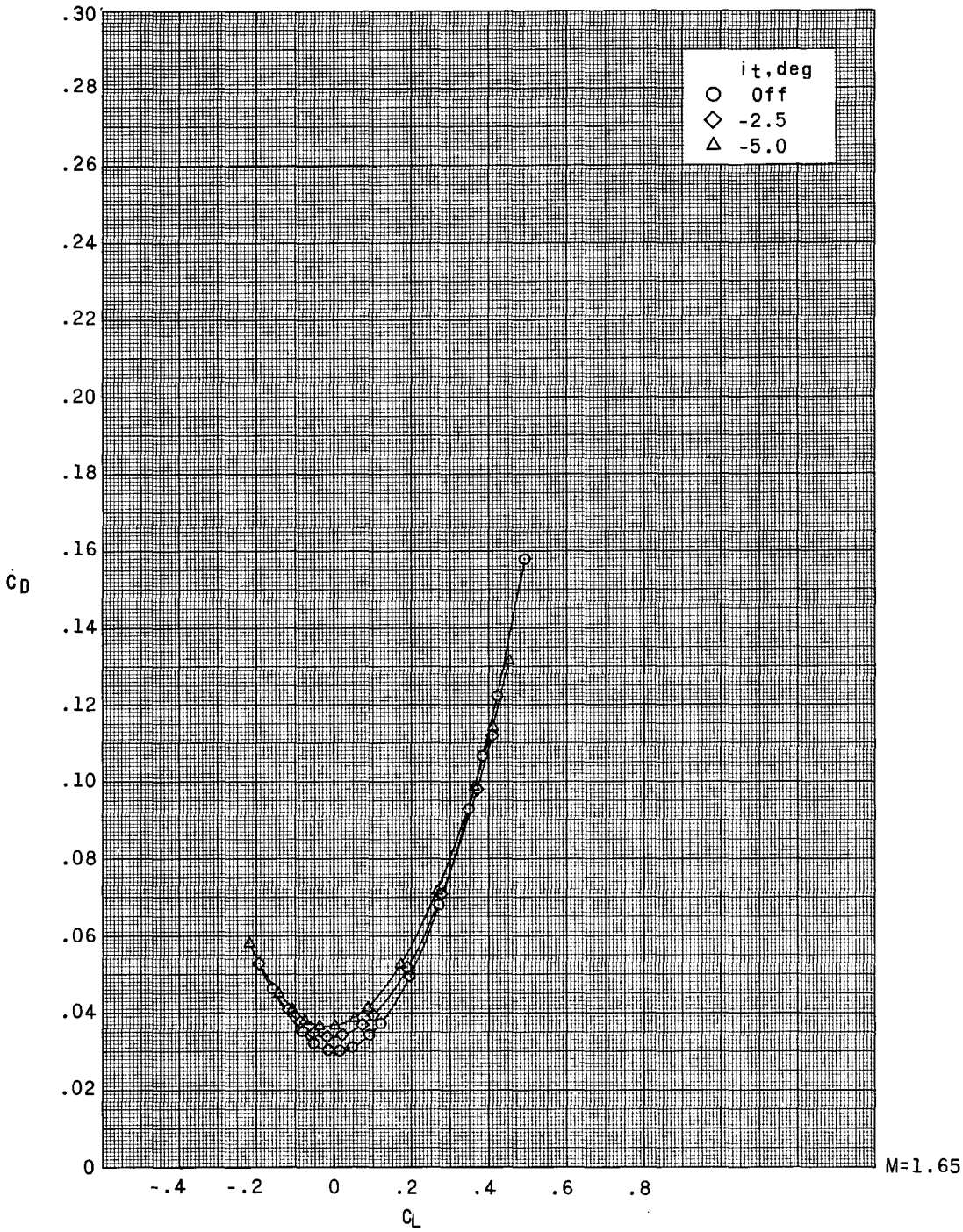

(b) Drag coefficient.

Figure 20.- Continued.

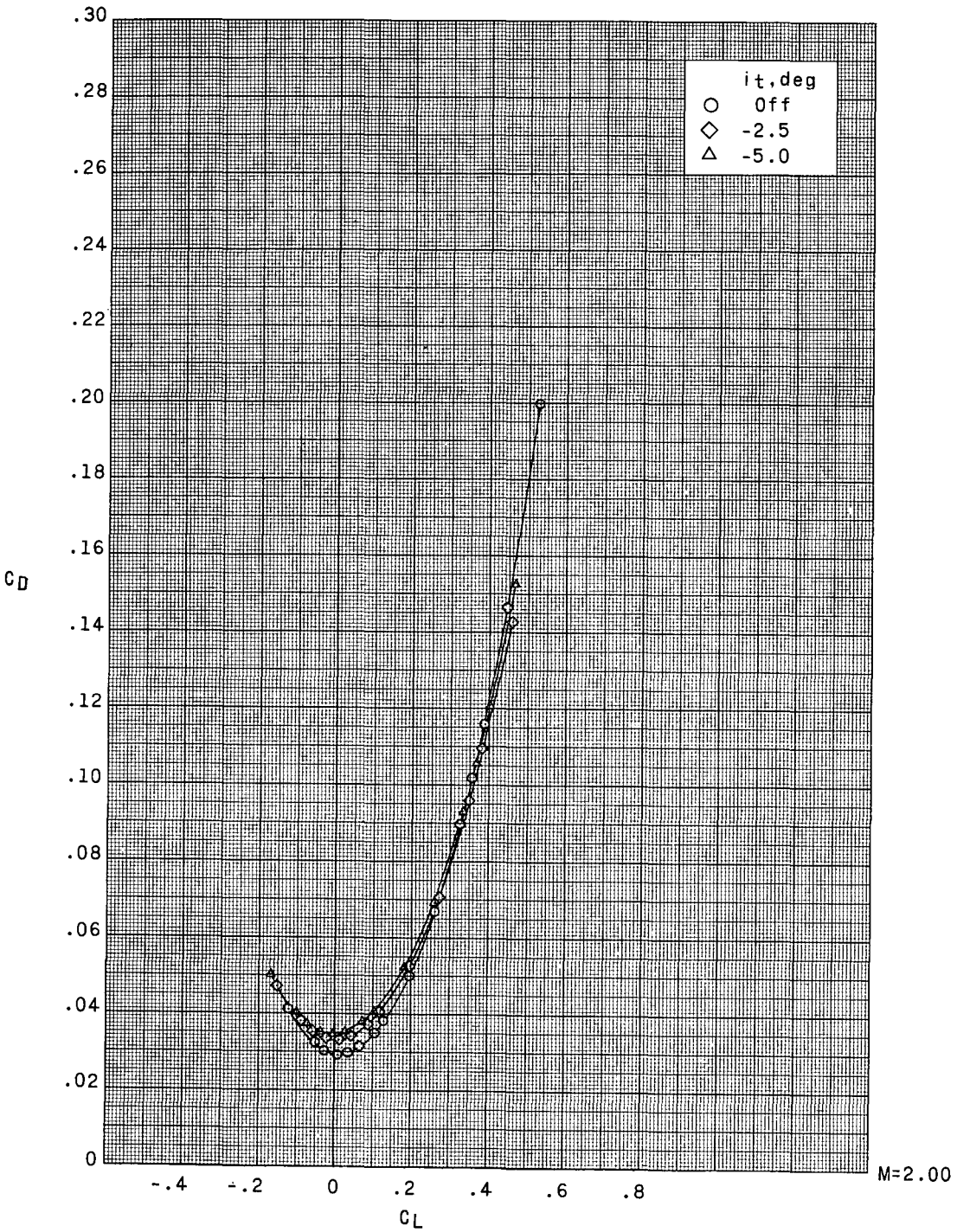

(b) Continued.

Figure 20.- Continued.

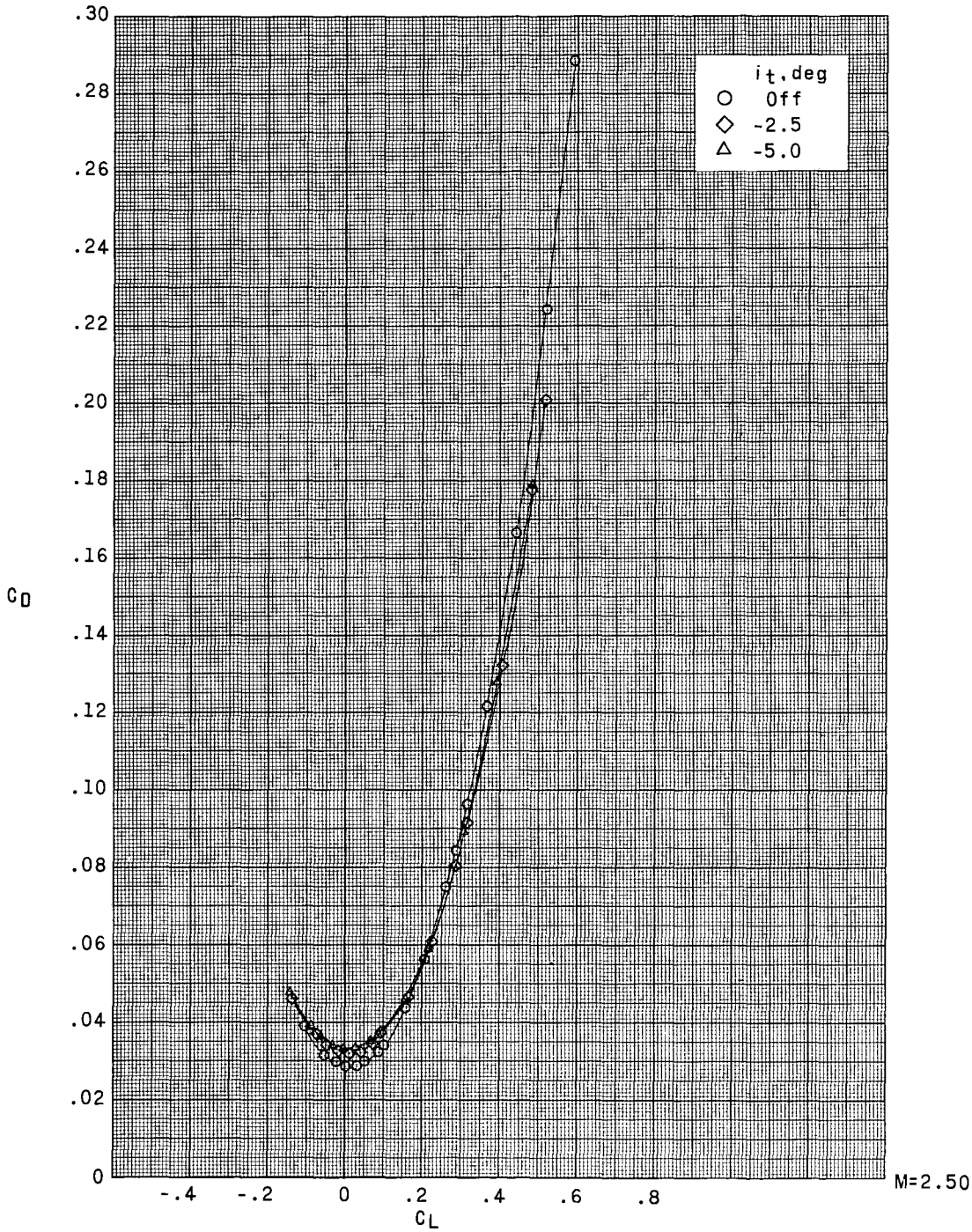

(b) Concluded.

Figure 20.- Continued.

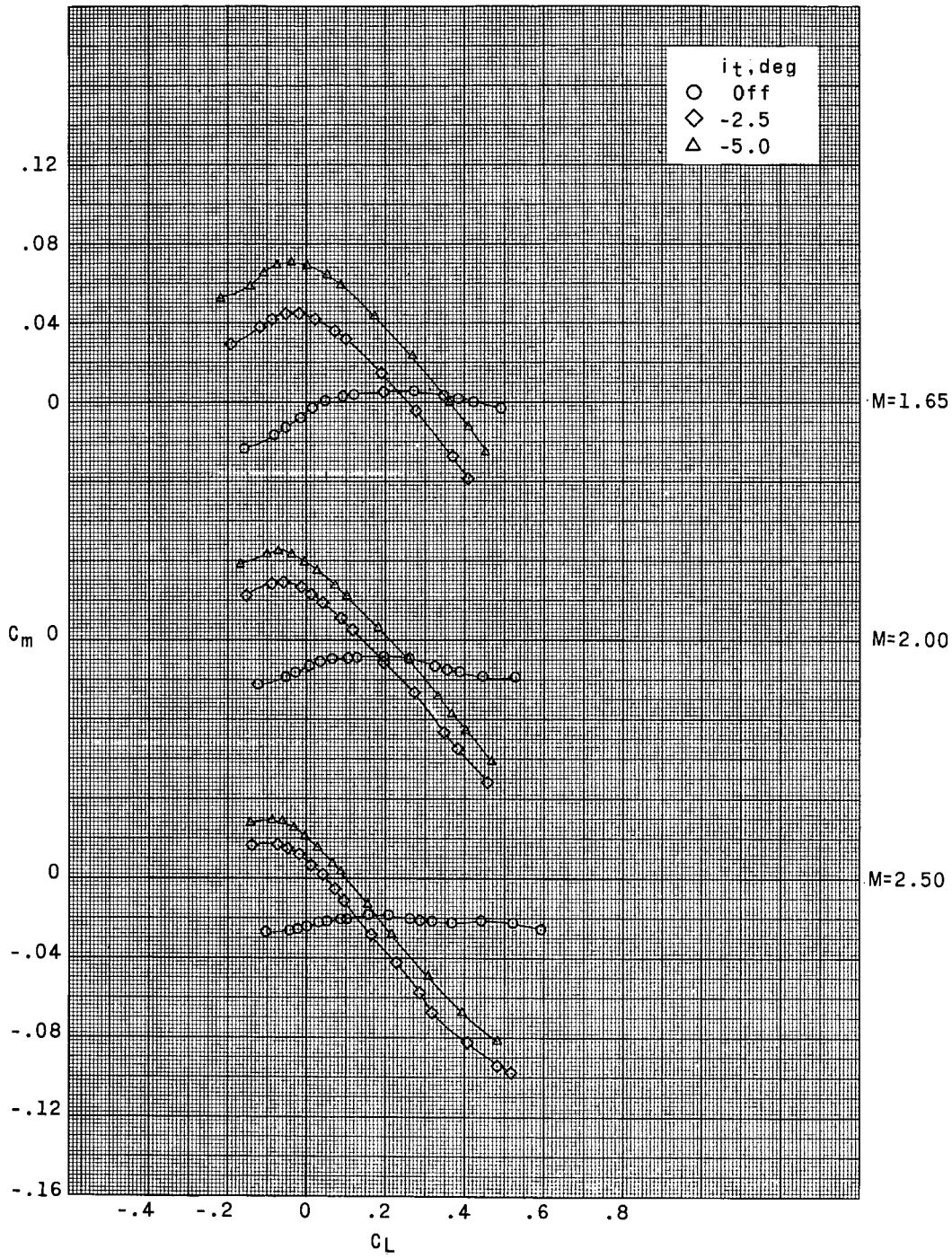

(c) Pitching-moment coefficient.

Figure 20.- Concluded.

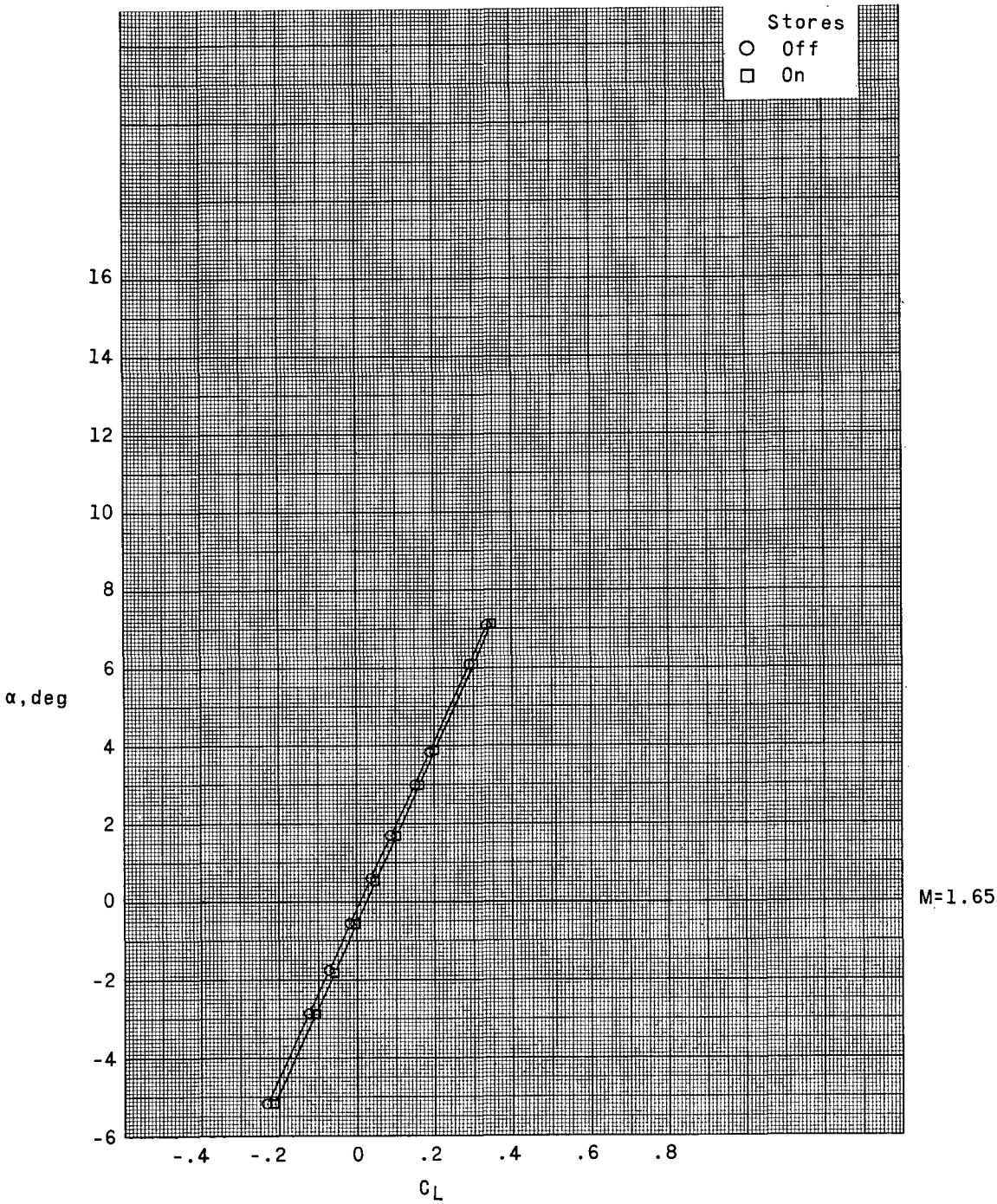

(a) Angle of attack.

Figure 21.- Effect of the addition of two GAR-8 stores at each wing-pivot point on the aerodynamic characteristics for configuration BW_2VH_1N at $\Lambda_{LE} = 75^{\circ}$ and $i_t = 0^{\circ}$.

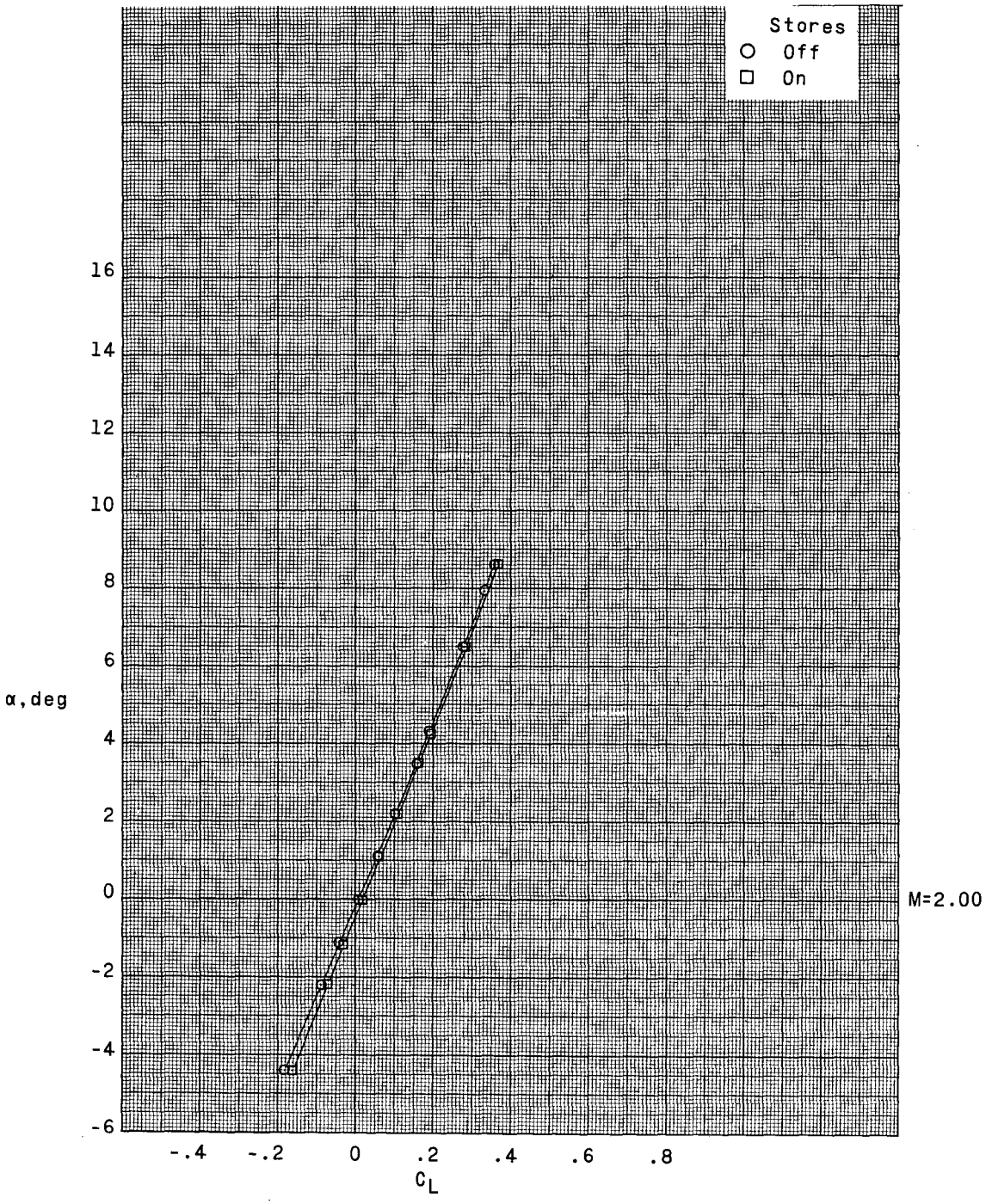

(a) Continued.

Figure 21.- Continued.

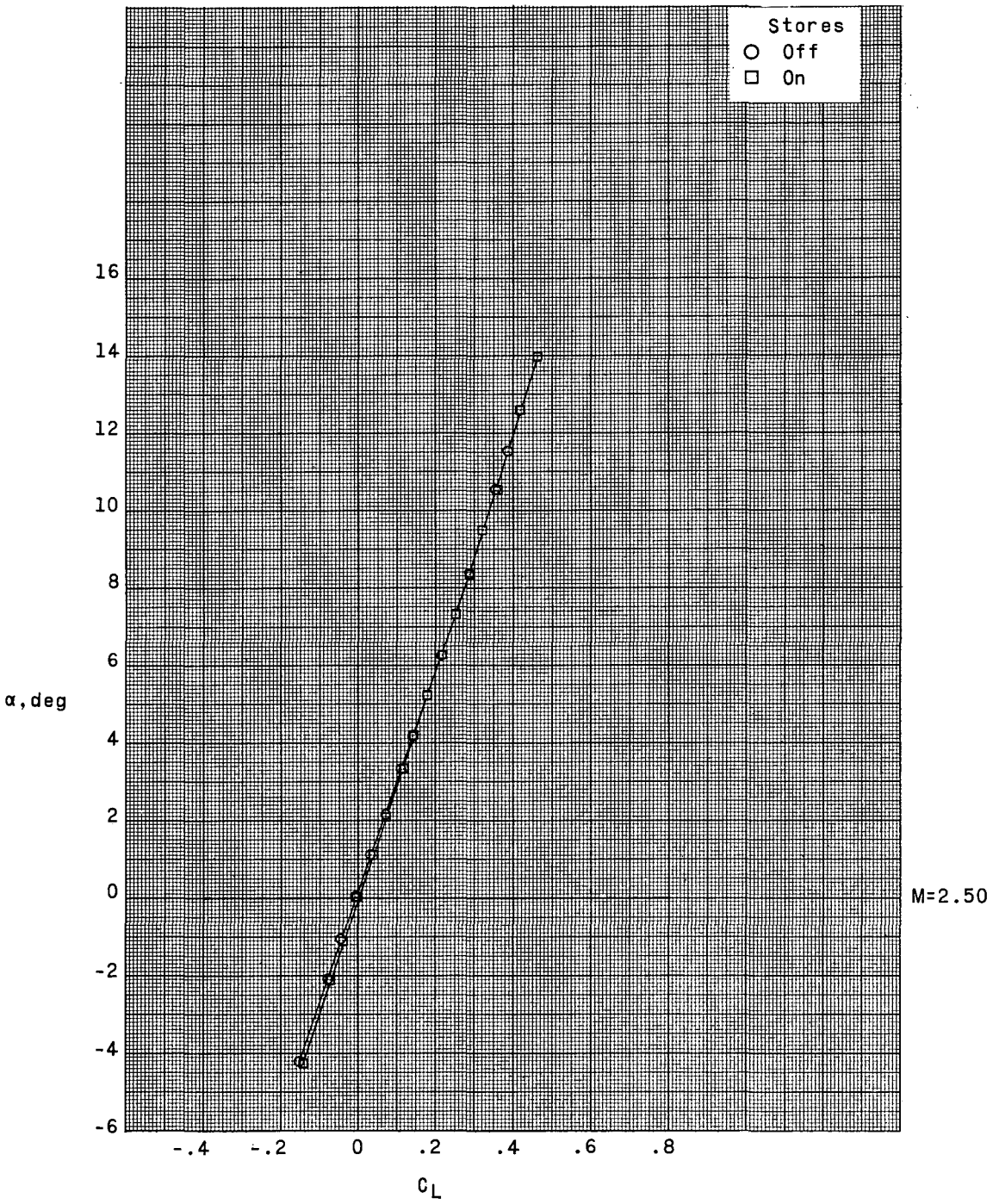

(a) Concluded.

Figure 21.- Continued.

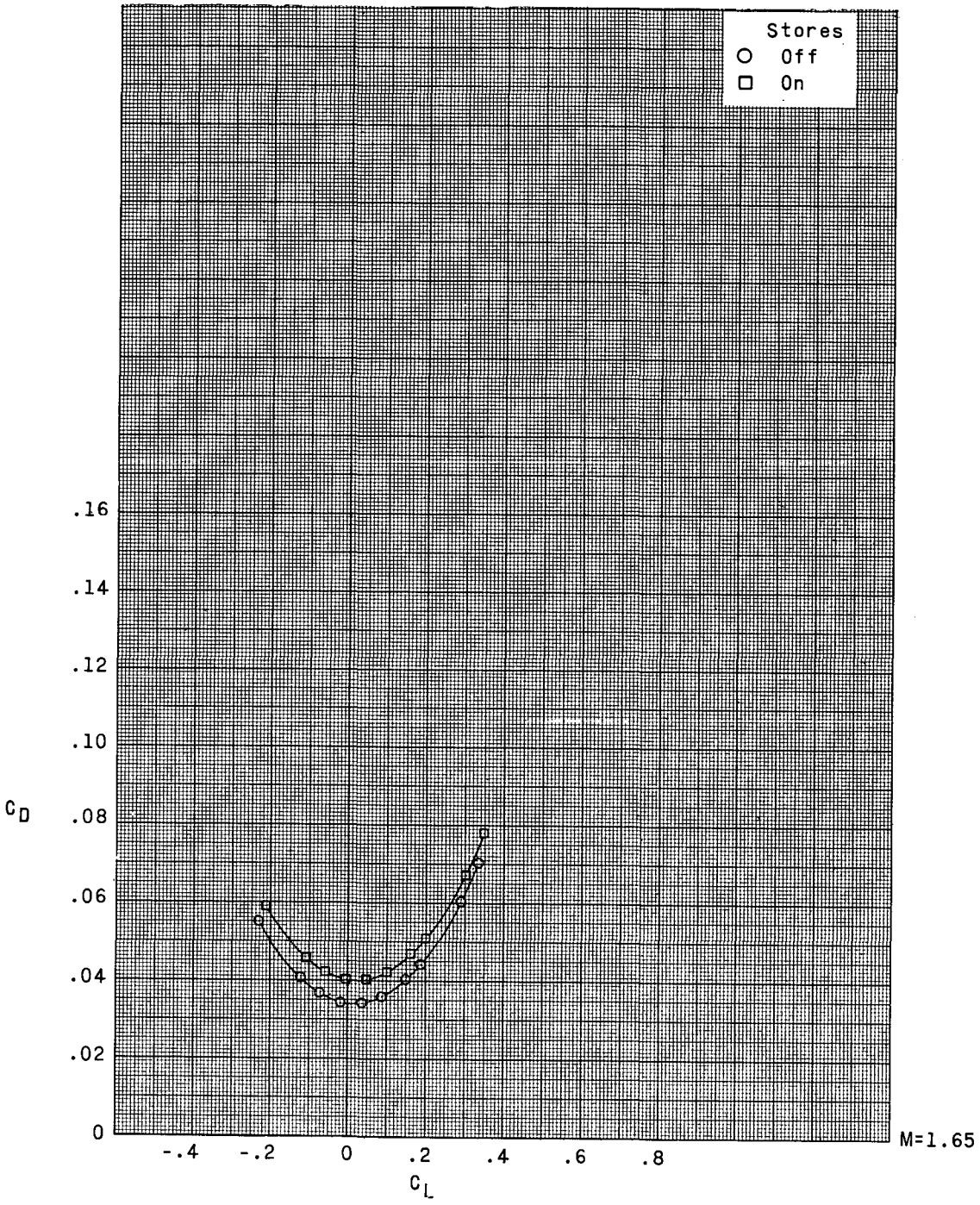

(b) Drag coefficient.

Figure 21.- Continued.

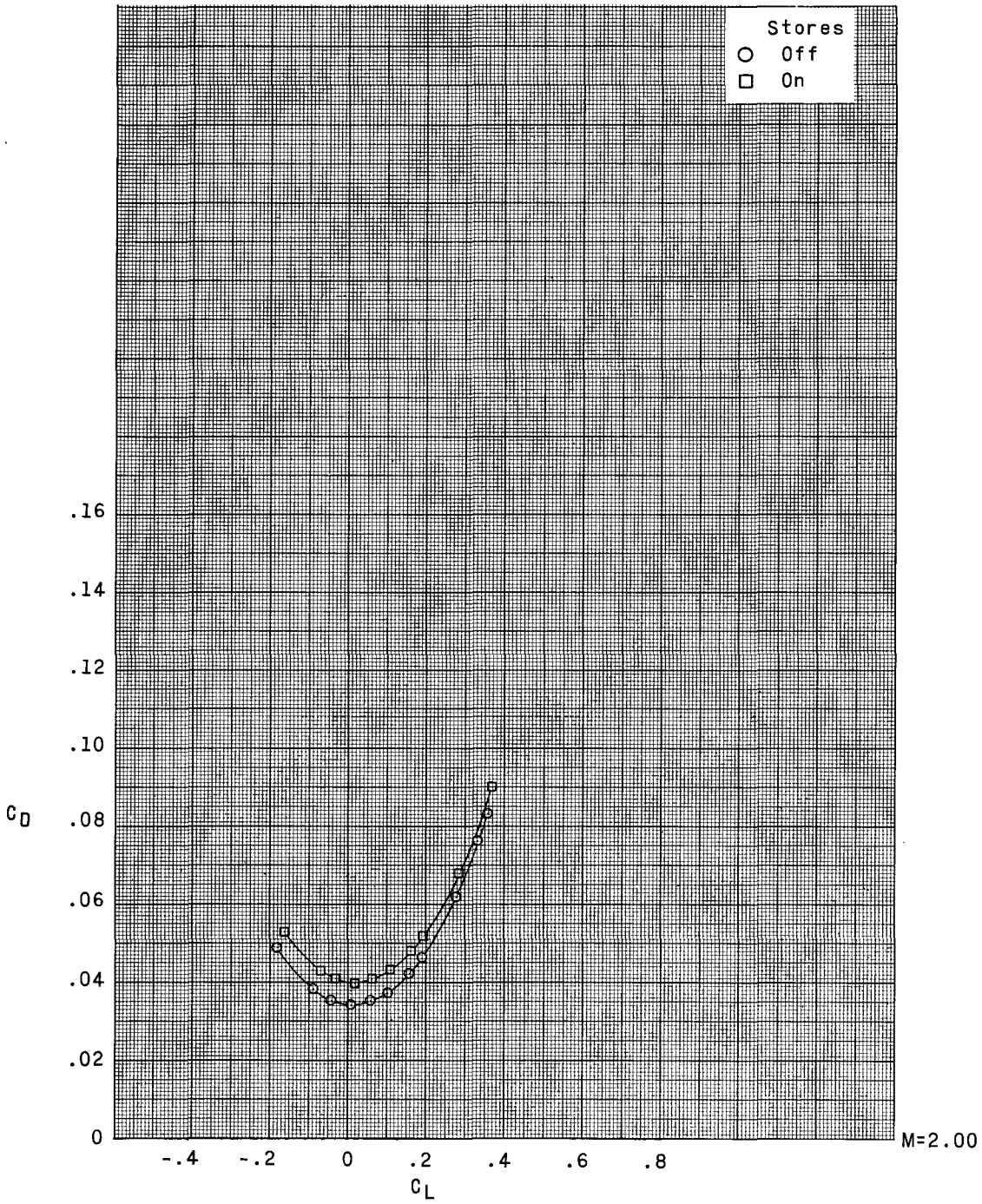

(b) Continued.

Figure 21.- Continued.

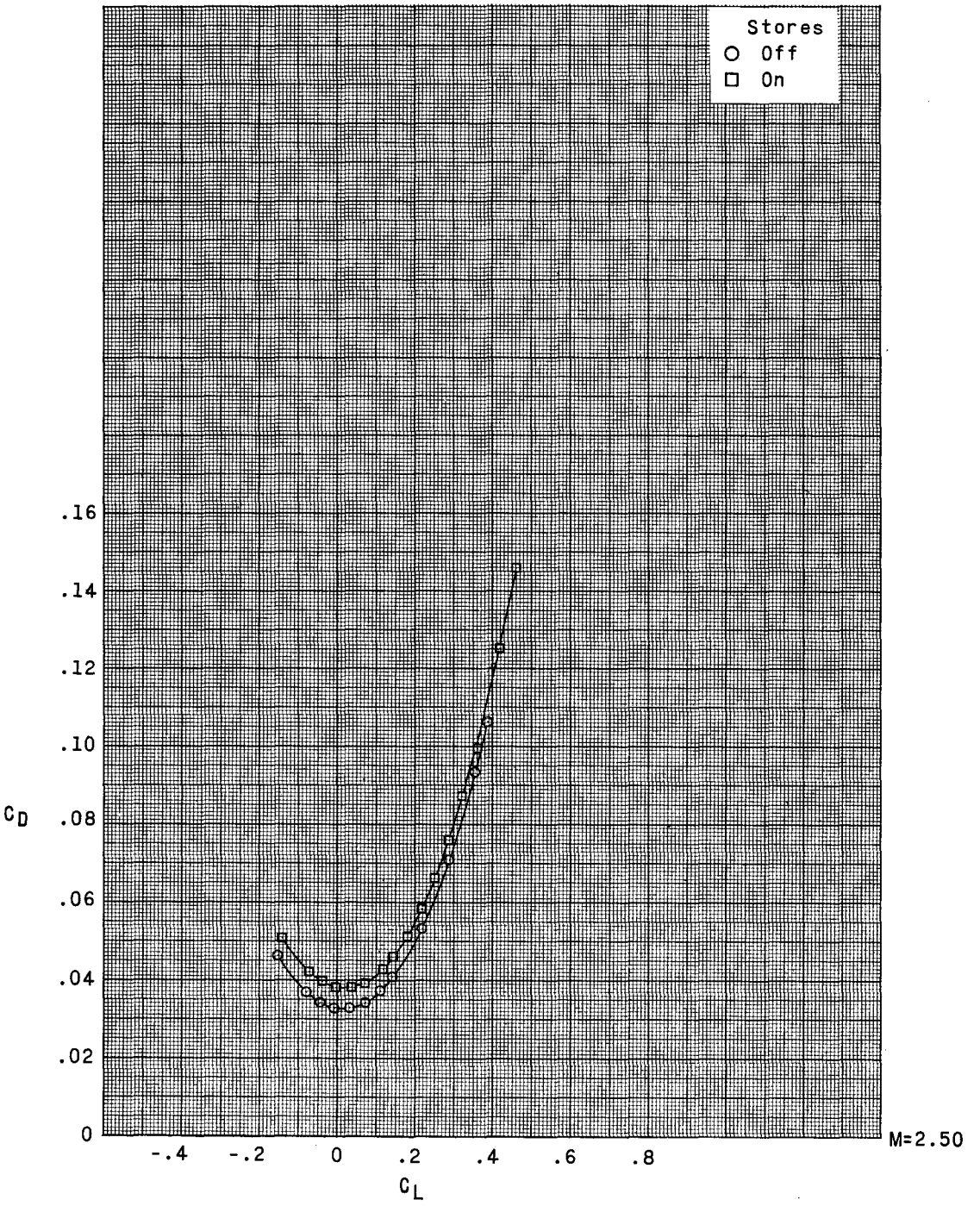

(b) Concluded.

Figure 21.- Continued.

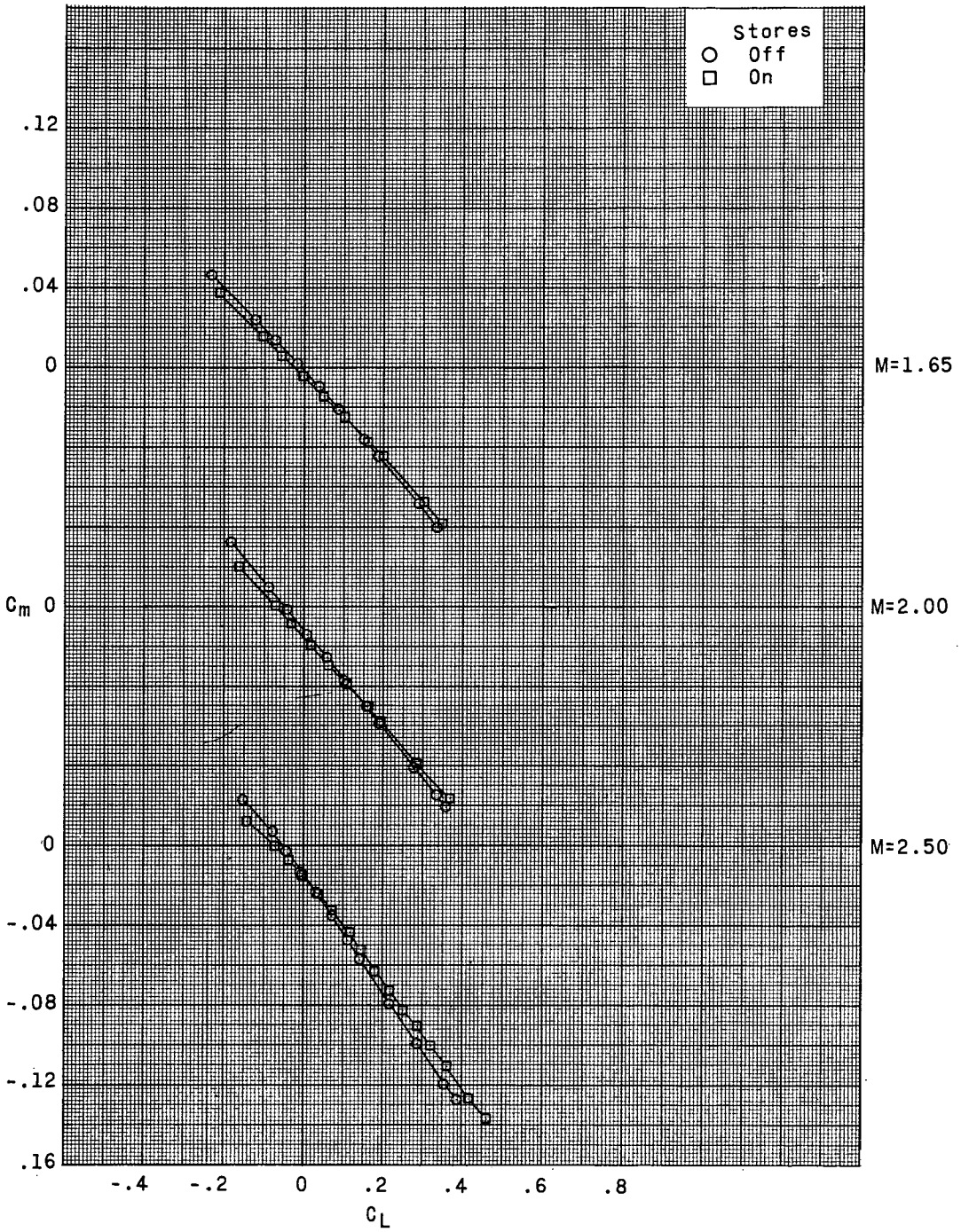

(c) Pitching-moment coefficient.

Figure 21.- Concluded.

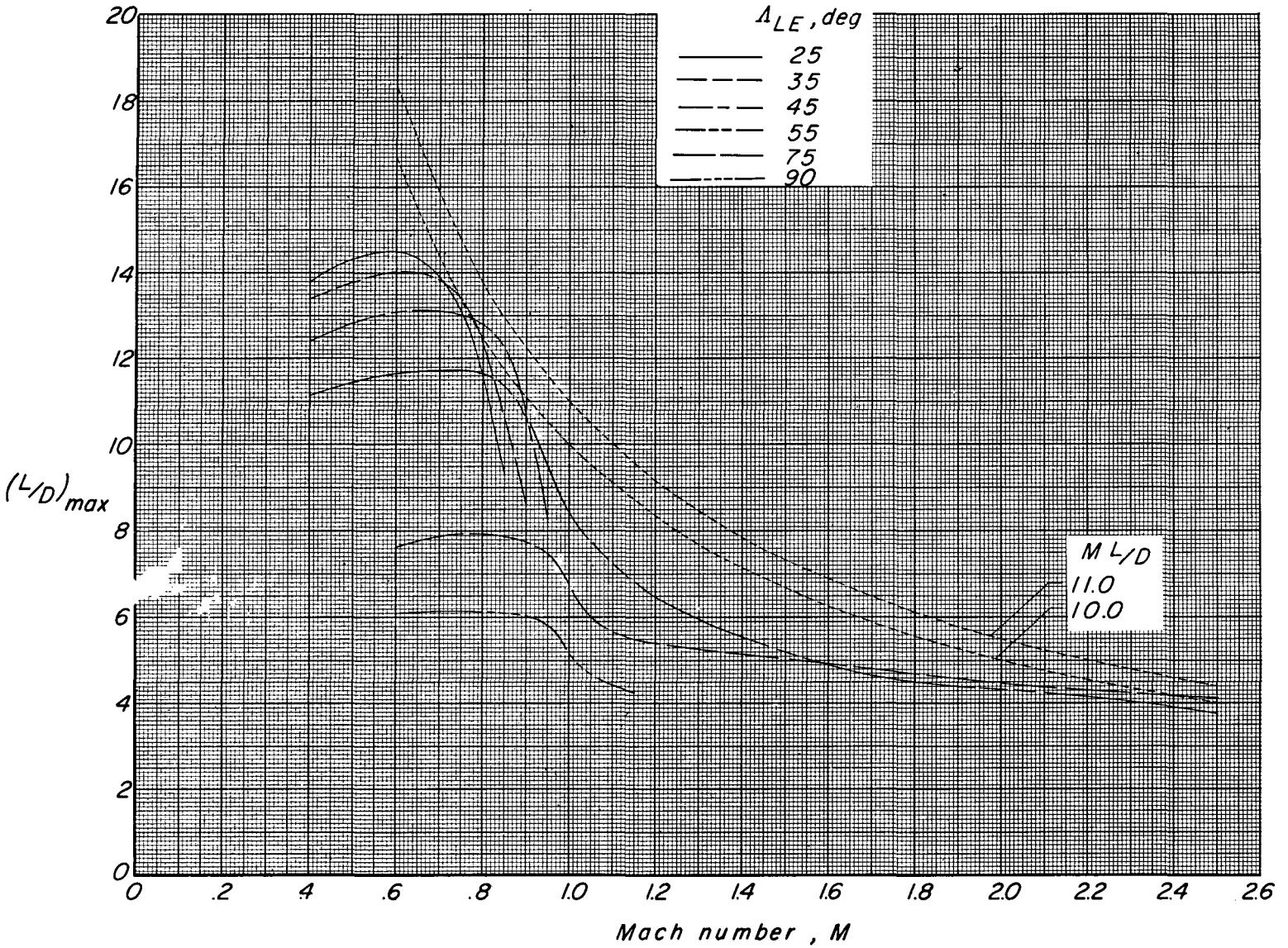

(a) $(L/D)_{max}$.

Figure 22.- $(L/D)_{max}$ and $C_{D,O}$ as functions of Mach number for configuration BW_1VH_1N with $i_t = 0^{\circ}$.

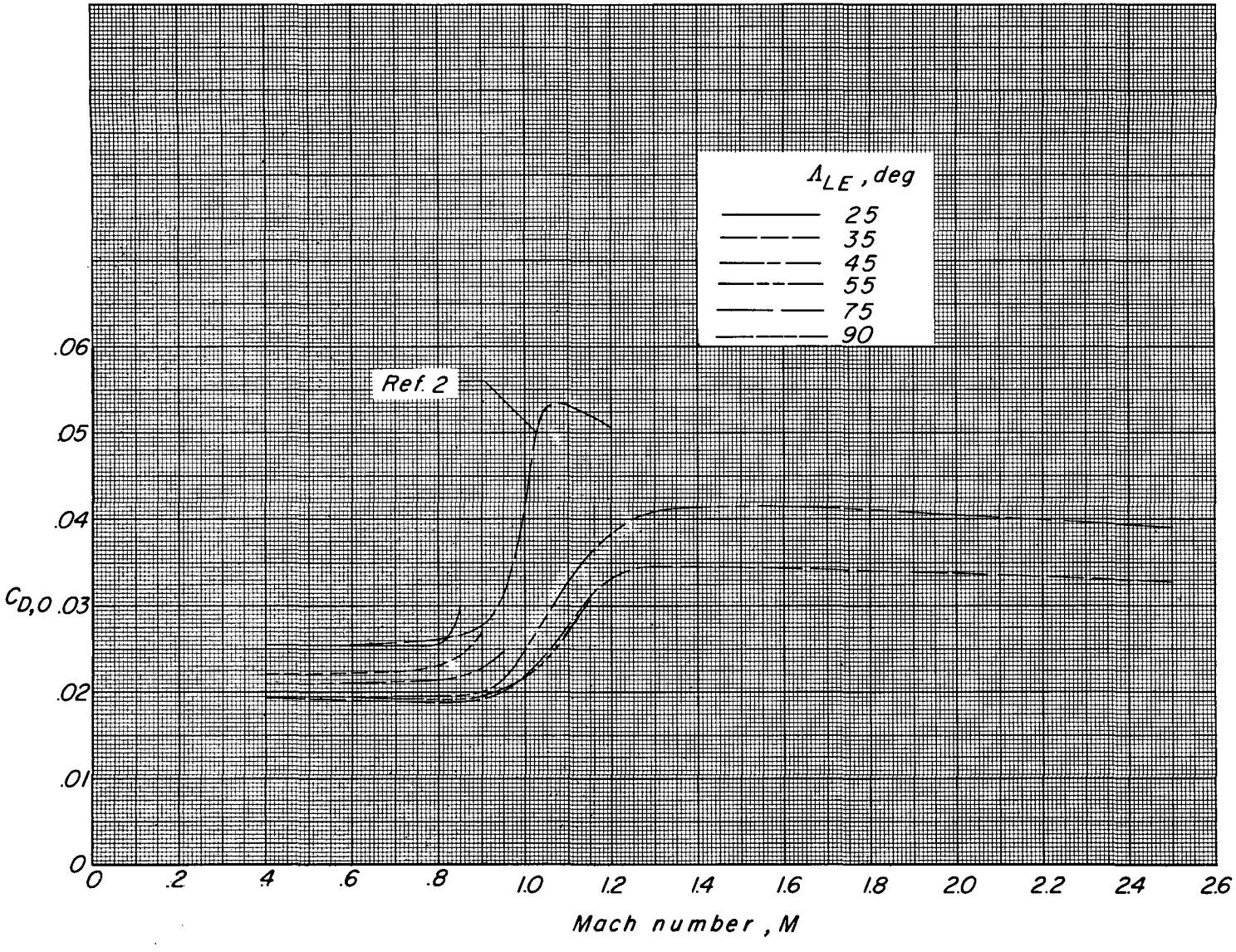

(b) $C_{D,0}$.

Figure 22.- Concluded.

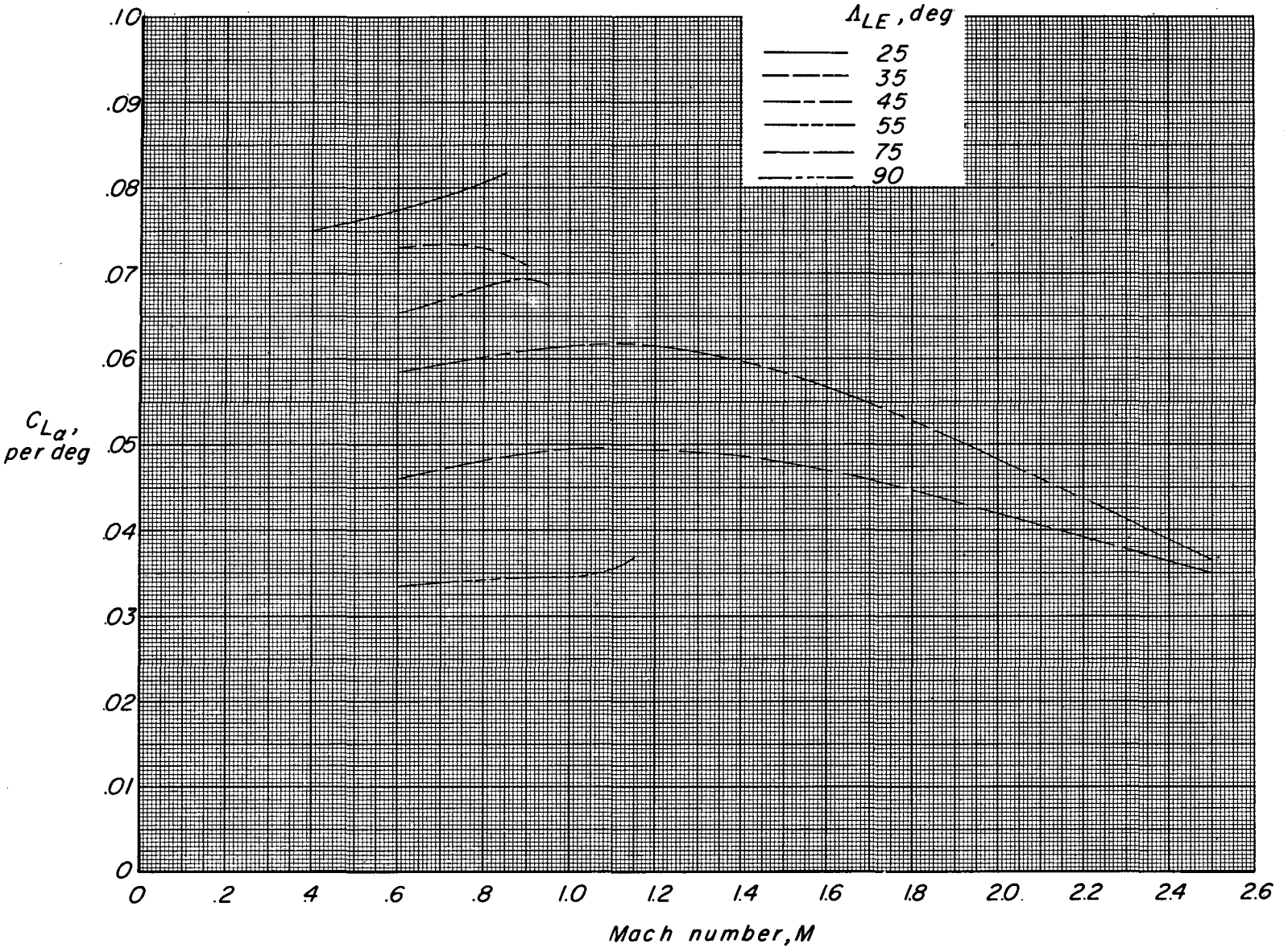

Figure 23.- Variation of C_{L_α} with Mach number for configuration BW_1VH_1N with $i_t = 0^\circ$.

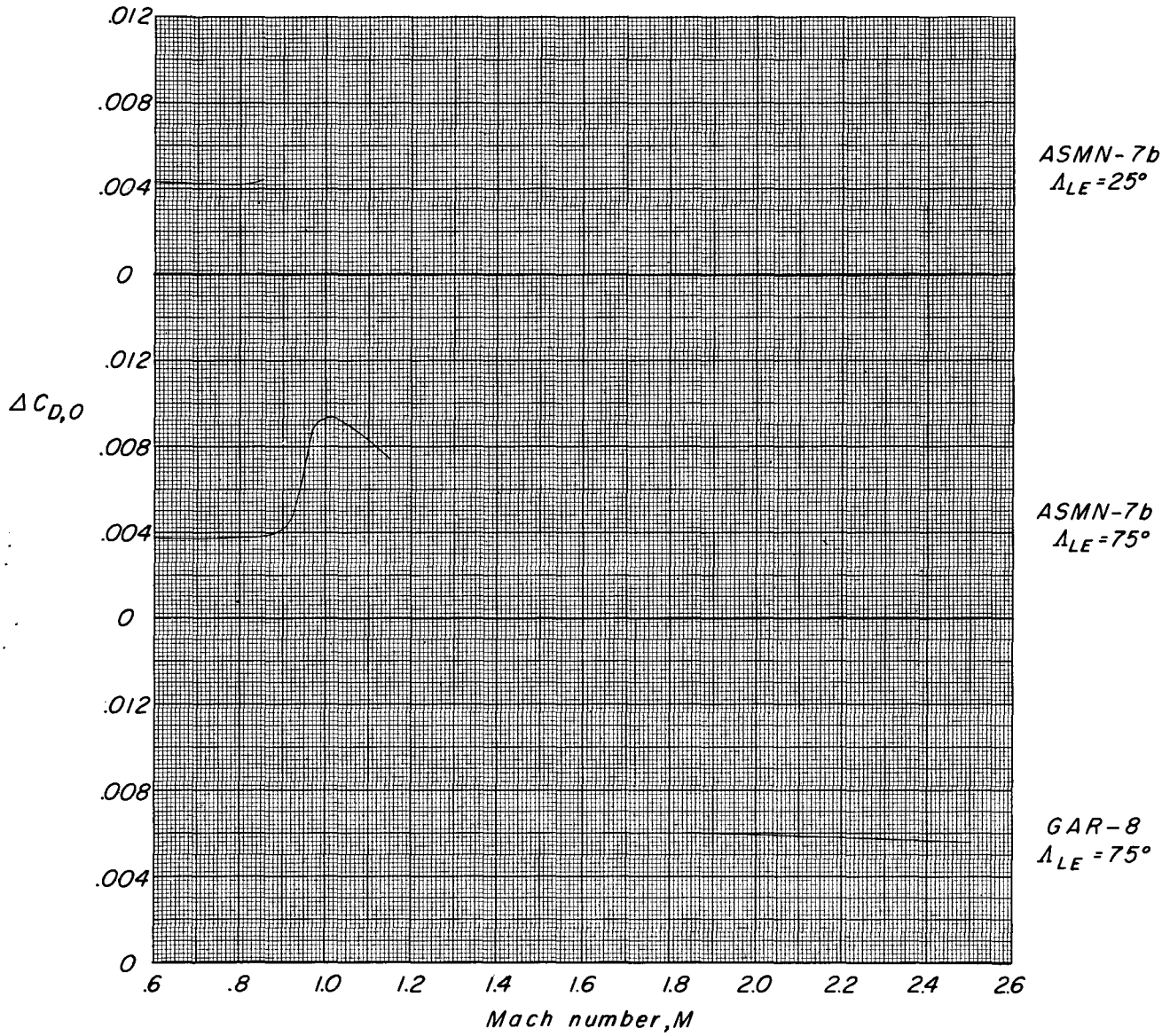

Figure 24.- Variation of incremental drag due to the addition of two ASM-N-7B and four GAR-8 stores with Mach number.

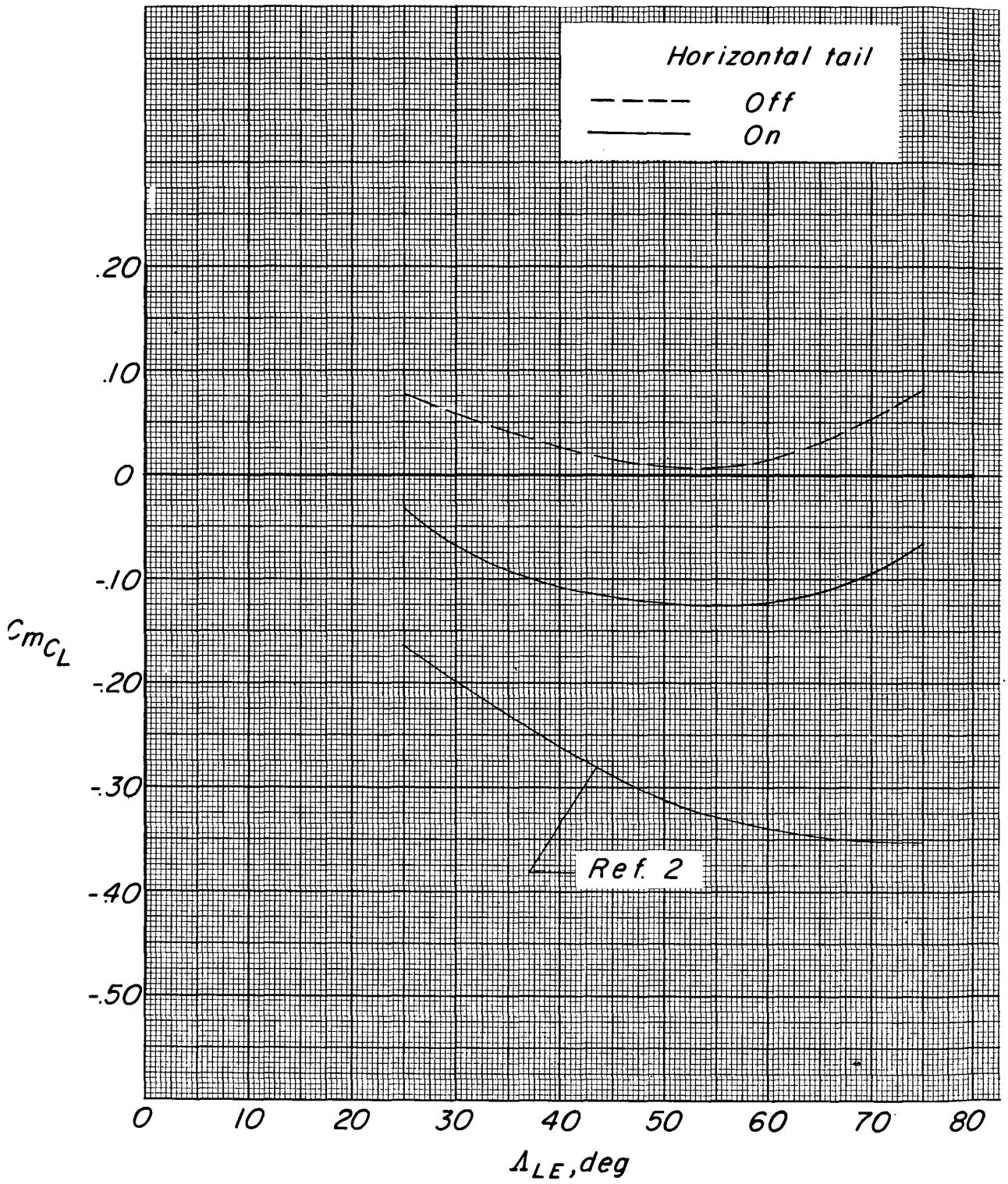

Figure 25.- Variation of longitudinal stability level with wing sweep at $M = 0.6$ for configuration BW_1VH_1N at $M = 0.6$ with $i_t = 0^{\circ}$. $C_L \approx 0.1$.

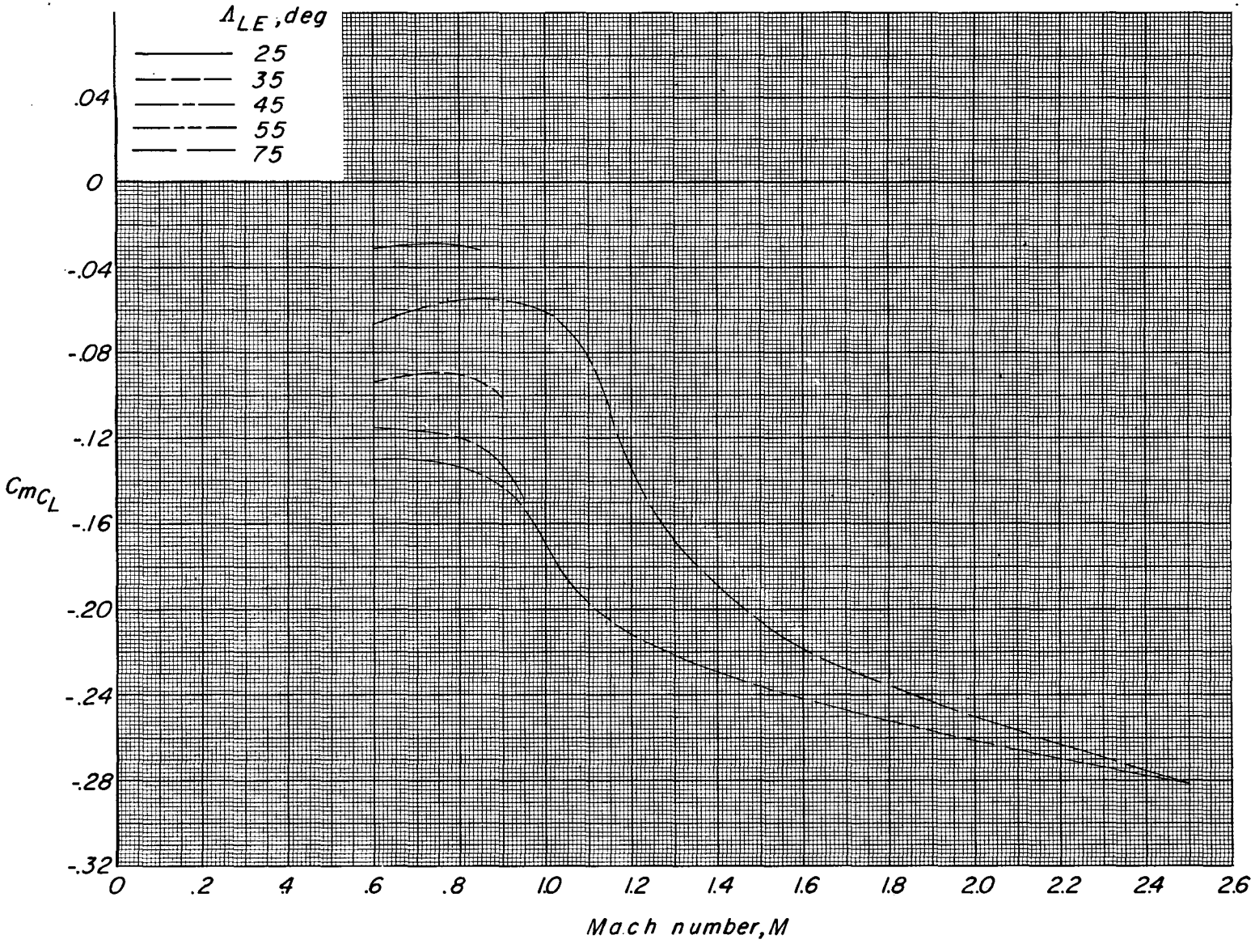

Figure 26.- Longitudinal stability level as a function of Mach number for configuration BW_1VH_1N with $i_t = 0^\circ$ at $C_L \approx 0.1$.

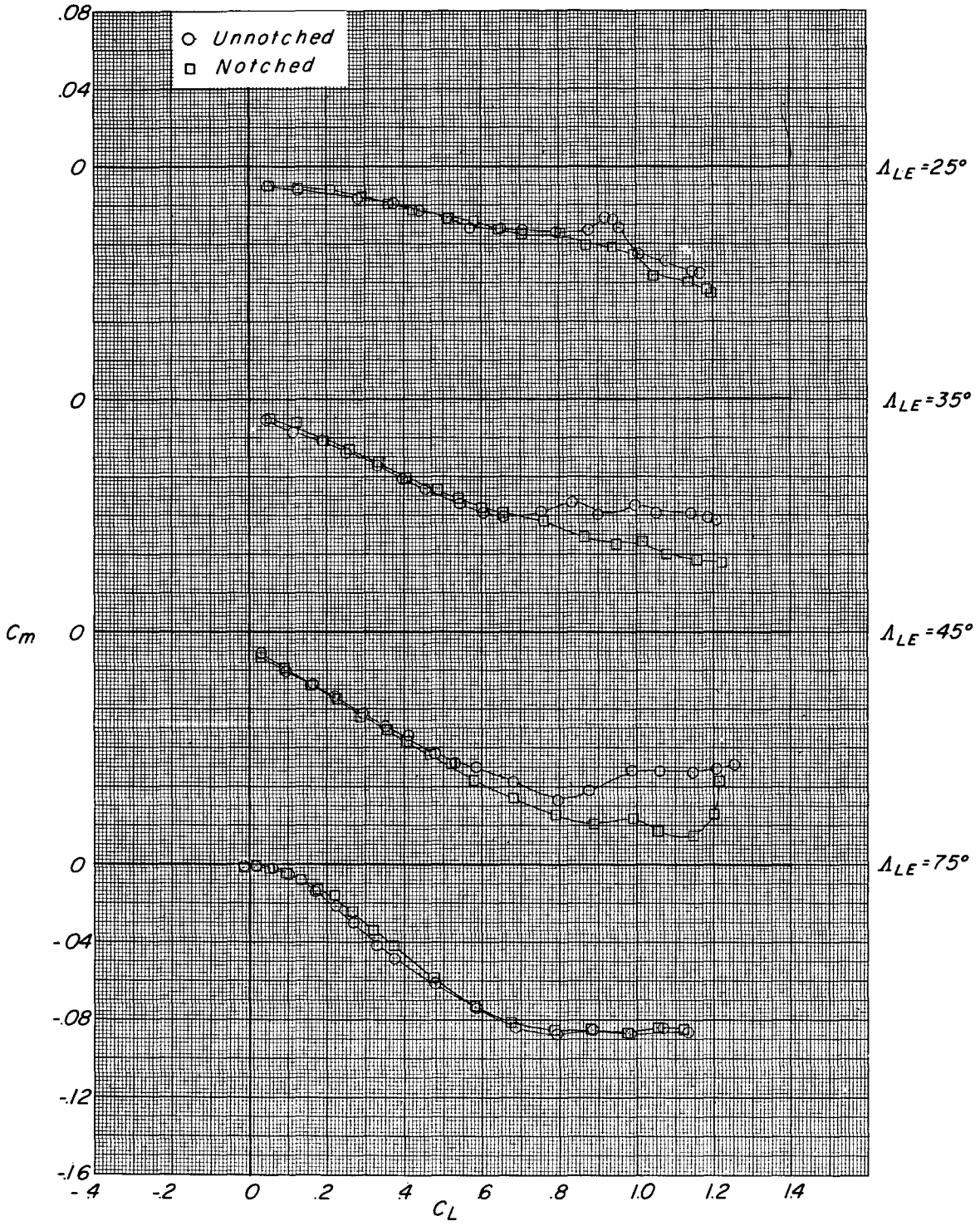

Figure 27.- Effect of notching the outboard wing panels for configuration BW_1VH_1N at $M = 0.28$ and $i_t = 0^\circ$.

NASA-Langley, 1963 L-3449